

## BANYAN. IX. THE INITIAL MASS FUNCTION AND PLANETARY-MASS OBJECT SPACE DENSITY OF THE TW HYA ASSOCIATION

JONATHAN GAGNÉ<sup>1,2</sup>, JACQUELINE K. FAHERTY<sup>1,3</sup>, ERIC E. MAMAJEK<sup>4,5</sup>, LISON MALO<sup>6,7</sup>, RENÉ DOYON<sup>7</sup>, JOSEPH C. FILIPPAZZO<sup>8</sup>, ALYCIA J. WEINBERGER<sup>1</sup>, JESSICA K. DONALDSON<sup>1</sup>, SÉBASTIEN LÉPINE<sup>9</sup>, DAVID LAFRENIÈRE<sup>7</sup>, ÉTIENNE ARTIGAU<sup>7</sup>, ADAM J. BURGASSER<sup>10</sup>, DAGNY LOOPER<sup>11</sup>, ANNE BOUCHER<sup>7</sup>, YURI BELETSKY<sup>12</sup>, SARA CAMNASIO<sup>13</sup>, CHARLES BRUNETTE<sup>7</sup>, GENEVIÈVE ARBOIT<sup>7</sup>

<sup>1</sup> Carnegie Institution of Washington DTM, 5241 Broad Branch Road NW, Washington, DC 20015, USA; jgagne@carnegiescience.edu

<sup>2</sup> NASA Sagan Fellow

<sup>3</sup> NASA Hubble Fellow

<sup>4</sup> Department of Physics & Astronomy, University of Rochester, Rochester, NY 14627, USA

<sup>5</sup> Jet Propulsion Laboratory, California Institute of Technology, 4800 Oak Grove Drive, Pasadena, CA 91109, USA

<sup>6</sup> Canada-France-Hawaii Telescope, 65-1238 Mamalahoa Hwy, Kamuela, HI 96743, USA

<sup>7</sup> Institute for Research on Exoplanets, Université de Montréal, Département de Physique, C.P. 6128 Succ. Centre-ville, Montréal, QC H3C 3J7, Canada

<sup>8</sup> Space Telescope Science Institute, 3700 San Martin Dr, Baltimore, MD 21218, USA

<sup>9</sup> Department of Physics and Astronomy, Georgia State University, 25 Park Place, Atlanta, GA 30302, USA

<sup>10</sup> Center for Astrophysics and Space Sciences, University of California, San Diego, 9500 Gilman Dr., Mail Code 0424, La Jolla, CA 92093, USA

<sup>11</sup> New York University Tisch School of the Arts, 721 Broadway, 10th floor, New York, NY 10003, USA

<sup>12</sup> Las Campanas Observatory, Carnegie Institution of Washington, Colina el Pino, Casilla 601 La Serena, Chile

<sup>13</sup> Department of Physics and Astronomy, Hunter College, City University of New York, NY 10065, USA

### ABSTRACT

A determination of the initial mass function (IMF) of the current, incomplete census of the 10 Myr-old TW Hya association (TWA) is presented. This census is built from a literature compilation supplemented with new spectra and 17 new radial velocities from on-going membership surveys, as well as a re-analysis of Hipparcos data that confirmed HR 4334 (A2 Vn) as a member. Though the dominant uncertainty in the IMF remains census incompleteness, a detailed statistical treatment is carried out to make the IMF determination independent of binning, while accounting for small number statistics. The currently known high-likelihood members are fitted by a log-normal distribution with a central mass of  $0.21_{-0.06}^{+0.11} M_{\odot}$  and a characteristic width of  $0.8_{-0.1}^{+0.2}$  dex in the  $12 M_{\text{Jup}}-2 M_{\odot}$  range, whereas a Salpeter power law with  $\alpha = 2.2_{-0.5}^{+1.1}$  best describes the IMF slope in the  $0.1-2 M_{\odot}$  range. This characteristic width is higher than other young associations, which may be due to incompleteness in the current census of low-mass TWA stars. A tentative overpopulation of isolated planetary-mass members similar to 2MASS J11472421-2040204 and 2MASS J11193254-1137466 is identified: this indicates that there might be as many as  $10_{-5}^{+13}$  similar members of TWA with hot-start model-dependent masses estimated at  $\sim 5-7 M_{\text{Jup}}$ , most of which would be too faint to be detected in 2MASS. Our new radial velocity measurements corroborate the membership of 2MASS J11472421-2040204, and secure TWA 28 (M8.5  $\gamma$ ), TWA 29 (M9.5  $\gamma$ ) and TWA 33 (M4.5 e) as members. The discovery of 2MASS J09553336-0208403, a young L7-type interloper unrelated to TWA, is also presented.

*Keywords:* stars:mass function — open clusters and associations: individual (TW Hya) — brown dwarfs — stars: kinematics and dynamics — stars: low-mass — methods: data analysis

### 1. INTRODUCTION

The study of young moving groups and associations has received much attention in recent years, in particular for their potential in hosting the brightest very low-mass substellar objects in the solar neighborhood. The youngest of these associations within 100 pc is TW Hya (TWA hereafter; e.g., see [de la Reza et al. 1989](#); [Kastner](#)

[et al. 1997](#); [Song et al. 2003](#); [Chauvin et al. 2004](#); [Mamajek 2005](#); [Zuckerman & Song 2004](#); [Weinberger et al. 2013](#); [Ducourant et al. 2014a](#); [Donaldson et al. 2016](#)), at an age of  $10 \pm 3$  Myr ([Bell et al. 2015](#)). Although this association has been well studied over more than a decade, many of its low-mass members are still missing since they are too faint to have been detected by the

Hipparcos mission (Perryman et al. 1997), and only a first estimate of its initial mass function (IMF) has been presented (Looper 2011).

Recent discoveries have identified the first few isolated planetary-mass objects in the solar neighborhood (e.g., Liu et al. 2013; Mace et al. 2013; Gagné et al. 2014a,c, 2015a,d) that are members of young associations. Their young age means that they still retain more heat from their formation process, and thus they are intrinsically brighter than similar objects at the age of the field. Field-age planetary mass objects are expected to have temperatures in the range  $\sim 250\text{--}500$  K, which correspond to the spectral class Y (Delorme et al. 2008; Cushing et al. 2011; Kirkpatrick et al. 2011, 2012; Tinney et al. 2012). Such objects are extremely faint, even at near-infrared (NIR) wavelengths (e.g.,  $M_K \geq 20$ ; Leggett et al. 2015). Younger planetary-mass objects are typically much brighter ( $M_K \sim 12\text{--}16$ ; e.g., Liu et al. 2013; Gagné et al. 2015d,a).

Two recent discoveries in particular demonstrate the interest of TWA as a laboratory for understanding this isolated planetary-mass population. 2MASS J11193254–1137466 (Kellogg et al. 2015, 2016) and 2MASS J11472421–2040204 (Schneider et al. 2016a) are both candidate members of TWA with spectral types L7 that display signs of youth, and with estimated masses as low as  $5\text{--}7 M_{\text{Jup}}$ . Their close distances to the Sun (29–33 pc) place them at the nearer side of the TWA spatial distribution. This result, as well as some recent indications that planetary-mass objects could be more abundant than expected in the young Tucana-Horologium Association (Gagné et al. 2015d), calls for an update of the IMF of TWA and an estimate of the space density of its planetary-mass members.

Various functional forms have been used in the literature to characterize the IMF of a stellar population. The first was introduced by Salpeter (1955):

$$\phi(\log_{10} m) = \frac{dN}{d \log_{10} m} = \phi_0 m^{1-\alpha}, \quad (1)$$

where  $\phi_0$  is the density of stars per logarithm mass per  $\text{pc}^3$  at  $m = 1 M_{\odot}$ .

The Salpeter IMF has been used to represent the IMF of field stars with masses in the range  $0.4\text{--}10 M_{\odot}$  with a slope of  $\alpha = 2.35$  (Salpeter 1955). However, steeper slopes have been measured for the more massive stars (e.g.,  $\alpha = 2.7 \pm 0.2$  in the  $1.1\text{--}1.6 M_{\odot}$  range or  $\alpha = 3.1 \pm 0.2$  in the  $1.6\text{--}4 M_{\odot}$  range; Schröder & Pagel 2003), whereas low-mass stars yield shallower slopes (e.g.,  $\alpha = 1.05$  in the  $0.1\text{--}1.0 M_{\odot}$  range; Reid & Gizis 1997, or  $\alpha = 1.2 \pm 0.3$  in the  $0.1\text{--}0.7 M_{\odot}$  range; Bastian et al. 2010).

Log-normal distributions have been introduced (Miller & Scalo 1979; Chabrier 2005) to represent this slope

variation as a function of the mass regime with a single functional form:

$$\phi(\log_{10} m) = \frac{\phi_t}{\sigma\sqrt{2\pi}} \exp\left(-\frac{(\log_{10} m - \log_{10} m_c)^2}{2\sigma^2}\right), \quad (2)$$

where  $m_c$  represents a characteristic mass where the IMF peaks,  $\sigma$  represents the characteristic width of the IMF in log space, and  $\phi_t$  is the space density of objects per unit logarithm mass at the peak of the IMF. Additional functional forms have also been introduced, such as multi-segmented power laws (Kroupa et al. 1993; Kroupa 2001), or a combination of a log-normal with power laws (Bastian et al. 2010).

Fitting such an IMF to field stars with masses in the range  $0.1\text{--}50 M_{\odot}$  has yielded typical values of  $m_c = 0.1 M_{\odot}$  and  $\sigma = 0.7$  dex (Miller & Scalo 1979). A subsequent determination of the field IMF from the Sloan Digital Sky Survey (Bochanski et al. 2011) yielded  $m_c = 0.18 M_{\odot}$  and  $\sigma = 0.34$  dex when counting all components of multiple systems, whereas an IMF treating systems as single objects yielded  $m_c = 0.25 M_{\odot}$  and  $\sigma = 0.28$  dex (Bochanski et al. 2010). Most field IMFs yield characteristic masses in the range  $0.15\text{--}0.25 M_{\odot}$  (Chabrier 2005).

IMF determinations in the brown dwarf regime ( $m \leq 0.075 M_{\odot}$ ) have yielded slopes of  $\alpha \leq 0$  (Metchev et al. 2008; Reylé et al. 2010; Burningham et al. 2010), indicating that the space density of brown dwarfs decreases with decreasing masses.

Current evidence suggests that the IMFs of young associations are similar to that of the field. Chabrier (2005) demonstrated that several young stellar associations are well described by a log-normal IMF similar to that of field stars, with  $m_c = 0.25 M_{\odot}$  and  $\sigma = 0.55$  dex (valid for  $m \leq 1 M_{\odot}$ ; see also Chabrier 2003; Moraux et al. 2003a). Jeffries (2012) further demonstrated this by obtaining a log-normal IMF with  $m_c = 0.25 M_{\odot}$  and  $\sigma = 0.52$  dex that adequately represents the IMF of several young stellar associations (e.g., Barrado Y Navascués et al. 2002; Moraux et al. 2003b; Jeffries et al. 2004; Barrado Y Navascués 2005; de Wit et al. 2006; Moraux et al. 2007; Luhman 2007; Oliveira et al. 2009; Caballero 2009), with the exception of Upper Scorpius, which might have an excess of brown dwarfs (Lodieu et al. 2007). It must be noted, however, that this last IMF was constructed with candidate members of Upper Scorpius that were not confirmed with spectroscopy, and could thus be subject to a high level of contamination from reddened background stars or extragalactic sources.

This paper presents a set of new spectroscopic and kinematic observations that furthers the census of TWA

members. An updated compilation of its members across spectral types A0–L7 is presented, which is then used to determine its IMF and to estimate the space density of its isolated planetary-mass members. In Section 2, new candidate members from the BASS-Ultracool and SUPERBLINK-south surveys and a re-analysis of Hipparcos are presented. In Section 3, new observations that consist of low- and high-resolution, optical and near-infrared spectroscopy are detailed. In Section 4, these new data are used to assign spectral types, assess signs of low-gravity, and measure the radial velocity of several TWA candidate members that originate from various surveys. In Section 5, the final list of TWA members and candidates is detailed, and their physical properties are estimated in Section 6. In Section 7, the completeness of the current census of TWA members is discussed. In Section 8, the IMF of TWA is constructed and discussed. In Section 9, the space density of its isolated planetary-mass members is assessed. This paper is concluded in Section 10.

## 2. NEW MEMBERS OF TW HYA

This section presents an update on TWA candidate members from the BANYAN All-Sky Survey (BASS; Gagné et al. (2015b); Section 2.1), and reports new candidate members of TWA that were uncovered by three new surveys. Section 2.2 describes the BASS-Ultracool survey that targets members of young moving groups with spectral types later than  $\sim$ L5; Section 2.3 describes a search for young low-mass, stellar moving group members from the SUPERBLINK-south proper motion catalog; and Section 2.4 describes a re-analysis of the Hipparcos (Perryman et al. 1997) survey data with the BANYAN II tool for bright members of young moving groups.

### 2.1. BASS

The BANYAN All-Sky Survey (BASS) was initiated by Gagné et al. (2015b) to identify new  $\sim$ M5–L5 candidate members of young moving groups in the solar neighborhood, including TWA. The BASS survey is based on a cross-match of the *Two Micron All-Sky Survey* (2MASS; Skrutskie et al. 2006) with the AllWISE (Wright et al. 2010; Kirkpatrick et al. 2014) survey, which yielded proper motion measurements with a precision of  $\sim$ 5–15 mas yr<sup>-1</sup>. An initial set of 98 970 potential nearby  $>$  M5 dwarfs was constructed from several selection criteria, e.g. a good 2MASS and AllWISE photometric quality, a  $J - K_S$  color consistent with spectral types M5–L5, no optical  $B2$ -band detection in USNO–A2.0, a proper motion larger than 30 mas yr<sup>-1</sup> and a sky position located further away than 15° from the Galactic plane. See Gagné et al. 2015b for the full details on selection criteria.

Moving group membership probabilities were assessed for all targets in this sample using the Bayesian Analysis for Nearby Young AssociatioNs II tool<sup>1</sup> (Gagné et al. 2014c; Malo et al. 2013). This resulted in a sample of 983 candidate members with Bayesian probabilities larger than 10% and estimated false-positive probabilities below 50%. As BANYAN II provides an estimate of the distance of each target assuming membership to the most probable moving group, further selection cuts based on the sequence of known young M5–L5 dwarfs in two color-magnitude diagrams (absolute  $W1$  versus  $J - K_S$  and absolute  $W1$  versus  $H - W2$ ) rejected 435 candidate members and divided the remaining candidates in two samples. The main BASS sample consists of 273 objects (including 54 TWA candidates) that are at least  $1\sigma$  redder than the field-age sequences in both color-magnitude diagrams, and the low-priority BASS (LP-BASS) sample consists of 275 objects (including 33 TWA candidates) that are redder than the field-age sequence by less than  $1\sigma$ . The BASS survey has an expected completeness of  $\sim$ 72% for TWA, based on the selection criteria mentioned above. The estimated false-positive rates are estimated to be below 30% and 80% for the main BASS and LP-BASS samples.

While the BASS survey was in construction and the selection criteria were still being refined, a subset of 312 candidate members (including 27 TWA candidates) was collected from partial and/or more permissive selection criteria; these candidates are designated as the PRE-BASS sample.

An initial spectroscopic follow-up of 182 candidate members of moving groups (including 36 TWA candidates) that were selected from BASS (106 targets), LP-BASS (27 targets) and PRE-BASS (49 targets) was presented by Gagné et al. (2015d). A fraction of 21% of these targets were found to be contaminants, consisting of old low-mass stars and brown dwarfs, or reddened background objects. A total of 18 TWA candidates were found to have spectroscopic signatures of youth, and 4 more were found to have a spectral type earlier than M5, for which the NIR spectroscopic follow-up could not constrain their age. Twelve of the TWA candidates with spectroscopic signatures of youth originated from the main BASS catalog, and three more originated from LP-BASS. A detailed spectroscopic follow-up of two TWA candidates from the main BASS sample (2MASS J12074836–3900043 and 2MASS J12474428–3816464) was also presented by Gagné et al. (2014a). A total of 70 TWA candidate members from the LP-BASS, BASS and PRE-BASS samples have not yet been

<sup>1</sup> Available at [www.astro.umontreal.ca/~gagne/banyanII.php](http://www.astro.umontreal.ca/~gagne/banyanII.php)

investigated for signs of low-gravity using spectroscopy, nor have they benefitted from radial velocity or parallax measurements. New radial velocity measurements, low-resolution near-infrared spectra and low-resolution optical spectra are presented in this paper for 9, 12 and 4 of these targets, respectively.

### 2.2. BASS-Ultracool

The BASS-Ultracool survey was recently initiated to identify the late-type ( $> L5$ ) members of young moving groups from a cross-match of 2MASS and AllWISE that were missed by the BASS survey due to the color and photometric quality cuts that were imposed on the 2MASS catalog entries (see Section 2.1 and Gagné et al. 2015b,d).

This ongoing survey is performed in multiple steps, the first of which consists of a re-analysis of 2MASS and AllWISE astrometry and photometry. This is done by cross-matching all entries of 2MASS and AllWISE, and using BANYAN II, without using photometry as an input, to assess the possible membership of all sources with  $W1 - W2 > 0.2$ . Including photometry in the BANYAN II analysis is avoided in this particular case, because the NIR sequences of young  $> L5$  brown dwarfs are poorly constrained at this time. The main survey results will be described in a future paper (J. Gagné et al., in preparation). This survey has already identified the first isolated T dwarf bona fide member of a young moving group: the AB Doradus member SDSS J111010.01+011613.1, with an estimated mass of  $10\text{--}12 M_{\text{Jup}}$  (Gagné et al. 2015a).

A total of 8 candidate members of TWA were identified to date in this first step of the BASS-Ultracool survey, which are listed in Table 1. Only the candidate members with BANYAN II probabilities above 60% were considered. The TWA Bayesian membership probabilities obtained from BANYAN II are listed, along with statistical distances (see Gagné et al. 2014c for a detailed description of how the membership probabilities are obtained). Estimated spectral types are also presented, based on a comparison of 2MASS and AllWISE photometry at the most probable TWA statistical distance with the young sequences of Gagné et al. (2015d).

BASS-UC 121 (2MASS J11193254–1137466) has been independently discovered by Kellogg et al. (2015) and confirmed as a likely candidate member of TWA with a radial velocity measurement by Kellogg et al. (2016). They note that it likely is the nearest known member of TWA, located at a kinematic distance of  $28.9 \pm 3.6$  pc. It has a very late spectral type (L7), and displays an unusually red NIR slope and weak K I absorption doublets at 1.117 and 1.125  $\mu\text{m}$ , which are both signs of low gravity and thus youth (e.g., see Kirkpatrick et al. 2006; Cruz et al. 2009; Allers & Liu 2013; Liu et al. 2013).

At the age of TWA ( $10 \pm 3$  Myr), this object has an estimated mass of  $5\text{--}7 M_{\text{Jup}}$ .

BASS-UC 56 (2MASS J11472421–2040204) has been independently discovered by Schneider et al. (2016a) as a young L7 candidate member of TWA. The similarities between this object and 2MASS J11193254–1137466 are remarkable, with their similar spectral types, distances (31–33 pc) and estimated masses (6–13  $M_{\text{Jup}}$ ). However, this object did not yet have a radial velocity confirmation of its TWA membership before the present work.

The remaining six candidate members were not previously known, and will be discussed in Section 4 in light of new data presented in this work.

### 2.3. SUPERBLINK-south

A search for new members of nearby, young associations was performed using the SUPERBLINK proper motion survey of the Southern hemisphere (SUPERBLINK-south; S. Lépine et al. in preparation). The SUPERBLINK-south catalog includes stars with total proper motions above  $40 \text{ mas yr}^{-1}$  in the region  $-33 < \text{Decl.} < 0$ , to an approximate magnitude limit of  $V < 20$ , and provides proper motions with a typical precision of  $\sim 11 \text{ mas yr}^{-1}$ . All stars are matched against the 2MASS all-sky point source catalog, and include optical blue (IIIaJ) and red (IIIaF) photographic magnitude estimates from the USNO-B1.0 catalog.

The 403 085 SUPERBLINK-south catalog entries were supplemented with *I*-band photometric data from the AAVSO Photometric All-Sky Survey (APASS-DR9; Henden et al. 2016). Potential young and nearby low-mass stars were selected by applying the following criteria: (1) A NUV detection in the Galaxy Evolution Explorer (GALEX) survey (Martin et al. 2005) must be present; (2) The declination must be located above  $-40^\circ$  and the right ascension must be located between 10 h and 14 h; (3) All 2MASS to WISE colors must be consistent with a spectral type of M0 or later (Pecaut & Mamajek 2013); (4) The apparent 2MASS  $K_S$  band magnitude must be fainter than 11.5; and (5) The AAVSO *I*-band magnitude must have error bars of 0.2 mag or smaller. These criteria yielded a set of 714 catalog entries.

The BANYAN I tool (Malo et al. 2013) was used to identify candidate members, using  $I_C$  and 2MASS *J*-band magnitudes, proper motions and sky positions as input observables. This analysis yielded fifteen TWA candidate members with a probability of 90% or more, and for which the absolute NUV magnitude is consistent with a young low-mass star (see Figure 1 of Rodriguez et al. 2011).

The known member TWA 5 A (M2IVe) was recovered, as well as the BASS candidate member 2MASS J10585054–2346206 and the LP-BASS candi-



**Table 1.** Candidate Members of TWA from the BASS-Ultracool Survey

BASS-UC Name	Designation	2MASS		
		$J$	$H$	$K_S$
BASS-UC 51	09553336–0208403	$17.11 \pm 0.24$	$> 15.56$	$14.79 \pm 0.12$
BASS-UC 55	11063147–4201251	$15.28 \pm 0.06$	$14.44 \pm 0.07$	$14.09 \pm 0.08$
BASS-UC 121	11193254–1137466	$> 17.29$	$15.606 \pm 0.14$	$14.62 \pm 0.11$
BASS-UC 56	11472421–2040204	$> 17.51$	$15.76 \pm 0.11$	$14.87 \pm 0.11$
BASS-UC 57	12021801–3110348	$14.91 \pm 0.04$	$14.20 \pm 0.03$	$13.84 \pm 0.05$
BASS-UC 58	12162481–2742007	$14.84 \pm 0.04$	$14.25 \pm 0.04$	$13.85 \pm 0.05$
BASS-UC 59	12194846–3232059	$15.66 \pm 0.06$	$14.97 \pm 0.06$	$14.59 \pm 0.08$
BASS-UC 60	12454194–3903106	$15.46 \pm 0.05$	$14.84 \pm 0.05$	$14.41 \pm 0.07$

Designation	AllWISE		$\mu_\alpha \cos \delta$ (mas yr <sup>-1</sup> )	$\mu_\delta$ (mas yr <sup>-1</sup> )	Estimated SpT <sup>a</sup>	Bayesian Prob. (%) <sup>b</sup>	Stat. Distance (pc)
	W1	W2					
095533.26–020841.6	$13.93 \pm 0.03$	$13.39 \pm 0.03$	$-123.9 \pm 14.8$	$-105.6 \pm 15.5$	L8	77.1	$24.1 \pm 2.8$
110631.37–420125.1	$13.87 \pm 0.03$	$13.65 \pm 0.03$	$-101.6 \pm 7.9$	$-0.3 \pm 7.7$	L0	94.7	$43.0^{+6.0}_{-5.6}$
111932.43–113747.7	$13.55 \pm 0.03$	$12.88 \pm 0.03$	$-148.5 \pm 15.4$	$-98.1 \pm 14.7$	L8	65.1	$25.3 \pm 2.8$
114724.10–204021.3	$13.72 \pm 0.03$	$13.09 \pm 0.03$	$-121.6 \pm 11.1$	$-74.2 \pm 11.9$	L8	84.5	$31.3 \pm 3.6$
120217.92–311035.1	$13.62 \pm 0.03$	$13.41 \pm 0.03$	$-98.6 \pm 7.6$	$-27 \pm 7$	M9.5	96.7	$44.6^{+5.2}_{-4.8}$
121624.74–274201.1	$13.66 \pm 0.03$	$13.43 \pm 0.03$	$-77.5 \pm 6.7$	$-31.2 \pm 6.5$	M9	94.8	$49.8^{+5.6}_{-5.2}$
121948.39–323206.1	$14.38 \pm 0.03$	$14.16 \pm 0.04$	$-70.2 \pm 7.7$	$-15.9 \pm 8.3$	L0	90.8	$56.2 \pm 6.4$
124541.87–390310.9	$14.22 \pm 0.03$	$13.95 \pm 0.04$	$-73.1 \pm 7.3$	$-22.3 \pm 7.4$	M9.5	95.3	$58.2^{+7.2}_{-6.8}$

<sup>a</sup>Photometric spectral types estimated from 2MASS and AllWISE photometry and the BANYAN II statistical distances (see [Gagné et al. 2014c](#) and [Gagné et al. 2015b](#) for a detailed explanation).

<sup>b</sup>Based on kinematics alone.

NOTE—See Section 2.2 for more details.

date member 2MASS J10542303–1507082. One further candidate member (2MASS J12000160–1731308) is presented in this paper. Three of the remaining 11 candidates were observed and rejected as members, and the remaining eight have not been observed yet; these 11 objects will be the subject of a future publication to identify young moving group members from SUPERBLINK-South.

New high-resolution optical spectra were obtained for the three SUPERBLINK-South targets described above, which are detailed in Section 3.5. Their TWA membership in light of these new data is discussed in Section 4.5. The full SUPERBLINK-south catalog will be presented in S. Lépine et al. (in preparation).

#### 2.4. A Re-Analysis of Hipparcos

A re-analysis of the Hipparcos catalog was performed to identify any missing bright members of TWA. In a first step, the proper motions and distances of all entries were used to identify candidate members with a TWA BANYAN II probability above 90%. The resulting 17 objects were then parsed to gather existing radial velocity measurements to refine the BANYAN II membership probability. The candidate members that were identified in this way are listed in Table 2. Four of these are known members of TWA (TWA 1, TWA 4, TWA 9

and TWA 11). Nine remaining objects have kinematics that are possibly consistent with TWA, although not all of them have radial velocity measurements. In the remainder of this section, we discuss each of these targets individually, to determine whether their global characteristics are consistent with membership to TWA.

**HIP 50032** is a moderately active ( $\log R'_{HK} = -4.38$ ; [Isaacson & Fischer 2010](#)) star with a low lithium abundance ( $\text{EW}(\lambda 6707) = 30 \text{ m}\text{\AA}$ ) compared to pre-main sequence K-type stars ([Tachihara et al. 2003](#)). Its absolute magnitude ( $M_V = 5.93$ ) calculated using its Hipparcos parallax ([van Leeuwen 2007a](#)) is consistent with a main sequence star. Its chromospheric activity, coronal X-ray emission ( $\log L_X/L_{\text{bol}} \simeq -4.5$ ), lithium abundance, and HR diagram position are all consistent with it being a Hyades-age interloper unrelated to TWA.

**HIP 52776** is a K4.5 V(k) star of modest chromospheric activity ( $\log R'_{HK} = -4.45$ ; [Gray et al. 2006](#)). Its lack of detectable lithium ( $A(\text{Li}) < 0.31$ ; [Delgado Mena et al. 2015](#)) suggests an age older than that of the Pleiades ( $\sim 120 \text{ Myr}$ ; [Stauffer et al. 1998](#)). It is a wide ( $234''$ ) companion to HIP 52787, a K1 V(k) star of similarly modest chromospheric activity ( $\log R'_{HK} = -4.42$ ; [Gray et al. 2006](#)) and detectable Li ( $\text{EW}(\lambda 6707) = 110 \text{ m}\text{\AA}$ ; [Torres et al. 2006a](#)), similar to that of  $\sim 0.2$ –

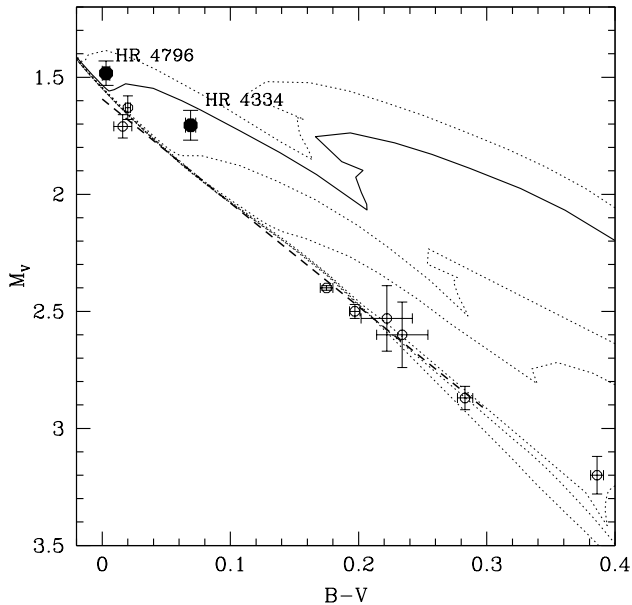


**Figure 1.** Color-magnitude diagram for young A-type stars. The filled circles are HIP 54477 (HR 4334) and TWA 11 (HR 4796). The open circles are six A-type members of the  $\beta$  Pictoris Moving Group from Mamajek & Bell (2014; age  $23 \pm 3$  Myr). Isochrones from the MIST/MESA tracks of Choi et al. (2016) are shown, ranging in age from 7–25 Myr ( $\log(\text{age}/\text{yr}) = 6.85, 6.9, 7.0, 7.1, 7.2, 7.3, 7.4$ ). The  $\log(\text{age}/\text{yr}) = 6.9$  isochrone (8 Myr) is drawn as a solid thick line. The thick dashed line is an empirical fit to the  $\beta$  Pictoris moving group stars ( $M_V = 1.594 + 4.431(B - V)$ ; between  $0.0 < B - V < 0.3$ ), and demonstrates that the Choi et al. (2016) solar metallicity isochrones do an excellent job fitting the  $\beta$  Pictoris zero age main sequence. Both HR 4796 and HR 4334 appear to be slightly pre-main sequence, as expected for  $\sim 7$ –10 Myr-old stars, thus HR 4334 has a color-magnitude position that is consistent with that expected for an A2V TWA member. See Section 2.4 for more information.

0.3 Gyr-old clusters such as M7, M34, and M35. The rotation period of HIP 52787 (6.579 days; Kiraga 2012) is consistent with a gyrochronological age of  $\sim 0.3$  Gyr using the calibration of Mamajek & Hillenbrand (2008), and its  $\log R'_{HK}$  is consistent with an age of  $\sim 0.4$  Gyr (Mamajek & Hillenbrand 2008). The absolute  $V$  magnitudes of HIP 52776 ( $M_V = 7.34$ ) and HIP 52787 ( $M_V = 5.70$ ), calculated using Hipparcos photometry and astrometry (ESA 1997; van Leeuwen 2007a), place both stars squarely on the main sequence. We conclude that the HIP 52776 + HIP 52787 pair are young ( $\sim 0.3$  Gyr) dwarf interlopers unrelated to TWA.

**HIP 54095** is a F2 V star according to Houk (1982), which translates to F3.5 V on the modern MK system (Pecaut & Mamajek 2016). David & Hillenbrand (2015) estimate an isochronal age in the  $1\sigma$  range 0.8–2.7 Gyr. It is detected in the *ROSAT* All-Sky Survey (Boller et al. 2016), however its X-ray luminosity is not particularly high for its bolometric luminosity

( $\log(L_X/L_{bol}) = -5.4$ ,  $\log L_X = 28.94$ ), and its X-ray emission is rather soft ( $\text{HR1} = -1.0$ ). There are multiple photometric metallicity estimates consistent with the star being slightly metal poor, with  $[\text{Fe}/\text{H}]$  in the range  $-0.28$  (Suchkov et al. 2003) to  $-0.15$  (Marsakov & Shevelev 1995). Most recently, Casagrande et al. (2011) estimate its metallicity at  $[\text{Fe}/\text{H}] = -0.19$  and  $[\text{M}/\text{H}] = -0.13$ , which would be at odds with that of young ( $< 10^8$  yr-old) stellar associations in the solar neighborhood. Its combination of effective temperature ( $T_{\text{eff}} = 6802$  K; Casagrande et al. 2011) and luminosity ( $\log L_{\odot} = 0.76$ ) would be consistent with a somewhat older pre-main sequence star ( $\sim 14$  Myr; see Fig. 6 of Pecaut et al. 2012 for comparison with F-type stars in the Sco-Cen subgroups), however the star seems to be somewhat under-luminous ( $\sim 0.2$  dex) if it were 10 Myr-old. There is currently no corroborating evidence to suggest that this star is coeval with TWA. It appears to be a slightly metal-poor main sequence early-type F dwarf.

**HIP 54477** (HR 4334) is a rapidly rotating A2 Vn star with  $v \sin i \simeq 230$  km s $^{-1}$  (Abt & Morrell 1995). The star was previously proposed as a candidate TWA member by Mamajek (2005, §2.5), but it was not assigned a TWA number<sup>2</sup>. In Figure 1, the color-magnitude position of HR 4334 is compared to HR 4796 (known TWA member; TWA 11) and six A-type members of the  $\sim 23$  Myr-old  $\beta$  Pictoris moving group from (Mamajek & Bell 2014, their Table 3). HR 4334 is consistent with being a  $9 \pm 1$  Myr-old pre-main sequence star just above the zero-age main sequence as defined empirically using the A-type  $\beta$  Pictoris members, and theoretically using the solar-composition MIST isochrones of Choi et al. (2016). The color-magnitude position of HR 4334 is located where one would predict an A2-type TWA member to lie. Since the kinematic properties of HIP 54477 are also a good match to those of TWA (its BANYAN II membership probability is 98.7% when distance and radial velocity are included), we suggest that it is a new bona fide member of TWA.

**HIP 54690** (CD-28 8704) is classified as a K5 V star by Uppgren et al. (1972). Although its kinematics match those of TWA members, its position on a  $V - J$  ( $1.96 \pm 0.03$ ; Egret et al. 1992; Skrutskie et al. 2006) versus  $M_V$  ( $7.1 \pm 0.2$ ) color-magnitude diagram is fully consistent with that of a main sequence star (e.g., see Bell et al. 2015, their Figure 10). A TWA-aged star with this  $V - J$  color would be expected to be at least 1 mag brighter. We conclude that HIP 54690 is an older

<sup>2</sup> HIP 54477 (as HD 96819) is accidentally listed with the age of the  $\beta$  Pictoris moving group ( $\sim 23$  Myr) in Table 1 of Meshkat et al. (2015) rather than the TWA group ( $\sim 10$  Myr).

interloper unrelated to TWA.

**HIP 55516** has been classified as a G8IV/V (Houk 1978) or G9 V (Lu 1982) star, and its absolute magnitude ( $M_V = 5.2 \pm 0.2$ ) calculated using its revised Hipparcos parallax of  $\varpi = 15.69 \pm 1.09$  mas (van Leeuwen 2007a) confirms its dwarf status. For its color ( $B - V = 0.76 \pm 0.02$ ; ESA 1997), a  $\sim 10$  Myr TWA member should have  $M_V \simeq 4.3$ , hence the star is a magnitude too faint to be a pre-main sequence TWA member. The star has not been detected in any X-ray surveys, nor has it been flagged as a variable star. Its predicted kinematic distance ( $\sim 42$  pc) based on its proper motion and the TWA velocity vector does not match its trigonometric parallax distance ( $\sim 64$  pc), despite its BANYAN II probability being high (99.8%). This apparent discrepancy between the two methods arises from the fact that HIP 55516 deviates from the mean  $UVW$  position of TWA members (by  $9 \pm 3$  km s $^{-1}$ ) in the direction where the BANYAN II model ellipsoid of TWA is most elongated. The isochrone mismatch precludes HIP 55516 from being as young as TWA, and we thus conclude that it is likely an older interloper star unrelated to TWA.

**HIP 58290** (HD 103840) is a G3 V star (Houk 1978), which on the modern MK system translates to approximately G1.5 V (Pecaut & Mamajek 2016). It has no X-ray detection in any reported survey, displays a low projected rotation ( $v \sin i = 2.7$  km s $^{-1}$ ; Nordström et al. 2004) and a dwarf surface gravity ( $\log g = 4.58$ ; Casagrande et al. 2011). The star has a low metallicity ( $[\text{Fe}/\text{H}] = -0.33$ ), which is corroborated by its intrinsic faintness ( $M_V = 5.22 \pm 0.07$ ), situating it  $\sim 0.6$  mag below the main sequence of Wright (2004, 2005) for its  $B - V$  color ( $0.61 \pm 0.01$ ). We conclude that HIP 58290 is an old, inactive, metal-poor interloper.

**HIP 59077** is classified as a G8/K0 V star by (Houk 1982), and has a wide, faint common proper motion companion  $56''$  away with colors consistent with a DA white dwarf (Hartkopf et al. 2013). HIP 59077 is slowly rotating ( $v \sin i = 1.8$  km s $^{-1}$  Głębocki & Gnaniński 2005) with an absolute magnitude  $M_V = 5.8 \pm 0.1$ , placing it near the main sequence. These indicators suggest that HIP 59077 is an older interloper unrelated to the  $\sim 10$  Myr-old TWA.

**HIP 59257** is a F6 V star (Houk 1978) that is listed by Hoogerwerf (2000) and Rizzuto et al. (2011) as a member of the  $\sim 16$  Myr-old (Mamajek et al. 2002) Lower Centaurus Crux (LCC) OB association. Its trigonometric distance of  $84.9 \pm 9.7$  pc would make it the furthest member of TWA, and is more consistent with a membership to LCC. It is likely that this star is thus an interloper from LCC that obtains a high Bayesian membership probability to TWA because no model of LCC is included in BANYAN II.

A detailed consideration of the properties of all new

Hipparcos candidate members that were uncovered in this section revealed them to be unrelated interlopers, with the exception of HIP 54477. A new assessment of its age based on the solar-composition MIST isochrones confirms that it is a bona fide member of TWA. After the completion of this survey for new members using Hipparcos data, the *Gaia* Data Release 1 (Lindgren et al. 2016) provided more precise trigonometric distances and proper motions for a number of targets detailed in this section. Although these new data did not affect the conclusions presented in this section, they are taken into account for refining membership probabilities in Section 5 where the list of TWA candidates and members is compiled.

### 3. OBSERVATIONS

Near-infrared and optical spectra of various resolutions were obtained at 5 facilities to measure the spectral types, spectroscopic indications of low-gravity (youth) and/or the radial velocity of TWA candidate members. The targets were selected for follow-up through a variety of heterogeneous surveys presented in Section 2 and were thus not selected in an optimal way from the final list of TWA candidate members compiled in this work. Most targets were selected from the BASS, LP-BASS and PRE-BASS samples presented in Section 2.1, and the remaining targets were selected from the BASS-Ultracool and SUPERBLINK-south surveys detailed in Sections 2.2 and 2.3. The observations are described in this section, and a detailed observing log is displayed in Table 3. The new spectra detailed in this section are presented in Appendix A.

#### 3.1. FIRE at Magellan/Baade

Three low- and ten mid-resolution near-infrared spectra were obtained for 9 TWA candidate members from 2013 December to 2016 February with the Folded-port InfraRed Echelle (FIRE; Simcoe et al. 2008, 2013) at the Magellan/Baade telescope. The  $0''.6$  slit was used in all cases, either in the high-throughput prism mode (resolving power of  $R \sim 450$ ) or in the high-resolution echelle mode ( $R \sim 6000$ ), both providing a wavelength coverage of  $0.8\text{--}2.45 \mu\text{m}$ . The data were obtained in an ABBA nodding pattern along the slit with two to six exposures of 500 to 900 s (echelle), or 8 exposures of 40 to 80 s (prism). This yielded signal-to-noise ratios per pixel of 40 or more, except in one observation at high airmass and with rapidly degrading seeing (2MASS 11472421–2040204 on 2016 January 23). A0-type spectral standards were obtained immediately after each science target at a similar airmass to ensure a proper telluric absorption correction.

Several high- and low-voltage internal flat fields were obtained at the beginning of every night, as well as ex-

**Table 2.** Candidate Members of TWA from Hipparcos

HIP Number	Other Names	Spectral Type	RA (hh:mm:ss.sss)	DEC (dd:mm:ss.ss)	$\mu_{\alpha} \cos \delta$ (mas yr <sup>-1</sup> )	$\mu_{\delta}$ (mas yr <sup>-1</sup> )	Trig. Dist. (pc)
50032	HD 88656	K2 V	10:12:52.77748	-28:30:48.1785	-49.84 ± 0.75	-24.65 ± 0.86	42.7 ± 1.7
52776	BD-21 3153	K4.5 V(k)	10:47:25.38730	-22:17:12.1792	-126.1 ± 1.4	-30.3 ± 1.2	32.6 ± 1.5
52787	HD 93528	K0 V	10:47:31.15457	-22:20:52.9160	-124.0 ± 0.9	-28.2 ± 0.8	34.5 ± 1.0
53911	TWA 1	K6 Ve	11:01:51.90671	-34:42:17.0323	-66.2 ± 1.9	-13.9 ± 1.5	53.7 ± 6.2
54095	HD 96033	F3.5 V	11:04:07.38096	-40:18:30.9042	-51.2 ± 0.6	-9.1 ± 0.4	81.8 ± 4.2
54477	HR 4334	A2 Vn	11:08:43.99954	-28:04:50.4127	-72.8 ± 0.4	-22.2 ± 0.5	55.7 ± 1.6
54690	CD-28 8704	K5 V	11:11:47.10817	-29:27:04.1717	-101.2 ± 1.7	-37.8 ± 1.5	47.8 ± 4.7
55505	TWA 4; HD 98800	K4 V	11:22:05.28975	-24:46:39.7571	-85.4 ± 1.7	-33.1 ± 2.1	44.9 ± 4.7
55516	HD 98870	G8 IV/V	11:22:14.75215	-48:56:43.3480	-88.8 ± 0.8	-15.5 ± 0.8	63.7 ± 4.4
57589	TWA 9	K7 IVe + M1	11:48:24.22320	-37:28:49.1537	-52.4 ± 2.4	-22.9 ± 1.7	46.8 ± 5.4
58290	HD 103840	G1.5 V	11:57:15.65407	-48:44:36.6582	-106.7 ± 0.6	-18.5 ± 0.6	38.6 ± 1.3
58363	HD 103933	F5 V	11:58:03.66897	-31:39:03.3795	-92.6 ± 0.6	-37.1 ± 0.3	57.2 ± 1.6
59077	HD 105227	G8/K0 V	12:06:54.69914	-38:06:23.2107	-82.8 ± 1.1	-45.5 ± 0.9	51.4 ± 3.3
59257	HD 105577	F6 V	12:09:20.45154	-42:50:18.4649	-47.0 ± 0.5	-10.0 ± 0.4	87.3 ± 4.6
60239	HD 107434	F6 V	12:21:09.57045	-38:18:09.8071	-55.6 ± 0.7	-20.1 ± 0.5	67.2 ± 3.2
61327	HD 109296	F8	12:33:55.44130	-48:36:05.2101	-63.3 ± 1.0	-24.1 ± 1.2	84.9 ± 9.7
61498	TWA 11; HR 4796	A0 V	12:36:01.03100	-39:52:10.2270	-56.7 ± 0.3	-25.0 ± 0.2	72.8 ± 1.8

HIP Number	RV (km s <sup>-1</sup> )	Ref.	Bayesian Prob. (%) <sup>a</sup>	$B - V$ (mag)	$M_V$ (mag)	Consistent Age? <sup>b</sup>	Membership <sup>c</sup>
50032	8.2 ± 0.2	(1)	96.7	0.88 ± 0.02	5.93 ± 0.09	N	R
52776	...	...	99.9	1.16 ± 0.02	7.3 ± 0.1	N	R
52787	23.4 ± 1.7	(2)	0.0	0.83 ± 0.02	5.70 ± 0.06	...	R
53911	13.4 ± 0.8	(3)	> 99.9	0.7 ± 0.1	7.3 ± 0.3	...	K
54095	...	...	99.8	0.369 ± 0.009	2.9 ± 0.1	N	R
54477	16 ± 5	(4)	98.7	0.069 ± 0.004	1.70 ± 0.06	Y	BF
54690	...	...	99.9	1.10 ± 0.02	7.1 ± 0.2	N	R
55505	9 ± 1	(3)	> 99.9	1.15 ± 0.04	5.6 ± 0.2	...	K
55516	14.1 ± 0.3	(5)	99.8	0.76 ± 0.02	5.3 ± 0.2	N	R
57589	9.5 ± 0.4	(3)	99.9	1.6 ± 0.4	7.8 ± 0.3	...	K
58290	7.9 ± 0.3	(5)	97.1	0.61 ± 0.01	5.22 ± 0.07	N	R
58363	15.2 ± 0.3	(4)	8.2	0.478 ± 0.008	3.30 ± 0.06	...	R
59077	10.1 ± 0.4	(5)	> 99.9	0.77 ± 0.03	5.8 ± 0.1	N	R
59257	3.8 ± 0.3	(5)	99.2	0.532 ± 0.003	3.2 ± 0.1	N	R
60239	-10.2 ± 0.3	(5)	0.0	0.54 ± 0.02	4.0 ± 0.1	...	R
61327	-8.0 ± 1.1	(6)	0.0	0.61 ± 0.03	4.8 ± 0.3	...	R
61498	7 ± 1	(5)	> 99.9	0.003 ± 0.003	1.47 ± 0.05	...	K

<sup>a</sup>Bayesian probability including all available measurements in the literature (position, proper motion, trigonometric distance and radial velocity when available).

<sup>b</sup>This Yes/No flag indicates whether the general properties of this object are consistent with the age of TWA (~10 Myr). Only the 9 stars with a high Bayesian membership probability that were not previously known as TWA members were investigated.

<sup>c</sup>K: Known member, R: Rejected, BF: New bona fide member.

NOTE—See Section 2.4 for more details.

**References**—(1) Chubak & Marcy 2011, (2) Jenkins et al. 2011, (3) Torres et al. 2006b, (4) Kharchenko et al. 2007, (5) Gontcharov 2006a, (6) Bilir et al. 2005.



ternal dome flats, which are used to build the slit illumination function. Several NeAr wavelength calibration lamps were obtained at the beginning of the night for the prism mode, whereas a single ThAr calibration lamp exposure was obtained after every target and telluric standard in echelle mode. The data were reduced with the Interactive Data Language (IDL) Firehose v2.0 package (Bochanski et al. 2009; Gagné et al. 2015c<sup>3</sup>; see Gagné et al. 2015d for more details on this reduction package).

### 3.2. GMOS at GEMINI-S and GEMINI-N

Optical spectra were obtained with GMOS (Hook et al. 2004) in queue mode at the Gemini-North and Gemini-South telescopes for 21 TWA candidate members from 2012 December to 2014 April. The R400 grating with a central wavelength setting of 800 nm were used with the OG515 filter and the 1'0 or 0'75 slits to obtain resolving powers of  $R \sim 950$  or  $R \sim 1250$  covering  $\sim 5900\text{--}10100\text{ \AA}$ . Four exposures of 45–1500 s were obtained to achieve signal-to-noise ratios of  $\sim 30\text{--}250$  per pixel on the science targets. The two first science exposures were obtained with a central wavelength of 800 nm, followed by a single flat-field exposure under the same settings. An additional flat exposure and the remaining two science exposures were obtained with a central wavelength of 805 nm. This ensures that the gaps between individual detectors do not result in gaps in the wavelength coverage of the final science spectra. Two CuAr lamp exposures were typically obtained at the end of each night, one for each central wavelength setting. The standard white dwarfs or bright stars G 191–2 B, LTT 2415, LTT 4816, CD–32 9927 were observed once per semester with each setting, as part of the regular Gemini calibrations and to correct for instrumental response. In most cases, only the central spectrum region was read on the detector to reduce readout time.

A single 10 s *i*- or *r*-band acquisition image was obtained before each target observation, followed by a single 20 s acquisition exposure with the slit on that was used to verify whether the target is a visual binary. In such cases, the position angle was adjusted to place both components within the slit.

The data were reduced with a custom IDL pipeline, which applies bias and flat field corrections, straightens the spectral traces, flags and ignores bad pixels, extracts the spectra on each detector separately using a 1D Moffat profile (Moffat 1969), performs wavelength calibration using the CuAr lamps and combines the spectra from individual detectors. Individual exposures are

then combined and corrected for instrumental response using the Gemini spectral standards. Six visual binaries were flagged from a visual inspection of the acquisition images, and extracted with a special algorithm that fits two Moffat profiles at every spectral position, yielding two individual spectra for the respective binary components.

The spectra that were reduced with the standards CD–32 9927 and G 191–2 B initially suffered from slope systematics at  $\gtrsim 850\text{ nm}$ . A correction to these systematics was developed for each standard star: this was done by calculating the ratio of each observed spectrum to that of a template M-type dwarf of the same spectral type and surface gravity that was re-sampled at the same resolution as the data. A linear polynomial was fit to the median of all slope corrections as a function of wavelength for the science targets that were observed with a given standard star, which was subsequently divided to the science spectra.

### 3.3. SPEX at IRTF

Low-resolution NIR spectra with a wavelength coverage of  $0.8\text{--}2.45\text{ }\mu\text{m}$  were obtained for 2 TWA candidate members with SpeX (Rayner et al. 2003) at the IRTF telescope on 2015 December 6. The 0'5 slit was used with the prism mode, yielding a resolving power of  $R \sim 120$ . Four to eight exposures of 180 s were obtained in an ABBA nodding pattern along the slit which yielded signal-to-noise ratios of  $\sim 20$  per pixel. This was followed by a standard SpeX calibration sequence consisting of 5 flat field exposures and 2 arc lamp exposures. The A0-type standard stars HD 79752 and HD 91398 were observed immediately after the science targets and at a similar airmass to correct for telluric absorption and instrument response. The data were reduced using the IDL SpeXTool v4.0 beta package<sup>4</sup> (Vacca et al. 2003; Cushing et al. 2004).

### 3.4. Flamingos-2 at GEMINI-S

Low-resolution NIR spectra were obtained with Flamingos-2 (Eikenberry et al. 2004) at Gemini-South in queue mode for 2 TWA candidate members, in 2015 April. The JH grism was used with the 0'72 slit, providing a resolving power of  $R \sim 500$  across  $0.9\text{--}1.73\text{ }\mu\text{m}$ . Sixteen to 36 exposures of 120 s were obtained, which yielded signal-to-noise ratios above 100 per pixel – these large numbers of exposures are required to correct for Flamingos-2 systematics such as fringing, which can otherwise artificially affect the spectral morphology. The A0-type spectral standards HD 92699 and HD 105764 were observed immediately after science target expo-

<sup>3</sup> Available at [https://github.com/jgagneastro/FireHose\\_v2/tree/v2.0](https://github.com/jgagneastro/FireHose_v2/tree/v2.0)

<sup>4</sup> Available at <http://irtfweb.ifa.hawaii.edu/~spex/>

tures and at a similar airmass to provide a correction for telluric absorption. Standard Flamings-2 calibrations (darks, flat fields and Ar wavelength calibration lamps) were obtained at the end of every night.

The data were reduced using the Red Flamings IDL pipeline<sup>5</sup> (see Gagné et al. 2015d for details). This pipeline performs spectral extraction, applies standard calibrations and corrects instrumental fringing.

**Table 3.** Log of Observations

2MASS Designation	UT Date	Slit (")	$T_{\text{Exp}}$ (s)	$N_{\text{Exp}}$	S/N	Standard Star	Input <sup>a</sup>
<b>Magellan/Baade FIRE, Echelle</b>							
08254335-0029110	131213	0.6	1310	2	65	HIP 35837	1
09553336-0208403	160123	0.6	5400	6	55	HD 79359	2
11020983-3430355	140512	0.6	1200	2	225	HIP 54890	1
11472421-2040204	160223	0.6	5454	6	40	HIP 61830	2
11472421-2040204	160123	0.6	5400	6	15 <sup>b</sup>	HD 79359	2
11480096-2836488	150531	0.6	3600	4	50	HIP 59351	1
12074836-3900043	151222	0.6	2400	4	95	HD 104647	1
12451416-4429077	160223	0.6	1816	4	120	HIP 70402	3
12563961-2718455	140512	0.6	1800	2	10	HD 116699	1
14112131-2119503	140512	0.6	1000	2	230	HIP 69639	1
<b>Magellan/Baade FIRE, Prism</b>							
11063147-4201251	160122	0.6	320	8	140	HD 102338	2
11472421-2040204	160122	0.6	640	8	70	HD 105992	2
12194846-3232059	160122	0.6	320	8	80	HD 102338	2
<b>IRTF SpeX, Prism</b>							
09553336-0208403	151206	0.5	1440	8	20	HD 79752	2
10212570-2830427	151206	0.5	720	4	20	HD 91398	1
<b>Gemini-South Flamings-2, JH grism</b>							
11034950-3409445	150426	0.72	1920	16	500	HD 92699	1
12451035-1443029	150427	0.72	4320	36	400	HD 105764	1
<b>CFHT, ESPaDOnS, Echelle</b>							
10190109-2646336	160421	...	1800	2	35	...	1
10284580-2830374	160418	...	1800	2	50	...	1
10585054-2346206	160124	...	1600	2	65	...	4
10585054-2346206	160611	...	1800	1	75	...	4
11023986-2507113	160421	...	1500	1	50	...	1
11152992-2954436	160421	...	1800	2	30	...	1
11382693-3843138	160612	...	1800	2	30	...	1
11393382-3040002	160421	...	1460	1	85	...	1
11423628-3859108	160516	...	1800	2	15	...	1
12000160-1731308	160115	...	500	1	65	...	4
12073145-3310222	160612	...	1790	1	50	...	5
12175920-3734433	160516	...	1800	2	20	...	1

Table 3 continued

<sup>5</sup> Available at [https://github.com/jgagneastro/red\\_flamings](https://github.com/jgagneastro/red_flamings)

Table 3 (continued)

2MASS Designation	UT Date	Slit (")	$T_{\text{Exp}}$ (s)	$N_{\text{Exp}}$	S/N	Standard Star	Input <sup>a</sup>
<b>Gemini-South and North GMOS, OG515/R400</b>							
08141769+0253199	130212	0.75	1120	4	115	G 191-2 B	1
08144321+2336045	140216	1.0	256	4	100	G 191-2 B	1
09512673-2220196	121205	0.75	1520	4	60	LTT 2415	1
10144705-3728151	140219	1.0	180	4	30	LTT 4816	1
10284580-2830374	130207	0.75	400	4	60	CD-32 9927	1
10455263-2819303	130208	0.75	6000	4	45	CD-32 9927	1
10542303-1507082	121208	0.75	360	4	20	LTT 2415	1
10585054-2346206	121210	0.75	400	4	70	LTT 2415	1
11112820-2655027	130206	0.75	400	4	95	CD-32 9927	1
11112984-2713320	130204	0.75	400	4	65	CD-32 9927	1
11195251-3917150	140312	1.0	188	4	35	LTT 4816	1
11504110-2356075	140412	1.0	1152	4	85	G 191-2 B	1
11532691-3015414	140412	1.0	440	4	115	G 191-2 B	1
12000160-1731308	140216	1.0	256	4	90	G 191-2 B	4
12041256+0514128	130303	0.75	600	4	250	G 191-2 B	1
12113180-3416537	140319	1.0	256	4	55	G 191-2 B	1
12175920-3734433	140221	1.0	180	4	35	LTT 4816	1
12214852-3652349	140412	1.0	256	4	20	G 191-2 B	1
12282569-3955014	130210	0.75	400	4	70	CD-32 9927	1
12421948-3805064	130207	0.75	400	4	70	CD-32 9927	1
12532702-3504151	140412	1.0	256	4	100	G 191-2 B	1

<sup>a</sup> 1: BASS survey (Gagné et al. 2015b), including the LP-BASS and PRE-BASS surveys (Gagné et al. 2015d); 2: BASS-Ultracool survey (see Section 2.2); 3: Looper (2011); 4: SUPERBLINK-south (S. Lépine et al., in preparation; see Section 2.3); 5: (Elliott et al. 2016)

<sup>b</sup> Poor weather conditions.

NOTE—See Section 3 for more details.

### 3.5. ESPaDOnS at CFHT

Two optical high-resolution spectra were obtained for 11 TWA candidates between 2016 January and June. The data were obtained in the Queue Service Observations (QSO) mode, using the ESPaDOnS optical high resolution spectropolarimeter (Donati et al. 2006) at the Canada-France-Hawaii Telescope (CFHT). The normal readout speed mode was used along with the *Star+Sky* mode, where a 1''6 optical fiber is placed on the science target and a 1''8 optical fiber is placed on the sky, which yielded a resolving power of  $R \sim 67\,000$  over 3670–10500 Å across 40 spectral orders. One or two exposures of 500–1800 s were used, resulting in signal-to-noise ratios of  $\sim 35$ –85 per pixel. The data were reduced by the QSO team using the Upena/Libre-Esprit pipeline (Donati et al. 1997).

## 4. DATA ANALYSIS

### 4.1. Spectral Typing

Spectral typing was performed using the method described by [Gagné et al. \(2015d\)](#) and K. Cruz et al. (submitted to AJ)<sup>6</sup>, i.e., the spectra were compared to templates built from a median combination of sets of previously established spectral standards. This was done within each of three separate bands ( $zJ$ ,  $H$  and  $K$ ) in the case of NIR spectra, or in the full 5900–10100 Å range in the case of optical spectra. Optical spectra that displayed  $H\alpha$  emission were flagged with the “e” suffix. The resulting spectral types are listed in Table 4.

The slope of all NIR spectra presented here were corrected using available photometry from 2MASS or the Vista Hemisphere Survey (VHS; PI McMahon, Cambridge, UK) to ensure that no systematic instrumental effects have affected them. The synthetic magnitudes of the spectra were calculated and compared to the measured values, and a linear relation was fitted to the synthetic-to-measured flux ratio as a function of the logarithm of wavelength. This relation was then used to correct the spectral data, such that deriving synthetic magnitudes from the corrected spectra yielded similar synthetic magnitudes as the 2MASS or VHS measurements. These corrections have only affected the FIRE data obtained in the prism mode.

#### 4.2. $H\alpha$ Emission

Young low-mass stars display enhanced  $H\alpha$  emission due to strong chromospheric activity, which persists for  $\sim 400$  Myr ([West et al. 2008](#)) and then for an additional  $\sim 6$ – $7$  Gyr in intermittence ([West et al. 2006, 2008](#); [Shkolnik et al. 2011](#); [Schmidt et al. 2015](#)). The presence of  $H\alpha$  emission at a given moment is thus not a strong indication of a very young age, however its absence can be used to constrain the age at  $\gtrsim 400$  Myr, and thus safely reject candidate members of TWA. There are 7 objects (spectral types M2–M5) in the GMOS data sample presented here that were rejected in this way. The  $H\alpha$  equivalent widths are listed in Table 4. There are no stars in the sample that display  $H\alpha$  strong enough to be classified as classical T Tauri stars, according to the criterion of [Barrado y Navascués & Martín \(2003\)](#); see their Table 1).

#### 4.3. Signs of Low Surface Gravity

Several spectral indices have been developed to identify signs of low surface gravity in the optical or near-infrared spectra of low-mass stars and brown dwarfs. In the optical, the equivalent width of the Na I (8183.3 and 8194.8 Å), K I (7665 and 7699 Å) and CrH (8611

and 9969 Å) absorption lines are known to be weaker in low-gravity atmospheres, due to the weaker effect of pressure broadening (e.g., [Kirkpatrick et al. 2006](#); [Cruz et al. 2009](#)). In the near-infrared, a similar effect is observed with the Na I (1.1396  $\mu\text{m}$ ), K I (1.1692, 1.7778, 1.2437 and 1.2529  $\mu\text{m}$ ) and FeH (0.998  $\mu\text{m}$ ) absorption lines ([Allers & Liu 2013](#)). In addition to this, the  $H$ -band continuum ( $\sim 1.5$ – $1.7$   $\mu\text{m}$ ) of low-gravity  $\geq M6$  dwarfs displays a typical triangular shape, which is a combined effect of decreased collision-induced absorption of the  $\text{H}_2$  molecule, and weaker absorption from the FeH molecule at  $\sim 1.6$ – $1.7$   $\mu\text{m}$  ([Rice et al. 2010](#); [Allers & Liu 2013](#)). [Kirkpatrick \(2005\)](#) and [Kirkpatrick et al. \(2006\)](#) have introduced the spectral typing suffixes  $\alpha$ ,  $\beta$  and  $\gamma$  to identify M and L dwarf with normal gravity, subtle signs of low gravity and strong signs of low gravity, respectively (see also [Cruz et al. 2009](#)).

The gravity-sensitive indices defined by [Kirkpatrick et al. \(1999\)](#) and [Cruz et al. \(2009\)](#) for the new GMOS data are presented in Table 4. In Figure 2, the optical indices derived from the GMOS data are compared with a field sequence, and with spectral indices of known giants and young ( $\leq 3$  Myr) dwarfs. Six objects display clear signs of low gravity in all of the sequences, and are thus assigned the  $\gamma$  suffix. All other 12 targets with spectral types  $\geq M4$  display spectral indices that are fully consistent with a field age, and are thus rejected as candidate members of TWA. None of the objects display ambiguous signs of low gravity that would justify the assignment of a  $\beta$  suffix. It can be seen that the sequences of field and young dwarfs merge at spectral types earlier than M4, and for this reason it is not possible to draw any conclusion regarding the age of the 9 targets that fall in this range using these low-gravity sensitive indices.

In the near-infrared, the gravity-sensitive spectral indices have been combined by [Allers & Liu \(2013\)](#) in a classification scheme that allows to assign a gravity class to  $R \sim 120$ – $1200$  spectra. The three possible gravity classes are field-gravity (FLD-G), intermediate-gravity (INT-G) and very low-gravity (VL-G), and have been shown to correspond age ranges that are similar to the  $\alpha$ ,  $\beta$  and  $\gamma$  suffixes described above. [Gagné et al. \(2015d\)](#) have also defined distinct NIR spectral templates for the three gravity classes that allow for a gravity classification based on a visual comparison, as described in Section 4.1.

There are 3 late-M targets for which new NIR data is presented in this work. Their names and respective spectral types, gravity classifications, and gravity scores are: 2MASS J12194846–3232059 (M7 FLD-G; score 0n00); 2MASS J11063147–4201251 (M8 FLD-G; score 0n00); and 2MASS J11034950–3409445 (M9 INT-G; score 1n10; see [Allers & Liu 2013](#) for a detailed de-

<sup>6</sup> See also <https://dx.doi.org/10.6084/m9.figshare.923587.v1> and [https://github.com/kelle/NIRTemplates\\_Manuscript/releases/tag/v1](https://github.com/kelle/NIRTemplates_Manuscript/releases/tag/v1)

Table 4. GMOS Optical Spectral Types and Indices

2MASS Designation	Opt. SpT <sup>a</sup>	Effect on Membership <sup>b</sup>	EW(H $\alpha$ ) (Å)	Cruz et al. (2009)		Kirkpatrick et al. (1999)	
				K-a	K-b	Na-a	Na-b
08141769+0253199	M5 e	LM $\rightarrow$ R	6.3 $\pm$ 0.4	2.27 $\pm$ 0.02	2.16 $\pm$ 0.02	1.21 $\pm$ 0.01	1.35 $\pm$ 0.01
08144321+2336045	M4 e	LM $\rightarrow$ R	8.0 $\pm$ 0.3	2.00 $\pm$ 0.01	1.80 $\pm$ 0.01	1.16 $\pm$ 0.01	1.14 $\pm$ 0.01
09512673-2220196 A	M5	CM $\rightarrow$ R	...	1.98 $\pm$ 0.02	1.83 $\pm$ 0.02	1.23 $\pm$ 0.02	1.33 $\pm$ 0.03
09512673-2220196 B	M5	CM $\rightarrow$ R	...	1.98 $\pm$ 0.02	1.81 $\pm$ 0.01	1.23 $\pm$ 0.03	1.33 $\pm$ 0.03
10144705-3728151 A	M3 pec	CM $\rightarrow$ R	...	1.61 $\pm$ 0.04	1.47 $\pm$ 0.04	1.13 $\pm$ 0.02	1.18 $\pm$ 0.03
10144705-3728151 B	M3 pec	CM $\rightarrow$ R	...	1.65 $\pm$ 0.05	1.46 $\pm$ 0.04	1.13 $\pm$ 0.02	1.18 $\pm$ 0.03
10284580-2830374	M5 $\gamma$ e	CM $\rightarrow$ CM	7.2 $\pm$ 0.6	2.26 $\pm$ 0.01	2.17 $\pm$ 0.01	1.12 $\pm$ 0.01	1.13 $\pm$ 0.01
10455263-2819303	M5.5 $\gamma$ e	CM $\rightarrow$ CM	5.8 $\pm$ 0.7	2.69 $\pm$ 0.01	2.44 $\pm$ 0.01	1.09 $\pm$ 0.01	1.21 $\pm$ 0.01
10542303-1507082	M5.5 e	CM $\rightarrow$ R	5.9 $\pm$ 0.6	2.38 $\pm$ 0.02	2.06 $\pm$ 0.02	1.23 $\pm$ 0.03	1.34 $\pm$ 0.03
10585054-2346206	M6 $\gamma$ e	CM $\rightarrow$ CM	8.4 $\pm$ 0.5	2.30 $\pm$ 0.01	2.09 $\pm$ 0.01	1.09 $\pm$ 0.01	1.16 $\pm$ 0.01
11112820-2655027	M6 $\gamma$ e	CM $\rightarrow$ CM	16.2 $\pm$ 0.8	2.70 $\pm$ 0.01	2.50 $\pm$ 0.01	1.10 $\pm$ 0.01	1.16 $\pm$ 0.01
11112984-2713320	M4.5 e	CM $\rightarrow$ R	3.7 $\pm$ 0.4	2.33 $\pm$ 0.02	2.09 $\pm$ 0.02	1.21 $\pm$ 0.01	1.29 $\pm$ 0.01
11195251-3917150 A	M2	CM $\rightarrow$ R	...	1.49 $\pm$ 0.01	1.38 $\pm$ 0.01	1.14 $\pm$ 0.02	1.17 $\pm$ 0.02
11195251-3917150 B	M2	CM $\rightarrow$ R	...	1.48 $\pm$ 0.01	1.34 $\pm$ 0.01	1.11 $\pm$ 0.01	1.15 $\pm$ 0.01
11504110-2356075	M6 e	R $\rightarrow$ R	3.2 $\pm$ 0.3	3.05 $\pm$ 0.03	2.62 $\pm$ 0.02	1.34 $\pm$ 0.01	1.47 $\pm$ 0.01
11532691-3015414	M4.5 e	R $\rightarrow$ R	2.0 $\pm$ 0.3	2.16 $\pm$ 0.01	1.94 $\pm$ 0.01	1.24 $\pm$ 0.01	1.33 $\pm$ 0.01
12000160-1731308 AB	M4 $\gamma$ e	LM $\rightarrow$ LM	3.9 $\pm$ 0.3	1.88 $\pm$ 0.01	1.74 $\pm$ 0.01	1.03 $\pm$ 0.01	1.06 $\pm$ 0.01
12041256+0514128	M5 e	R $\rightarrow$ R	9.6 $\pm$ 0.4	2.42 $\pm$ 0.01	2.28 $\pm$ 0.01	1.26 $\pm$ 0.01	1.39 $\pm$ 0.01
12113180-3416537	M2	CM $\rightarrow$ R	...	1.41 $\pm$ 0.01	1.26 $\pm$ 0.01	1.15 $\pm$ 0.01	1.20 $\pm$ 0.01
12175920-3734433	M5 $\gamma$ e	CM $\rightarrow$ CM	7.4 $\pm$ 0.6	2.53 $\pm$ 0.02	2.28 $\pm$ 0.02	1.10 $\pm$ 0.02	1.19 $\pm$ 0.02
12214852-3652349 A	M4 e	CM $\rightarrow$ R	5.6 $\pm$ 1.9	1.94 $\pm$ 0.09	1.74 $\pm$ 0.08	1.22 $\pm$ 0.02	1.30 $\pm$ 0.02
12214852-3652349 B	M4 e	CM $\rightarrow$ R	5.4 $\pm$ 1.7	1.96 $\pm$ 0.09	1.79 $\pm$ 0.08	1.22 $\pm$ 0.03	1.30 $\pm$ 0.03
12282569-3955014 A	M4 e	CM $\rightarrow$ R	5.2 $\pm$ 0.3	1.91 $\pm$ 0.01	1.68 $\pm$ 0.01	1.19 $\pm$ 0.01	1.25 $\pm$ 0.01
12282569-3955014 B	M3.5 e	CM $\rightarrow$ CM	5.0 $\pm$ 0.3	1.91 $\pm$ 0.01	1.68 $\pm$ 0.01	1.20 $\pm$ 0.01	1.24 $\pm$ 0.01
12421948-3805064 A	M3 e	LM $\rightarrow$ LM	3.2 $\pm$ 0.3	1.85 $\pm$ 0.01	1.65 $\pm$ 0.01	1.22 $\pm$ 0.01	1.28 $\pm$ 0.01
12421948-3805064 B	M3 e	LM $\rightarrow$ LM	3.4 $\pm$ 0.3	1.86 $\pm$ 0.01	1.64 $\pm$ 0.01	1.21 $\pm$ 0.01	1.25 $\pm$ 0.01
12532702-3504151	M3 e	CM $\rightarrow$ CM	4.5 $\pm$ 0.2	1.56 $\pm$ 0.01	1.43 $\pm$ 0.01	1.11 $\pm$ 0.01	1.18 $\pm$ 0.01

2MASS Designation	Kirkpatrick et al. (1999)							
	Rb-a	Rb-b	Cs-a	Cs-b	CrH-a	CrH-b	FeH-a	FeH-b
08141769+0253199	1.09 $\pm$ 0.01	1.04 $\pm$ 0.01	1.04 $\pm$ 0.01	1.02 $\pm$ 0.01	0.97 $\pm$ 0.01	1.03 $\pm$ 0.01	0.97 $\pm$ 0.01	1.30 $\pm$ 0.01
08144321+2336045	0.97 $\pm$ 0.01	1.04 $\pm$ 0.01	0.99 $\pm$ 0.01	1.01 $\pm$ 0.01	0.99 $\pm$ 0.01	1.02 $\pm$ 0.01	0.98 $\pm$ 0.01	1.20 $\pm$ 0.01
09512673-2220196 A	1.04 $\pm$ 0.01	1.05 $\pm$ 0.01	1.03 $\pm$ 0.01	1.02 $\pm$ 0.02	0.92 $\pm$ 0.01	0.97 $\pm$ 0.03	0.95 $\pm$ 0.01	1.09 $\pm$ 0.04
09512673-2220196 B	1.05 $\pm$ 0.01	1.05 $\pm$ 0.01	1.03 $\pm$ 0.01	1.02 $\pm$ 0.01	0.92 $\pm$ 0.01	0.99 $\pm$ 0.03	0.96 $\pm$ 0.01	1.09 $\pm$ 0.04
10144705-3728151 A	0.98 $\pm$ 0.03	1.04 $\pm$ 0.01	0.96 $\pm$ 0.01	0.99 $\pm$ 0.02	0.97 $\pm$ 0.01	...	0.98 $\pm$ 0.02	1.24 $\pm$ 0.05
10144705-3728151 B	0.98 $\pm$ 0.02	1.04 $\pm$ 0.01	0.97 $\pm$ 0.01	0.98 $\pm$ 0.02	0.96 $\pm$ 0.01	...	0.97 $\pm$ 0.02	1.27 $\pm$ 0.05
10284580-2830374	1.07 $\pm$ 0.01	1.01 $\pm$ 0.01	1.07 $\pm$ 0.01	1.01 $\pm$ 0.01	0.88 $\pm$ 0.01	0.96 $\pm$ 0.01	0.97 $\pm$ 0.01	1.14 $\pm$ 0.01
10455263-2819303	1.02 $\pm$ 0.01	1.06 $\pm$ 0.01	1.05 $\pm$ 0.01	1.01 $\pm$ 0.01	0.91 $\pm$ 0.01	0.99 $\pm$ 0.02	0.96 $\pm$ 0.01	1.13 $\pm$ 0.03
10542303-1507082	1.04 $\pm$ 0.01	1.05 $\pm$ 0.02	1.05 $\pm$ 0.02	1.01 $\pm$ 0.02	0.95 $\pm$ 0.02	1.00 $\pm$ 0.02	0.96 $\pm$ 0.02	1.23 $\pm$ 0.02
10585054-2346206	1.01 $\pm$ 0.01	1.08 $\pm$ 0.01	1.06 $\pm$ 0.01	1.04 $\pm$ 0.02	0.89 $\pm$ 0.01	1.01 $\pm$ 0.02	0.96 $\pm$ 0.01	1.17 $\pm$ 0.02
11112820-2655027	1.05 $\pm$ 0.01	1.05 $\pm$ 0.01	1.12 $\pm$ 0.01	1.05 $\pm$ 0.01	0.90 $\pm$ 0.01	0.97 $\pm$ 0.01	0.98 $\pm$ 0.01	1.17 $\pm$ 0.01
11112984-2713320	0.98 $\pm$ 0.01	1.06 $\pm$ 0.01	1.00 $\pm$ 0.01	1.00 $\pm$ 0.01	0.95 $\pm$ 0.01	1.03 $\pm$ 0.02	0.99 $\pm$ 0.01	1.18 $\pm$ 0.02
11195251-3917150 A	1.00 $\pm$ 0.01	1.04 $\pm$ 0.01	0.94 $\pm$ 0.01	1.00 $\pm$ 0.02	0.95 $\pm$ 0.01	...	0.97 $\pm$ 0.01	1.13 $\pm$ 0.04
11195251-3917150 B	1.00 $\pm$ 0.01	1.05 $\pm$ 0.01	0.93 $\pm$ 0.01	1.00 $\pm$ 0.01	0.98 $\pm$ 0.01	...	0.97 $\pm$ 0.01	1.21 $\pm$ 0.02
11504110-2356075	1.08 $\pm$ 0.01	1.04 $\pm$ 0.01	1.07 $\pm$ 0.01	1.02 $\pm$ 0.01	0.98 $\pm$ 0.01	1.04 $\pm$ 0.01	1.04 $\pm$ 0.01	1.37 $\pm$ 0.01
11532691-3015414	1.06 $\pm$ 0.01	1.03 $\pm$ 0.01	1.03 $\pm$ 0.01	1.00 $\pm$ 0.01	0.99 $\pm$ 0.01	1.03 $\pm$ 0.01	0.95 $\pm$ 0.01	1.24 $\pm$ 0.01
12000160-1731308 AB	0.97 $\pm$ 0.01	1.02 $\pm$ 0.01	0.99 $\pm$ 0.01	1.01 $\pm$ 0.01	0.96 $\pm$ 0.01	1.02 $\pm$ 0.01	0.97 $\pm$ 0.01	1.13 $\pm$ 0.01
12041256+0514128	1.07 $\pm$ 0.01	1.05 $\pm$ 0.01	1.05 $\pm$ 0.01	1.03 $\pm$ 0.01	0.98 $\pm$ 0.01	1.02 $\pm$ 0.01	1.00 $\pm$ 0.01	1.32 $\pm$ 0.01
12113180-3416537	1.01 $\pm$ 0.01	1.04 $\pm$ 0.01	0.92 $\pm$ 0.01	1.00 $\pm$ 0.01	0.99 $\pm$ 0.01	1.02 $\pm$ 0.01	0.94 $\pm$ 0.02	1.08 $\pm$ 0.01
12175920-3734433	0.98 $\pm$ 0.01	1.08 $\pm$ 0.01	1.04 $\pm$ 0.01	1.05 $\pm$ 0.02	0.88 $\pm$ 0.01	...	1.00 $\pm$ 0.01	1.35 $\pm$ 0.04
12214852-3652349 A	1.07 $\pm$ 0.04	1.04 $\pm$ 0.02	1.02 $\pm$ 0.01	1.01 $\pm$ 0.01	0.98 $\pm$ 0.01	1.01 $\pm$ 0.02	0.89 $\pm$ 0.01	1.21 $\pm$ 0.03
12214852-3652349 B	1.06 $\pm$ 0.04	1.03 $\pm$ 0.03	1.01 $\pm$ 0.01	1.01 $\pm$ 0.01	0.98 $\pm$ 0.01	1.00 $\pm$ 0.03	0.95 $\pm$ 0.01	1.22 $\pm$ 0.04
12282569-3955014 A	1.00 $\pm$ 0.01	1.04 $\pm$ 0.01	0.97 $\pm$ 0.01	1.01 $\pm$ 0.01	0.99 $\pm$ 0.01	1.01 $\pm$ 0.02	1.00 $\pm$ 0.01	1.15 $\pm$ 0.01
12282569-3955014 B	1.01 $\pm$ 0.01	1.04 $\pm$ 0.01	0.97 $\pm$ 0.01	1.01 $\pm$ 0.01	1.00 $\pm$ 0.01	0.98 $\pm$ 0.01	1.00 $\pm$ 0.01	1.14 $\pm$ 0.01
12421948-3805064 A	1.02 $\pm$ 0.01	1.03 $\pm$ 0.01	0.99 $\pm$ 0.01	0.97 $\pm$ 0.01	0.98 $\pm$ 0.01	0.95 $\pm$ 0.01	1.00 $\pm$ 0.01	1.12 $\pm$ 0.01
12421948-3805064 B	1.02 $\pm$ 0.01	1.02 $\pm$ 0.01	1.01 $\pm$ 0.01	1.00 $\pm$ 0.01	0.98 $\pm$ 0.01	0.95 $\pm$ 0.01	0.99 $\pm$ 0.01	1.12 $\pm$ 0.01
12532702-3504151	1.03 $\pm$ 0.01	1.03 $\pm$ 0.01	0.99 $\pm$ 0.01	1.00 $\pm$ 0.01	0.98 $\pm$ 0.01	1.01 $\pm$ 0.01	0.96 $\pm$ 0.01	1.13 $\pm$ 0.01

<sup>a</sup> Optical spectral type. “e” indicates H $\alpha$  emission,  $\gamma$  indicates a low surface gravity and “pec” indicates other peculiar features. See Section 4.1 for more details.<sup>b</sup> Previous membership status  $\rightarrow$  Updated membership status, based on the inclusion of new age constraints based on spectroscopic indices. See Section 4 for more detail. R: Rejected; LM: Low-likelihood candidate member; CM: Candidate member, HM: High-likelihood candidate member; BF: Bona fide member.



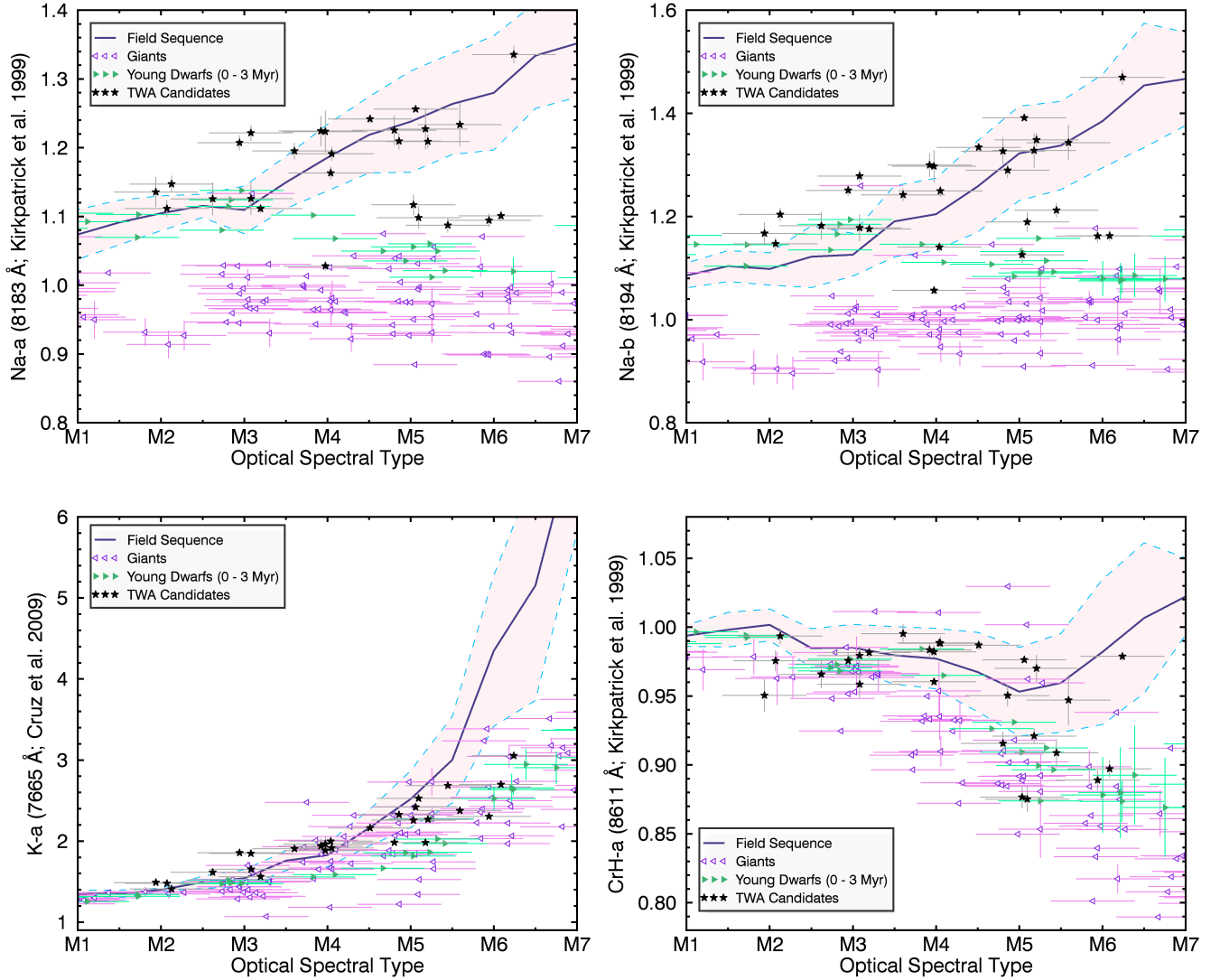


**Figure 2.** Gravity-sensitive spectral indices for giant stars (leftwards purple triangles), young ( $\leq 3$  Myr) dwarfs (rightwards green triangles) and new observations of TWA candidate members (black stars). A sequence of field-age dwarfs is displayed as a thick, dark blue line and its scatter is represented by the light pink region that is encompassed with dashed pale-blue lines. These spectral indices do not allow for a distinction between young and field  $\leq M3$  dwarfs, however they can identify giants even at these early types. Six of the new  $\geq M4$  candidates members have spectral indices that are systematically lower than the field sequence, indicating a young age. Twelve others show signs of an older age and can thus be rejected as candidate members of TWA. See Section 4.3 for more details.

scription of the gravity scores). The first two targets are rejected as TWA candidate members, due to their lack of low-gravity signatures. The visual spectral type classifications are consistent with the Allers & Liu (2013) index-based gravity classes for the three targets (M7, M8 and M9  $\beta$ , respectively).

NIR spectral types of new TWA candidates fromLooper (2011) were revised using the spectral stan-

dards of Gagné et al. (2015d), since no low-gravity NIR standards or templates were available at the time of their discovery. All subtypes remained unchanged, but all objects were classified with the  $\gamma$  gravity class (2MASS J10455263–2819303, M6  $\gamma$ ; 2MASS J11064461–3715115, M9  $\gamma$ ; 2MASS J11112820–2655027 or TWA 37, M6  $\gamma$ ; 2MASS J12035905–3821402 or TWA 38, M8  $\gamma$ ; 2MASS J12071089–3230537 or TWA 31, M6  $\gamma$ ; and 2MASS J12520989–4948280, M8  $\gamma$ ).

**Table 5.** FIRE Radial Velocity Measurements

2MASS Designation	Other Name	RV <sup>a</sup> (km s <sup>-1</sup> )	$v \sin i$ (km s <sup>-1</sup> )	EW(Li) (mÅ)	S/N per pixel	UT Date (ddmmyy)	Effect on Membership <sup>b</sup>
08254335–0029110	...	17 ± 3	...	...	79	131213	R → R
09553336–0208403	BASS-UC 51	-20 ± 4	...	...	60	160123	CM → R
11020983–3430355	TWA 28	9 ± 3	...	...	230	140512	HM → BF
11472421–2040204	BASS-UC 56	9 ± 5	...	...	15	160123	...
11472421–2040204	BASS-UC 56	7 ± 3	...	...	45	160223	...
11472421–2040204 <sup>c</sup>	BASS-UC 56	7 ± 3	...	...	...	...	CM → HM
11480096–2836488	...	6 ± 3	...	...	55	150531	CM → CM
12074836–3900043	...	6 ± 3	...	...	100	151222	CM → HM
12451416–4429077	TWA 29	8 ± 3	...	...	120	160223	HM → BF
12563961–2718455	...	-19 ± 4	...	...	15	140512	CM → R
14112131–2119503	...	-13 ± 3	...	...	230	140512	R → R

<sup>a</sup> Radial velocity.

<sup>b</sup> Previous membership status → Updated membership status, based on the inclusion of the new radial velocity measurement in BANYAN II. See Section 4.4 for more detail. R: Rejected; LM: Low-likelihood candidate member; CM: Candidate member, HM: High-likelihood candidate member; BF: Bona fide member. A few candidates have been rejected either by additional information after they were observed with GMOS; this explains the few cases with a mention R → R.

<sup>c</sup> Error-weighted combination of the two measurements (weights are determined before the application of the ±3 km s<sup>-1</sup> systematic error).

NOTE—See Section 4.4 for more details.

#### 4.4. FIRE/Echelle Radial Velocity Measurements

Radial velocities were measured for all FIRE-echelle spectra by comparing them with zero-velocity CIFIST 2011 BT-Settl spectra (Baraffe et al. 2015; Allard et al. 2012). The IDL implementation of the amoeba Nelder-Mead downhill simplex algorithm (Nelder & Mead 1965) was used to fit a forward model to the data in several fixed wavelength windows located in the  $H$  band, which provides the highest signal-to-noise data. The 4 free parameters that were used in this forward modelling approach are (1) the radial velocity Doppler shift, (2) the characteristic width of the instrumental line spread function, and (3) a two-parameters multiplicative linear correction to the spectral flux density continuum to account for instrumental systematics.

The instrumental LSF was assumed to be Gaussian, and no telluric model was needed as telluric standard

observations were used to correct the science spectra as described in Section 3.1. The Firehose pipeline generates spectra that are corrected for barycentric velocity variations and placed in a vacuum wavelength reference, thus removing the need to account for these effects or to determine a wavelength solution as part of the forward model.

The BT-Settl model that minimizes the  $\chi^2$  value in the  $H$  band when compared to the science spectrum was selected for the radial velocity determination, and the radial velocity fitting was performed in fifteen 0.02  $\mu\text{m}$ -wide segments regularly distributed in the 1.5100–1.5535  $\mu\text{m}$  range to account for any systematics and limit the effects of bad pixels. This method is very similar to that used by Gagné et al. (2015a) and Burgasser et al. (in preparation) to measure radial velocities using FIRE-echelle spectra, and is known to pro-

duce RVs that are limited to a  $3 \text{ km s}^{-1}$  precision due to systematics (this assessment of precision was obtained by performing similar RV measurements on radial velocity standard stars). The average of all individual 15 measurements was taken as the radial velocity measurement, and their standard deviation, added in quadrature to the  $3 \text{ km s}^{-1}$  systematic error, was taken as the measurement error.

These new radial velocity measurements are displayed in Table 5, along with their updating effect on TWA membership, when used as an additional input to BANYAN II.

#### 4.5. *ESPaDOnS/CFHT Measurements*

Heliocentric radial velocities and projected rotational velocities for the 11 ESPaDOnS/CFHT spectra were measured using the method described by Malo et al. (2014), which consists in performing a cross-correlation of the data with an observed radial velocity standard star of a similar spectral type. Lithium absorption lines were clearly detected for 8/11 spectra, and their equivalent widths were measured using the method of Malo et al. (2014). These detections ensure that the objects in question are younger than  $\sim 80\text{--}200$  Myr, depending on their spectral types.

There are a few objects that were observed only with ESPaDOnS for which no spectral types were yet determined in the literature. The method of Riaz et al. (2006) was used to estimate their spectral types based on the TiO5 spectral index. All resulting measurements are reported in Table 6.

#### 4.6. *Discussion of Individual Objects*

In this section, we discuss several individual objects for which the new data presented here require special attention.

##### 4.6.1. *2MASS J11423628–3859108*

The ESPaDOnS spectrum of 2MASS J11423628–3859108 differs significantly from that of an M- or later-type dwarf, hence we conclude that it is likely a background star contaminant and reject it from the sample of TWA candidate members.

##### 4.6.2. *2MASS J11112820–2655027*

2MASS J11112820–2655027 (TWA 37; M6  $\gamma$ e) is the star in the GMOS data sample that has an H $\alpha$  equivalent

width closest to the Barrado y Navascués & Martín (2003) criterion for Classical T Tauri stars although it does not meet it, with  $\text{EW}(\text{H}\alpha) = 16.2 \pm 0.8 \text{ \AA}$ : at this spectral type,  $\text{EW}(\text{H}\alpha) \geq 24.1 \text{ \AA}$  would be required to categorize it as a classical T Tauri star.

The  $W3$  and  $W4$  WISE magnitudes of TWA 37 are well detected (catalog entry WISE J111128.13–265502.9) at  $W3 = 8.77 \pm 0.02 \text{ mag}$  ( $46\sigma$ ) and  $W4 = 8.31 \pm 0.23$  ( $4.7\sigma$ ), however it does not present conclusive signs of an infrared excess. Its  $W1 - W4$  color ( $0.93 \pm 0.23$ ) is not red enough to respect the  $W1 - W4 > 1.0$  criterion of Schneider et al. (2012b) for infrared excess (see also Schneider et al. 2012a), and a comparison with predictions from BT-Settl models places the infrared excess of this source at a significance below  $3\sigma$  in these two photometric bands (see Boucher et al. 2016).

##### 4.6.3. *2MASS J12000160–1731308 AB*

The Na-a index (Kirkpatrick et al. 1999) of 2MASS J12000160–1731308 AB (M4  $\gamma$ e; see Table 4 and Figure 2) could be weak enough for a giant star instead of a young brown dwarf, however this possibility is rejected by the presence of H $\alpha$  emission in its spectrum (with an H $\alpha$  equivalent width of  $3.9 \pm 0.3 \text{ \AA}$ ).

##### 4.6.4. *2MASS J09553336–0208403: A New young L7 dwarf*

Although the new radial velocity measurement presented here rejects 2MASS J09553336–0208403 as a possible member of TWA (see Section 4.4), its very red  $J - K_S$  color ( $2.14 \pm 0.02$ ), triangular-shaped  $H$ -band continuum and weak K I absorption lines (see Table 7 and Figure 3(a)) are indicative of a low surface gravity. Using the young spectral type– $K_S$ -magnitude sequence of Gagné et al. (2015d), the spectrophotometric distance of 2MASS J09553336–0208403 is estimated at  $30.5 \pm 9.0 \text{ pc}$ . A likelihood analysis based on the BT-Settl models (see Gagné et al. 2014c) yields a mass estimate of  $18 \pm 6 M_{\text{Jup}}$  at this distance when adopting a conservative age range of 1–200 Myr. This upper age limit was chosen at the approximate boundary where low-gravity spectral indices become inapparent in the NIR spectra of brown dwarfs and low-mass stars (e.g., Allers & Liu 2013).

**Table 6.** Measurements from ESPaDOnS Optical Spectra

2MASS Designation	Other Name	RV (km s <sup>-1</sup> )	$v \sin i$ (km s <sup>-1</sup> )	EW(H $\alpha$ ) (Å)	EW(Li) (mÅ)	Li Age <sup>a</sup> (Myr)	S/N /pix	Spectral Type	UT Date (ddmmyy)	Effect on Membership <sup>b</sup>
10190109–2646336	...	$-3.1 \pm 0.3$	$24 \pm 2$	$4.0 \pm 0.1$	$< 27$	$> 100$	35	M5e	160421	CM → R
10284580–2830374	TWA 34	$12.4 \pm 0.3$	$15 \pm 2$	$8.7 \pm 0.1$	$630 \pm 20$	$< 200$	50	M6e	160418	CM → HM
10585054–2346206	...	$8.1 \pm 0.3$	$22 \pm 2$	$8.7 \pm 0.1$	$620 \pm 20$	$< 200$	65	M6e	160124	...
10585054–2346206	...	$8.2 \pm 0.3$	$24 \pm 2$	$7.9 \pm 0.3$	$680 \pm 60$	$< 200$	75	M6e	160611	...
10585054–2346206 <sup>c</sup>	...	$8.2 \pm 0.2$	$23 \pm 2$	$8.6 \pm 0.1$	$630 \pm 20$	$< 200$	...	M6e	...	CM → CM
11023986–2507113	...	$17.3 \pm 0.3$	$8.4 \pm 0.9$	$3.29 \pm 0.06$	$26 \pm 4$	$< 80$	50	M4e	160421	CM → LM
11152992–2954436	...	$13.3 \pm 0.2$	$5 \pm 1$	$3.51 \pm 0.08$	$71 \pm 6$	$< 80$	30	M4e	160421	CM → CM
11382693–3843138	...	$18.7 \pm 0.4$	$24 \pm 2$	$4.9 \pm 0.1$	$53 \pm 9$	$< 100$	30	M5e	160612	CM → LM
11393382–3040002	TWA 33	$5.8 \pm 0.7$	$15 \pm 2$	$3.88 \pm 0.07$	$590 \pm 10$	$< 150$	85	M5.5e	160421	HM → BF
11423628–3859108	...	...	...	...	...	...	15	<M0	160516	CM → R
12000160–1731308 <sup>d</sup>	...	$-0.1 \pm 0.8$	$59 \pm 4$	$3.9 \pm 0.1$	$720 \pm 30$	$< 200$	65	M6e	160115	R → R
12073145–3310222	...	$-9.0 \pm 0.2$	$3 \pm 1$	$-0.45 \pm 0.02$	$< 12$	...	50	~M0	160612	CM → R
12175920–3734433	...	$5 \pm 3$	$32 \pm 5$	$10.6 \pm 0.9$	$850 \pm 20$	$< 200$	20	M6e	160516	CM → HM

<sup>a</sup> Age limit based on the detection of Li,  $T_{\text{eff}}$  estimated from spectral types (see Pecaut & Mamajek 2013) and the lithium depletion boundaries of Basri (1998).

<sup>b</sup> Previous membership status → Updated membership status, based on the inclusion of the new radial velocity measurement in BANYAN II. See Section 4.4 for more detail. R: Rejected; LM: Low-likelihood candidate member; CM: Candidate member, HM: High-likelihood candidate member; BF: Bona fide member.

<sup>c</sup> Error-weighted combination of the two epochs.

<sup>d</sup> Possible spectral binary.

NOTE—See Section 4.4 for more details.

#### 4.6.5. 2MASS J10212570–2830427: A young L5 $\beta$ dwarf

The low-resolution NIR spectrum of 2MASS J10212570–2830427 (Figure 3(b)) displays a triangular-shaped  $H$ -band continuum and a unusually red slope. Using the spectral templates of Gagné et al. (2015d) yields a spectral type of L5 $\beta$ . A higher-resolution spectrum will be necessary to confirm whether these characteristics are clearly due to a young age.

#### 4.6.6. The Isolated Planetary-Mass Object 2MASS J11472421–2040204

As mentioned in Section 2.2, 2MASS J11472421–2040204 has been reported as a candidate member of TWA by Schneider et al. (2016a), using its sky position, proper motion, spectrophotometric distance and tentative indications of youth. The very red  $J - K_S$  color ( $2.57 \pm 0.03$ ) and triangular-shaped  $H$ -band continuum of 2MASS J11472421–2040204 were used to determine that it is likely a young L7 substellar object. However, it has been discussed in the literature that these characteristics could also be potentially caused by other effects, such as a high metallicity or unusual cloud thickness, without needing to invoke a young age (Allers & Liu 2013; Marocco et al. 2014; Aganze et al. 2016).

As one of the first few high-priority discoveries of

the BASS-Ultracool survey, 2MASS J11472421–2040204 (BASS-UC 56) was observed with FIRE in both the prism and echelle modes. The new FIRE-echelle spectrum allowed a radial velocity measurement that strengthened the TWA membership (see Section 4.4), as well as a diagnosis of the surface gravity based on the strength of the K I absorption lines at 1.168–1.179  $\mu\text{m}$  and 1.243–1.253  $\mu\text{m}$ . The relative strength of these absorption lines, along with the other characteristics mentioned above, can be used to safely determine whether 2MASS J11472421–2040204 is a young L7 dwarf.

In Table 7, the K I equivalent widths as defined by McLean et al. (2003) are compared to those of other known young L7 dwarfs and to those of field L7 dwarfs (McLean et al. 2003). The weak K I equivalent widths of 2MASS J11472421–2040204 demonstrate that it has a low surface gravity, and is thus a young substellar object, as suspected by Schneider et al. (2016a).

Only a parallax measurement is still needed before this object can be assigned as a bona fide member of TWA. Since its spectrophotometric distance matches its BANYAN II kinematic distance (Schneider et al. 2016a), it is likely that this object is a member of TWA (see also Faherty et al. 2016a).



**Table 7.** *J*-Band K I Equivalent Widths of L7-type Objects

Name	EW(K I) <sup>a</sup> (Å)			
	1.169 $\mu\text{m}$	1.177 $\mu\text{m}$	1.243 $\mu\text{m}$	1.254 $\mu\text{m}$
PSO J318.5–22 <sup>b</sup>	2 $\pm$ 1	3 $\pm$ 1	1.7 $\pm$ 0.6	1.3 $\pm$ 0.7
J1119–1137 <sup>c</sup>	1.2 $\pm$ 0.6	3.9 $\pm$ 0.6	1.9 $\pm$ 0.3	3.1 $\pm$ 0.3
J1147–2040 <sup>d</sup>	3.0 $\pm$ 0.7	4.4 $\pm$ 0.7	3.4 $\pm$ 0.3	3.0 $\pm$ 0.3
J0955–0208 <sup>e</sup>	2.3 $\pm$ 0.7	4.6 $\pm$ 0.7	2.9 $\pm$ 0.3	3.7 $\pm$ 0.3
Field L7 <sup>f</sup>	6.0–7.0	9.0–10.0	4.0–6.0	5.5–7.5

<sup>a</sup> As defined by [McLean et al. \(2003\)](#).

<sup>b</sup> The complete PSO designation is PSO J318.5338–22.8603; the FIRE spectrum of [Faherty et al. \(2016b\)](#) was used.

<sup>c</sup> The complete 2MASS designation is 2MASS J11193254–11374661; the FIRE spectrum of [Kellogg et al. \(2016\)](#) was used.

<sup>d</sup> The complete 2MASS designation is 2MASS J11472421–2040204.

<sup>e</sup> The complete 2MASS designation is 2MASS J09553336–0208403.

<sup>f</sup> Complete range of values for field L7 dwarfs obtained by [McLean et al. \(2003\)](#)

NOTE—See Section 4.6.6 for more details.

## 5. A COMPILATION OF THE TW HYA MEMBERS AND CANDIDATES

In light of the new data presented in this work, an updated list of members and candidate members of TWA is compiled in this section. A discussion on the confusion between members of TWA and LCC is presented in Section 5.1. The final list of TWA objects is displayed in Tables 12 (kinematic properties), 13 (spectrophotometric properties) and 14 (final BANYAN II membership probabilities). The final BANYAN II probabilities listed in Table 14 take into account positions, proper motions, radial velocities and/or trigonometric distances, when available. In addition to this, 2MASS and WISE photometry were used for all objects with spectral types  $\geq$  M5 to constrain the distance using two color-magnitude diagrams ( $M_{W1}$  versus  $J - K_S$ , and  $M_{W1}$  versus  $H - W2$ ), as described by [Gagné et al. \(2014c\)](#).

A proper motion was calculated from the 2MASS and ALLWISE astrometries for all members and candidate members of TWA using the method of [Gagné et al. \(2015b\)](#). The resulting measurements were adopted only when the proper motion was more accurate than those available in the literature. These measurements are reported in Table 12 along with all kinematic properties.

Objects that show all the necessary observational evidence for TWA membership (signs of youth, proper motion, radial velocity and trigonometric distance) and have Bayesian probabilities above 90% are assigned the *bona fide member* (BF) status (all have Bayesian membership probabilities above 98%). Those that are miss-

ing only one of these measurements and have a Bayesian membership probability above 90% are assigned the *high-likelihood candidate member* (HM) status. Objects that are members of other groups, have properties that are inconsistent with the age of TWA, or have Bayesian membership probabilities below 1% are rejected (R). All remaining objects are divided between *candidate members* (CM; Bayesian probability  $\geq$  20%) or *low-likelihood candidate members* (LM; Bayesian probability  $<$  20%). Two systems (TWA 6 AB and TWA 31) respect all of the observational criteria for *bona fide members*, but have a significantly lower Bayesian membership probability. These two objects are further discussed below.

In Table 8, a list of all known binaries in the present sample is reported, along with their projected separations. 2MASS J12421948–3805064 B was discovered in this work as a visual binary in the GMOS follow-up, using the *i*-band acquisition image that preceded the spectral data acquisition. The two components were placed in the slit, which allowed for a separate data extraction and spectral typing of the two components.

**TWA 6 AB** and **TWA 31** were identified as candidate members of TWA by [Song et al. \(2003\)](#) and [Shkolnik et al. \(2011\)](#). At the present stage, they benefit from full kinematic measurements, but display slight discrepancies with other TWA members in *XYZ* and *UVW* spaces, resulting in relatively low Bayesian membership probabilities of 62.5% and 68.4%. These two objects are discussed in more detail in Section 5.1.

**TWA 9 AB** has been identified as a candidate member of TWA by [Song et al. \(2003\)](#). [Weinberger et al. \(2013\)](#) and [Ducourant et al. \(2014a\)](#) noted that this object seems slightly older ( $38 \pm 18$  Myr; [Ducourant et al. 2014a](#)) than other TWA members from a comparison with the [Baraffe et al. \(1998\)](#) and [Siess et al. \(2000\)](#) evolutionary models. [Weinberger et al. \(2013\)](#) used a trigonometric distance measurement to show that it is relatively discrepant to other TWA members in *UVW* space. [Pecaut & Mamajek \(2013\)](#) argued that all of these discrepancies were possibly explained by the Hipparcos distance if it is in error by  $\approx 3\sigma$ , as adopting a distance of  $\approx 70$  pc (rather than  $46.8 \pm 5.4$  pc) would solve both the isochronal age and kinematic discrepancy. A recent trigonometric distance measurement of  $52.1 \pm 3.0$  pc ([Ducourant et al. 2014b](#)) made this scenario seem unlikely, however a more precise measurement from the *Gaia* Data Release 1 ([Lindegren et al. 2016](#)) places TWA 9 at  $75.7 \pm 1.7$  pc, corroborating the hypothesis of [Pecaut & Mamajek \(2013\)](#). In this paper, we adopt the *Gaia* distance measurement, which makes TWA 9 a *bona fide member* of TWA.

**TWA 21** was identified by [Song et al. \(2003\)](#) as a candidate member of TWA. [Ducourant et al. \(2014a\)](#) noted that this object seemed slightly older ( $25 \pm 7$  Myr)

than other TWA members from a comparison with the Baraffe et al. (1998) and Siess et al. (2000) evolutionary models. Using all available kinematic data from the literature, TWA 21 is instead an excellent match (98.2%) to the Carina association ( $45_{-7}^{+11}$  Myr; Torres et al. 2008; Bell et al. 2015), although its age seems slightly lower than that of the Carina association. A more detailed analysis of this object will be required to confirm whether it is a new bona fide member of Carina, however this scenario seems likely and it is therefore rejected from the census of TWA members and candidates.

**TWA 22 AB** was identified as a candidate member of TWA by Song et al. (2003), a claim that was subsequently questioned by Mamajek (2005) using the method of convergent proper motion. Teixeira et al. (2009) used a trigonometric distance measurement to confirm that it is not a member of TWA, and suggested that it is rather a member of the young  $\beta$  Pictoris moving group ( $24 \pm 3$  Myr; Zuckerman et al. 2001a; Bell et al. 2015). This is consistent with the resulting BANYAN II classification (99.7% membership to  $\beta$  Pictoris).

**Table 8.** Multiple Systems in TWA

2MASS Designation	Other Name	Type <sup>a</sup>	Host Name	$N_*$ <sup>b</sup> 2MASS	$N_*$ <sup>b</sup> AllWISE	Sep. <sup>c</sup> (")	Ref.
10023100–2814280 A	1002–2814 A	P	...	2	2	...	...
10023100–2814280 B	1002–2814 B	C	1002–2814 A	2	2	0.56	(1)
10120908–3124451 A	TWA 39 A	P	...	2	2	...	...
10120908–3124451 B	TWA 39 B	C	TWA 39 A	2	2	1.0	(2)
10182870–3150029 A	TWA 6 A	P	...	2	2	...	...
10182870–3150029 B	TWA 6 B	C	TWA 6 A	2	2	SB	(3)
11015191–3442170	TWA 1	P	...	1	1	...	...
11020983–3430355	TWA 28	C	TWA 1	1	1	735.6	(4)
11091380–3001398 A	TWA 2 A	P	...	2	2	...	...
11091380–3001398 B	TWA 2 B	C	TWA 2 A	2	2	0.56	(3)
11102788–3731520 Aa	TWA 3 Aa	P	...	3	3	...	...
11102788–3731520 Ab	TWA 3 Ab	C	TWA 3 Aa	3	3	SB	(5)
11102788–3731520 B	TWA 3 B	C	TWA 3 Aa	3	3	1.4	(6)
11211723–3446454 A	TWA 13 A	P	...	2	2	...	...
11211723–3446454 B	TWA 13 B	C	TWA 13 A	2	2	5	(7)
11220530–2446393 Aa	TWA 4 Aa	P	...	4	4	...	...
11220530–2446393 Ab	TWA 4 Ab	C	TWA 4 Aa	4	4	0.2	(8)
11220530–2446393 Ba	TWA 4 Ba	C	TWA 4 Aa	4	4	0.8	(9)
11220530–2446393 Bb	TWA 4 Bb	C	TWA 4 Ba	4	4	SB	(10)
11315526–3436272 Aa	TWA 5 Aa	P	...	2	2	...	...
11315526–3436272 Ab	TWA 5 Ab	C	TWA 5 Aa	2	2	0.066	(11)
11315526–3436272 B	TWA 5 B	C	TWA 5 Aa	1	1	2.0	(12)
11324116–2652090	TWA 8 B	C	TWA 8 A	1	1	13.1	(4)
11324124–2651559	TWA 8 A	P	...	1	1	...	...
11321822–3018316	TWA 30 B	C	TWA 30 A	1	1	80.2	(13)
11321831–3019518	TWA 30 A	P	...	1	1	...	...
11392944–3725531	HIP 56863 A	P	...	1	2	...	...
11392960–3725538	HIP 56863 B	C	HIP 56863 A	1	2	3.34	(14)
11482422–3728491	TWA 9 A	P	...	1	1	...	...
11482373–3728485	TWA 9 B	C	TWA 9 A	1	1	6.0	(3)
12072738–3247002 Aa	TWA 23 A	P	...	3	3	...	...
12072738–3247002 Ab	TWA 23 B	C	TWA 23 A	3	3	SB2	(15)
12073346–3932539 A	TWA 27 A	P	...	1	1	...	...
12073346–3932539 b	TWA 27 b	C	TWA 27 A	1	1	0.78	(17)
12074836–3900043	TWA 40	C	TWA 27 A	1	1	1977.2	(4)
12100648–4910505	HIP 59315	P	...	1	1	...	...
12265135–3316124 A	TWA 32 A	P	...	2	2	...	...

*Table 8 continued*

Table 8 (*continued*)

2MASS Designation	Other Name	Type <sup>a</sup>	Host Name	$N_*$ <sup>b</sup> 2MASS	$N_*$ <sup>b</sup> AllWISE	Sep. <sup>c</sup> (")	Ref.
12265135–3316124 B	TWA 32 B	C	TWA 32 A	2	2	0.656	(15)
12313807–4558593 A	TWA 20 A	P	...	2	2	...	...
12313807–4558593 B	TWA 20 B	C	TWA 20 A	2	2	SB	(18)
12345629–4538075 A	TWA 16 A	P	...	2	2	...	...
12345629–4538075 B	TWA 16 B	C	TWA 16 A	2	2	0.61	(19)
12354893–3950245	TWA 11 C	C	TWA 11 A	1	1	174.9	(4)
12360055–3952156	TWA 11 B	C	TWA 11 A	1	1	7.6	(3)
12360103–3952102	TWA 11 A	P	...	1	1	...	...
12421948–3805064 A	1242–3805 A	P	...	2	2	...	...
12421948–3805064 B	1242–3805 B	C	1242–3805 A	2	2	1.53	(20)

<sup>a</sup>Type of system component (P: Primary; C: Companion).

<sup>b</sup>Number of known unresolved components in the 2MASS or AllWISE entry.

<sup>c</sup>Separation to host component. SB indicates a spectroscopic binary for which the separation was not measured.

NOTE—See Section 5 for more details.

**References**—(1) Janson et al. 2012b; (2) Riedel et al. 2014; (3) Webb et al. 1999; (4) 2MASS catalog (Skrutskie et al. 2006); (5) Kastner et al. 1997; (6) Reipurth & Mikkola 2015; (7) Stock & Wroblewski 1972; (8) Tokovinin 1999; (9) Torres et al. 2008; (10) Boden et al. 2005; (11) Konopacky et al. 2007; (12) Weinberger et al. 2013; (13)Looper et al. 2010a; (14) Fabricius et al. 2002; (15) Shkolnik et al. 2011; (16) Elliott et al. 2016; (17) Chauvin et al. 2004; (18) Jayawardhana et al. 2006; (19) Zuckerman et al. 2001b; (20) this paper.

**2MASS J102825000–3959230** was identified as a candidate member of TWA as part of the PRE-BASS survey, which consists of objects that were selected and observed while the BASS survey (Gagné et al. 2015b) selection criteria were still getting refined, and was subsequently rejected (see Gagné et al. 2015d for more discussion on the PRE-BASS survey). A recent radial velocity measurement of  $20 \pm 2 \text{ km s}^{-1}$  (Murphy et al. 2015) rejects it as a possible member of TWA, making it instead a candidate member of Carina with a Bayesian membership probability of 51.4%.

### 5.1. *The Confusion Between TW Hya and the LCC Association*

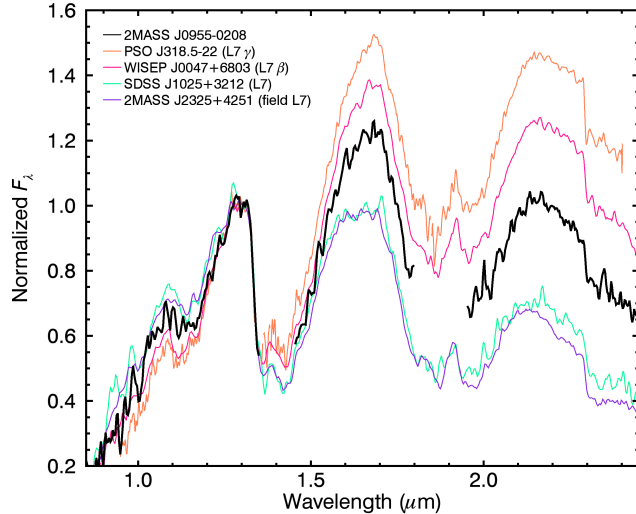
Before a final list of TWA candidates and members can be properly constructed, it is necessary to address the possible confusion between TWA and the LCC OB association. This slightly older ( $\sim 16 \text{ Myr}$ ; Mamajek et al. 2002) and more distant association ( $\sim 120 \text{ pc}$ ; de Zeeuw et al. 1999) is located in the same region of the sky as TWA, which causes confusion between the members of the two groups. Furthermore, the members of both associations have similar space velocities  $UVW$ .

It has been demonstrated, for example, that several objects that were thought to be members of TWA (TWA 12, 14, 15, 17, 18, 19 and 24) are probable members of LCC (Mamajek & Feigelson 2001; Lawson & Crause 2005; Mamajek 2005). Mamajek (2005) sug-

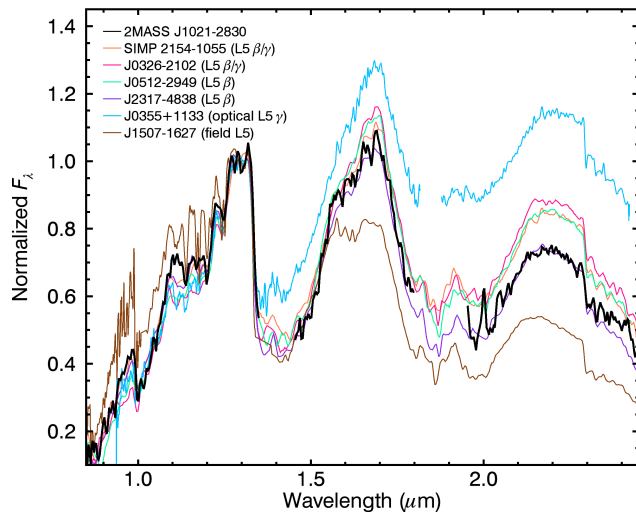
gested a separation at a Solar distance of  $\sim 85 \text{ pc}$  to differentiate between the two groups, as this distance delimitates two populations of stars with distinct compositions, ages and rotation periods (Lawson & Crause 2005).

A new version of the BANYAN II tool, which will include a larger number of associations, is currently under construction. The final version of this tool, BANYAN  $\Sigma$ , will be presented in a future publication, but at this stage it is already in a state where it can be used to flag likely LCC contaminants in our sample. All LCC members compiled by de Zeeuw et al. (1999) and Preibisch & Mamajek (2008) that have signs of youth, radial velocity and distance measurements were used to build a spatial-kinematic model that is similar to those of BANYAN II (see Gagné et al. 2014c). The probabilities of this new tool are not yet calibrated to yield true contamination rates and the model of the field population is still incomplete, however it is already possible to calculate the Bayes factor between the LCC and TWA hypotheses.

Any TWA candidate in our sample that has an LCC/TWA Bayes factor above 1 is thus likely to be a contaminant from LCC. There are 44 such systems in our sample (including TWA 6 and TWA 31); they were flagged in Table 14 and excluded from the sample for the remainder of this work. Only 9/44 of these objects would also have been rejected by the Mamajek



(a) 2MASS J09553336-0208403



(b) 2MASS J10212570-2830427

**Figure 3.** NIR SpeX spectra of 2MASS J09553336-0208403 and 2MASS J10212570-2830427 compared with field and young substellar objects of the same spectral types. Both objects display a trinangular  $H$ -band continuum and red  $J-K$  colors, which are telltale signs of a low surface gravity. All spectra were normalized by their median in the 1.27–1.33  $\mu\text{m}$  range. The full names of the reference spectra given in the legends are, from top to bottom; PSO J318.5338-22.8603 (Liu et al. 2013), WISEP J004701.06+680352.1 (Gizis et al. 2012), SDSS J102552.43+321234.0 (Chiu et al. 2006), 2MASS J23254530+4251488 (Cruz et al. 2007), SIMP J21543454-1055308 (Gagné et al. 2014b), 2MASS J032642250-2102057 (Gizis et al. 2003), 2MASS J05120636-2949540 (Cruz et al. 2003), 2MASS J23174712-4838501 (Reid et al. 2008), 2MASS J03552337+1133437 (Reid et al. 2008), and 2MASS J150747690-1627386 (Reid et al. 2000). See Section 3.3 for more details.

(2005) criterion, 7/9 from their trigonometric distance and 2/35 from their TWA statistical distance. A criterion based on only the distance separation between TWA and LCC is therefore not reliable to distinguish LCC contaminants when using a kinematic distance estimate instead of a trigonometric distance measurement.

Objects that have been defined as high-likelihood candidates or bona fide members but that have a non-negligible probability of being an LCC interloper (the threshold is defined as an LCC/TWA Bayes factor above 0.1) were demoted to ambiguous candidate members (CM) until more information is available. This was the case for only one object (not counting those with a LCC/TWA Bayes factor above 1): 2MASS J11152992-2954436, which has an LCC/TWA Bayes factor of  $\sim 0.9$ .

In Figure 4, an update on the Figure 3 of Mamajek (2005) is presented; two LCC members from de Zeeuw et al. (1999) are located between 80–85 pc; HIP 59781 and HIP 50520. Both objects have a 0% BANYAN II TWA membership probability. This figure also shows that three stars located at R.A.  $< 10^{\text{h}}40^{\text{m}}$  (R.A.  $< 160^{\circ}$ ) and well within  $\sim 85$  pc of the Sun are likely contaminants from LCC according to their LCC/TWA Bayes factor. It thus seems that a clear separation between TWA and LCC members lies at  $\sim 80$  pc rather than  $\sim 85$  pc, and that it is only valid for R.A.  $> 160^{\circ}$ ; the members of LCC and TWA that are located East of this boundary cannot be discriminated with a simple distance criterion.

The TWA member that is closest to the  $\sim 80$  pc boundary is TWA 29 at a distance of  $79 \pm 13$  pc (Weinberger et al. 2013); it would be useful to obtain a more precise distance measurement to clarify whether TWA 29 falls within a distance of 80 pc. The *Gaia* mission (Perryman et al. 2001; Gaia Collaboration 2016) will likely answer this question, as TWA 29 is present in the Initial *Gaia* Source List (Smart & Nicastrò 2013) with a magnitude of  $G = 16.8 \pm 0.4$  (The *Gaia* Data Release 1 does not provide its parallax measurement; Lindegren et al. 2016). Even when this large distance error bar is adopted, the LCC/TWA Bayes factor of TWA 29 remains very small at  $\sim 3\%$ , hence it seems unlikely that it is a contaminant from LCC even if it were located above 80 pc.

## 5.2. Possible Common Proper-Motion Systems

A few studies have uncovered potential common proper motion (CPM) systems in TWA. It has been suggested by Kastner et al. (2008) that TWA 11 C and TWA 11 A are a CPM pair; by Scholz et al. (2005) that TWA 1 and TWA 28 are a possible CPM pair; by Looper et al. (2010a) that TWA 30 A and TWA 30 B are a CPM pair; and Elliott et al. (2016) have sug-



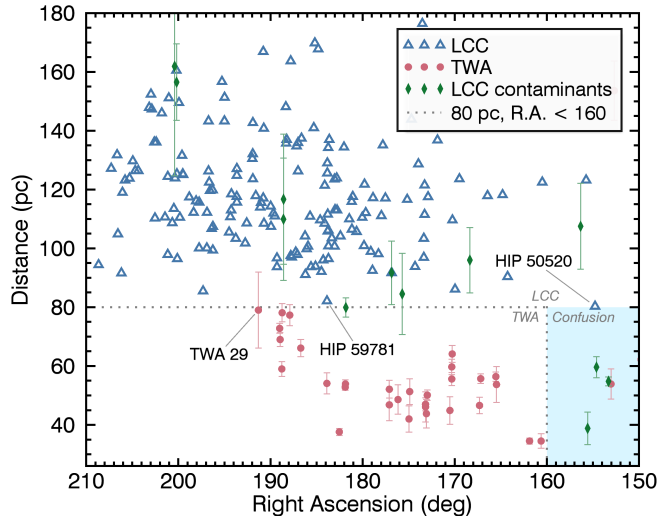


**Figure 4.** Distance as a function of right ascension for the current TWA census (red circles), and members of the LCC association (blue triangles). Likely LCC members that contaminated the current TWA sample before the application of BANYAN  $\Sigma$  are displayed with green diamonds. This figure is an update on Figure 3 of Mamajek (2005). Mamajek (2005) suggest a distance threshold of 85 pc to distinguish between members of LCC and TWA; this updated census seems to warrant a slight modification to a distance threshold of 80 pc, which is only valid at R.A. > 160. It can be seen that East of this boundary (pale blue shaded region), the statistical distance cannot discriminate likely LCC contaminants from true TWA members. See Section 5.1 for more details.

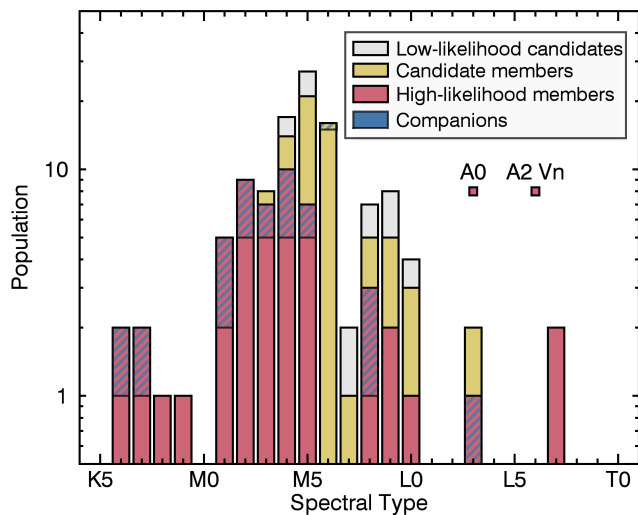


**Figure 5.** Spectral type histogram of members and candidate members of TWA. Optical spectral types are preferred when they are available. The bona fide members TWA 11 A and HIP 54477 with respective spectral types A0 and A2 Vn are located outside of range, and are represented with square symbols. Known companions are represented with diagonal blue stripes, and are assumed to have the same spectral type as the primary star when the brightness ratio is close to unity. See Section 5 for more details.

gested 3 additional new potential CPM companions to known TWA members: 2MASS J11130416-4516056 (TWA 14), 2MASS J12073145-3310222 (TWA 23) and 2MASS J12090628-3247453 (TWA 23). Since TWA 14 is a likely member of LCC (see Section 5.1), the former system is not discussed here. There is, however, a fundamental problem with the two latter CPM companions suggested by Elliott et al. (2016). Placing 2MASS J12073145-3310222 at the distance of TWA 23 would make its absolute  $K_S$ -band magnitude ( $7.35 \pm 0.06$ ) too faint for a K9-type dwarf by more than almost 4 mag. By comparison, the K9 bona fide member TWA 25 has an absolute  $K_S$ -band magnitude of  $3.6 \pm 0.1$ . Similarly, placing 2MASS J12090628-3247453 at the distance of TWA 23 would mean that its absolute  $K_S$ -band magnitude is  $8.32 \pm 0.06$ , again much too faint for an M1 dwarf (the M1-type bona fide member TWA 13 A has an absolute  $K_S$ -band magnitude of  $4.59 \pm 0.07$  after correcting for its binary nature). It is therefore very likely that both these objects are not related to TWA 23, or even to the TWA association. This is consistent with the fact that we measure an ES-PaDONs RV of  $-9.0 \pm 0.2 \text{ km s}^{-1}$  for 2MASS J12073145-3310222, which safely rejects it from TWA.

In addition to these, Gagné et al. (2014a) have discovered an isolated planetary-mass candidate member of TWA (2MASS J12074836-3900043) that is located relatively close ( $\sim 57'$ , corresponding to 181 000 AU at 52.8 pc) to TWA 27 on the sky. While this fact has not been discussed in the discovery paper, it has triggered discussions on the possibility that 2MASS J12074836-3900043 is a CPM companion of TWA 27 (Niall Deacon, priv. comm. 2014).

Since the determination of false-positive probabilities of CPM discoveries in young associations requires a different approach than those in the field (e.g., see Deacon et al. 2016), a determination of the false-positive probabilities of the possible CPM systems mentioned above is carried out in this section.

The development in this section aims at addressing the following question: *What is the probability that any two members of TWA will have observables that are similar to a CPM system simply by chance?* To answer this, it is possible to model the distribution of the  $XYZ$  Galactic positions and  $UVW$  space velocities of its members as a six-dimensional multivariate Gaussian distribution. If  $\mathbf{Q}$  is a six-dimensional vector that contains the  $XYZUVW$  coordinates, the multivariate Gaussian distribution is obtained by calculating the covariance matrix  $\Sigma$  of the  $XYZUVW$  positions of the members and their mean position  $\mathbf{Q}_0$ . The spatial density distri-

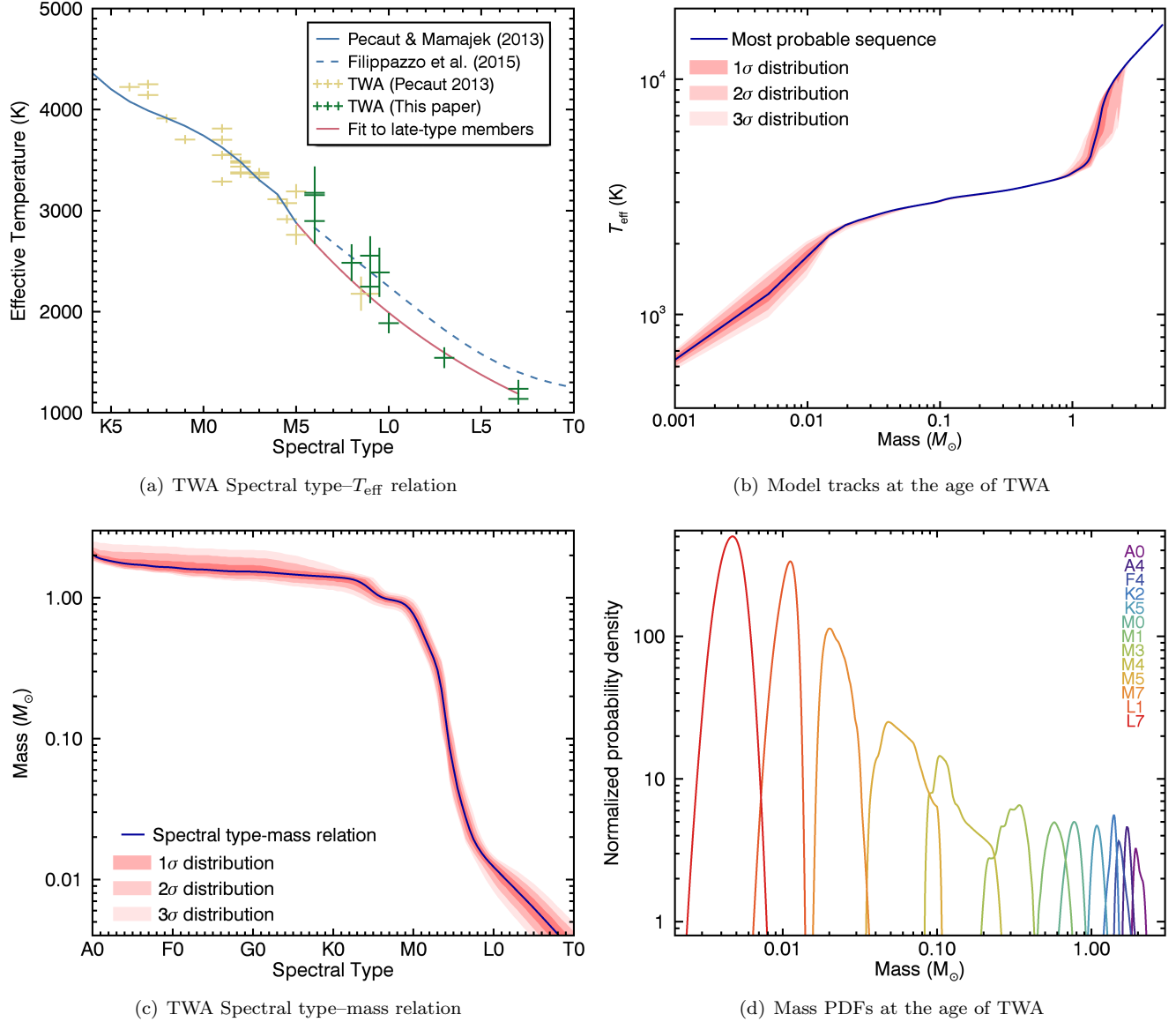


**Figure 6.** Panel a: Extension of the Pecaut & Mamajek (2013) spectral type– $T_{\text{eff}}$  relation (blue line) to the  $> M5$  regime (red line) using late-type members of TWA and the  $T_{\text{eff}}$  determination method of Filippazzo et al. (2015). The dashed blue line is the spectral type– $T_{\text{eff}}$  relation of field stars calculated by Filippazzo et al. (2015) at the age of the field. Young stars are expected to have a lower  $T_{\text{eff}}$  at a fixed spectral type. It is possible that the sample of M6–M9 TWA stars is contaminated by unresolved binaries, which would explain that some objects lie above the young  $T_{\text{eff}}$  sequence.

Panel b: Posterior PDFs for evolutionary model tracks obtained from the Baraffe et al. (2015;  $\leq 1.4 M_{\odot}$ ) and Siess et al. (2000;  $> 1.4 M_{\odot}$ ) models, at the age of TWA ( $10 \pm 3$  Myr; Bell et al. 2015).

Panel c: Mass– $T_{\text{eff}}$  relations for TWA, obtained from a combination of the relations displayed in Panels a and b.

Panel d: Mass posterior PDFs as a function of spectral type, obtained from the spectral type–temperature relation displayed in Panel a and the model tracks presented in Panel b. See Section 6 for more details.

bution of the TWA members is then described as:

$$P(\mathbf{Q}|\mathbf{Q}_0, \mathbf{\Sigma}) = N_{\text{tot}} \frac{e^{-\frac{1}{2}(\mathbf{Q}-\mathbf{Q}_0)^T \mathbf{\Sigma}^{-1}(\mathbf{Q}-\mathbf{Q}_0)}}{\sqrt{(2\pi)^3 |\mathbf{\Sigma}|}}, \quad (3)$$

where  $N_{\text{tot}}$  is the total number of members. Such a distribution is equivalent to the freely rotating Gaussian ellipsoids used in BANYAN II (Gagné et al. 2014c) if the spatial-dynamic terms of the covariance matrix are set to zero. The covariance matrix  $\mathbf{\Sigma}$  and mean value  $\mathbf{Q}_0$  of the  $XYZUVW$  coordinates were calculated for all bona fide and high-likelihood members of TWA. Only primaries were used in this calculation, to avoid introducing artificial biases in the structure of TWA. Kinematic distances or radial velocities were used when the measurements were not available.

A set of  $10^5$  artificial associations were then randomly drawn from the multivariate gaussian distribution of TWA described in Equation (3). These artificial associations were created with the same number (34) of bona fide and high-likelihood systems as the current TWA census. The fraction of simulations that had any two members with proper motions, radial velocities, distances and sky positions at least as close together as a given common proper motion system was then counted.

Similar simulations were carried out for each potential CPM pair, the results of which are presented in Table 9. It can be seen that most of the proposed potential CPM pairs have relatively low probabilities of being located this close by pure chance, given the spatial structure of TWA. 2MASS J12074836–3900043 has the largest probability (0.7%) of a chance alignment. Obtaining a precise trigonometric distance would be helpful to determine whether it is a common proper motion companion of TWA 27, however it will be treated conservatively as an isolated object in the remainder of this work.

**Table 9.** Potential Common Proper Motion Objects

Companion Name	Primary Name	Angular Sep. (")	Physical Sep. (AU)	$P_A^a$ (%)
TWA 30 B	TWA 30 A	80.2	$3\,500 \pm 400$	$< 10^{-6}$
TWA 11 C	TWA 11 A	174.9	$14\,400 \pm 300$	$9 \cdot 10^{-4}$
TWA 28	TWA 1	735.6	$160\,000 \pm 20\,000$	$8 \cdot 10^{-3}$
J1207–3900 <sup>d</sup>	TWA 27	1977.2	$181\,000 \pm 3\,000$	0.7

<sup>a</sup> Chance alignment probability, assuming membership to TWA.

<sup>b</sup> The complete 2MASS designation is 2MASS J12073145–3310222.

<sup>c</sup> The complete 2MASS designation is 2MASS J12090628–3247453.

<sup>d</sup> The complete 2MASS designation is 2MASS J12074836–3900043.

NOTE—See Section 5.2 for more details.

### 5.3. An Update on TWA Names

In light of the revisions to the list of TWA candidates and members presented here, it will be useful to assign new TWA names to the list that is currently available in the literature. The TWA numbers up to TWA 33 have been defined without ambiguity, however TWA 34 and TWA 35 have each been assigned to two distinct objects: TWA 34 stands for 2MASS J12520989–4948280 (Looper 2011) or 2MASS J10284580–2830374 (Murphy et al. 2015), whereas TWA 35 stands for 2MASS J13265348–5022270 (Looper 2011) or 2MASS J12002750–3405371 (Murphy et al. 2015). Here, the definitions of Murphy et al. (2015) are adopted since it was the first refereed work to use both names. Furthermore, 2MASS J12520989–4948280 was found here to be a likely LCC contaminant, and 2MASS J13265348–5022270 has a 0% BANYAN II TWA membership probability; both objects were thus rejected from the current TWA sample. The names TWA 36 through 38 have been defined by Looper (2011) without ambiguity in the literature and refer to objects that are still credible candidate members; they were thus adopted in this work. To our knowledge, no TWA name with a number above TWA 38 has been defined yet (with the exceptions of TWA 45 and TWA 46 discussed below).

There are seven high-likelihood candidates and bona fide members of TWA that currently do not have a TWA name. We therefore suggest assigning the names TWA 39 AB to SCR 1012–3124 AB (2MASS J10120908–3124451 AB; Riedel et al. 2014), TWA 40 to 2MASS J12074836–3900043 (Gagné et al. 2014a), TWA 41 to 2MASS J11472421–2040204 (Schneider et al. 2016a), TWA 42 to 2MASS J11193254–1137466 (Kellogg et al. 2016), TWA 43 to HIP 54477 (Section 2.4), and TWA 44 to 2MASS J12175920–3734433 (Section 4.5).

Two additional TWA names have been introduced for new candidate members of TWA reported by Donaldson et al. (2016): TWA 45 for 2MASS J11592786–4510192 and TWA 46 for 2MASS J12354615–4115531. One last high-likelihood candidate member of TWA was discovered by Riedel et al. (2016) while this paper was in review; we therefore assign the name TWA 47 to SCR 1237–4021 (2MASS J12371238–4021480; Riedel et al. 2016).

The distribution of spectral types for the final TWA candidates and members is presented in Figure 5. This figure demonstrates that there are only two massive (< K-type) members of TWA, and that all of its M6–M7 candidate members still remain to be confirmed as bona fide members. Furthermore, it is likely that several K-type members are still missing due to the lack of an all-sky survey targeting such members of TWA.

## 6. ESTIMATION OF PHYSICAL PARAMETERS

In order to obtain a mass estimate for the candidate members of TWA, either their absolute magnitudes or effective temperatures must first be measured, and then translated to masses using evolutionary models. Since the multiplicity rate of TWA members is high, we choose to rely on effective temperature measurements over absolute magnitudes such that the effect of unknown binaries is minimized.

### 6.1. *Effective Temperatures of Early-Type Members*

The spectral types of all objects with spectral types M5 or earlier are translated to an effective temperature using the relations for young stars developed by [Pecaut & Mamajek \(2013\)](#). This is done by drawing a set of  $10^7$  Gaussian random numbers distributed around each spectral type (error bars of 0.5 subtypes were assumed), and interpolating them into a set of temperatures with the aforementioned spectral type– $T_{\text{eff}}$  relations.

**Table 10.** Empirical Bolometric Luminosity and Semi-Empirical  $T_{\text{eff}}$  Measurements

2MASS Designation	TWA Name	Spectral Type	Data Used <sup>a</sup>	$\log_{10}(L_*/L_{\odot})$	Radius ( $R_{\text{Jup}}$ )	$T_{\text{eff}}$ (K)
<b>Bona Fide Members and High-Likelihood Candidate Members of TWA</b>						
12265135–3316124 A	TWA 32 A	M5	di	$-1.71 \pm 0.04$	$4.5 \pm 0.3$	$3200 \pm 100$
12073346–3932539 A	TWA 27 A	M8 pec	doi	$-2.59 \pm 0.02$	$2.4 \pm 0.1$	$2640 \pm 70$
11020983–3430355	TWA 28	M8.5 $\gamma$	di	$-2.54 \pm 0.03$	$2.4 \pm 0.1$	$2680 \pm 80$
11395113–3159214	TWA 26	M9 $\gamma$	doi	$-2.71 \pm 0.09$	$2.2 \pm 0.2$	$2600 \pm 200$
12451416–4429077	TWA 29	M9.5 $\gamma$	doi	$-2.9 \pm 0.1$	$2.0 \pm 0.2$	$2400 \pm 200$
12074836–3900043	TWA 40	L0 $\gamma$	oi	$-3.47 \pm 0.08$	$1.67 \pm 0.04$	$1890 \pm 90$
12073346–3932539 b	TWA 27 b	L3 $\gamma$ pec	di	$-3.59 \pm 0.02$	$1.62 \pm 0.01$	$1800 \pm 20$
11472421–2040204	TWA 41	L7 pec(red)	i	$-4.51 \pm 0.07$	$1.40 \pm 0.03$	$1140 \pm 50$
11193254–1137466	TWA 42	L7 pec(red)	i	$-4.3 \pm 0.1$	$1.44 \pm 0.05$	$1240 \pm 80$
<b>Candidate Members of TWA</b>						
10284580–2830374	TWA 34	M5 $\gamma$ e	oi	$-1.9 \pm 0.1$	$4.0 \pm 0.5$	$3100 \pm 300$
12175920–3734433	TWA 44	M5 $\gamma$ e	o	$-1.9 \pm 0.1$	$3.9 \pm 0.4$	$3100 \pm 200$
10585054–2346206	...	M6 $\gamma$ e	o	$-1.7 \pm 0.1$	$4.5 \pm 0.5$	$3200 \pm 300$
11112820–2655027	TWA 37	M6 $\gamma$ e	oi	$-1.7 \pm 0.1$	$4.4 \pm 0.5$	$3200 \pm 300$
12574941–4111373	...	M6 $\gamma$	i	$-2.2 \pm 0.1$	$3.0 \pm 0.3$	$2900 \pm 200$
12035905–3821402	TWA 38	M8 $\gamma$	i	$-2.80 \pm 0.09$	$2.1 \pm 0.2$	$2500 \pm 200$
11064461–3715115	...	M9	oi	$-3.1 \pm 0.1$	$1.8 \pm 0.1$	$2300 \pm 200$
11480096–2836488	...	L3 $\beta$	i	$-3.9 \pm 0.1$	$1.56 \pm 0.03$	$1500 \pm 100$

<sup>a</sup>Data used to derive the measurements presented in this table. d: trigonometric distance (otherwise kinematic distance assuming membership to TWA is used); i: NIR spectrum and photometry, o: optical spectrum and photometry.

NOTE—See Section 6 for more details.

### 6.2. *Effective Temperatures of Late-Type Members*

In the case of later-type ( $\gtrsim$  M6) targets, estimating effective temperatures is more delicate, especially because there are relatively large deviations in spectral types ( $\geq$  1–2 subtypes) depending upon what wavelength regime and/or spectral typing method is used. This is especially true for young substellar objects, in part because too few of them are known, which has yet prevented the construction of definite and reliable spectral standards.

For this reason, [Filippazzo et al. \(2015\)](#) developed an empirical method to estimate the bolometric luminos-

ity of an object using all available spectrophotometric data. A model-dependent radius must then be derived from this bolometric luminosity measurement, assuming an age of  $10 \pm 3$  Myr for all TWA objects ([Bell et al. 2015](#)). The inferred radius and empirical bolometric luminosity are then translated to an effective temperature using the Stefan-Boltzmann law. One major advantage of this method is that the result is weakly dependent on model systematics, as  $T_{\text{eff}}$  depends on the square root of the assumed radius, and as the radii of  $\sim 10$  Myr-old substellar objects only span a factor of  $\sim 2$  depending on the mass of the object.

The method of [Filippazzo et al. \(2015\)](#) was therefore used to estimate the effective temperature of targets in the TWA sample for which resolved NIR and/or optical photometry and spectroscopy were available. The resulting bolometric luminosities,  $T_{\text{eff}}$  and radii measurements are presented in Table 10. All measurements in common with those presented by [Faherty et al. \(2016a\)](#) and [Filippazzo et al. \(2015\)](#) agree within  $1.3\sigma$ . The differences are due to slightly different distance estimates (either because a different kinematic tool was used or because no radial velocity was available at the time), or because different spectra were used.

The resulting  $T_{\text{eff}}$  estimates were assumed to be described by Gaussian PDFs. A linear power law was then adjusted to the derived  $T_{\text{eff}}$  values as a function of spectral type, which yielded:

$$T_{\text{eff}} = 10^{3.46 - 0.0321(x-5)}, \quad (4)$$

where  $x$  is the numerical spectral type (e.g., M6 = 6, L0 = 10). The resulting spectral type– $T_{\text{eff}}$  relation is displayed in Figure 6(a) and is associated with a temperature scatter of 140 K. Note that this relation should only be used within the spectral type range M5–L7. It is likely that the slope of the spectral type– $T_{\text{eff}}$  relation will flatten at the L/T transition, however this remains to be demonstrated at such a young age.

To avoid the aforementioned problems (unknown unresolved binaries are of special concern given the high binary fraction in TWA), the spectral type– $T_{\text{eff}}$  relations of [Pecaut & Mamajek \(2013;  \$\leq\$  M5, see Section 6.1\)](#) and Equation (4;  $>$  M5) are used in the remainder of this work to transform gaussian spectral type PDFs into temperature PDFs.

### 6.3. Mass Estimates

The [Baraffe et al. \(2015\)](#) and [Siess et al. \(2000\)](#) model masses were separately interpolated on a regular  $10^4 \times 10^4$  logarithmic grid of  $T_{\text{eff}}$  and ages that span 400–17 000 K and 1 Myr–12 Gyr, respectively. The two grids were combined by adopting the [Baraffe et al. \(2015\)](#) masses below  $1.4 M_{\odot}$  and the [Siess et al. \(2000\)](#) models otherwise. The [Siess et al. \(2000\)](#) models overpredict  $T_{\text{eff}}$  by up to 500 K ( $\sim 14\%$ ) compared to [Baraffe et al. \(2015\)](#) in the mass range where both models are available ( $0.1$ – $1.4 M_{\odot}$ ); the [Baraffe et al. \(2015\)](#) models were adopted in this range as they include a more thorough treatment of convection, which is particularly important in this range of masses and age. The resulting mass– $T_{\text{eff}}$  relations that are obtained from a random draw along a log-normal distribution at the age of TWA ( $10 \pm 3$  Myr; [Bell et al. 2015](#)) are displayed in Figure 6(b). A combination of these model tracks with the spectral type– $T_{\text{eff}}$  relations derived above allows calculating mass–SpT tracks at the age of TWA; these are

displayed in Figure 6(c).

The model grid described above was used to transform the  $10^7$  Monte Carlo  $T_{\text{eff}}$  determinations of each target to a mass PDF, while assuming the same log-normal age prior as above. The resulting mass PDF functions are displayed for a selection of spectral types spanning A0 to L7 in Figure 6(d).

## 7. THE COMPLETENESS OF THE CURRENT TWA CENSUS

Measuring an accurate IMF for TWA requires computing the completeness as a function of mass for the census of TWA members. It is however not possible to determine it given current data; the set of TWA candidates and members presented here originates from 39 distinct surveys that are based on different selection criteria, several of which are still not completed or do not provide enough information to determine the survey completeness or the overlap between different surveys. For this reason, the IMF that is determined in Section 8 should be taken as preliminary until a single all-sky survey with a well defined completeness as a function of mass is carried out.

The *Gaia* Data Release 1 ([Lindegren et al. 2016](#)) does not allow to build a sample of TWA candidate members for which a completeness as a function of mass can be determined, because of several systematic effects and the heterogeneous nature of the sample ([Gaia Collaboration et al. 2016](#)). The full release of the *Gaia* mission will however provide a unique opportunity to assemble a well behaved sample of TWA candidates and members and re-visit the IMF of TWA, while taking completeness into account. The full release will include the full astrometric solution of 33/40 of the bona fide members and high-likelihood candidate members of TWA compiled in Section 5, as well as 35/44 of the candidate members and 12/16 of the low-likelihood candidate members. It will also likely uncover additional low-mass members of TWA.

In the low-mass regime, all current surveys for TWA members are at best limited by the 2MASS sensitivity. This is true even though the AllWISE survey is more sensitive to substellar objects than 2MASS, because proper motions derived from the WISE mission data alone are not precise enough to identify new TWA candidate members without relying on 2MASS (the typical precision is of 100–3000  $\text{mas yr}^{-1}$  for  $W1 \sim 13$ – $18$ ; [Kirkpatrick et al. 2014](#)). For this reason, the completeness limit of TWA candidates imposed by 2MASS is informative as it provides the best-case scenario for the completeness of low-mass TWA members. This completeness is determined in Section 7.1.

In Section 7.2, the completeness of the Hipparcos survey that was presented in Section 2.4 will be examined



to determine a mass regime within which completeness is constant as a function of mass.

### 7.1. The 2MASS Completeness of Low-Mass TWA Members

Although the census of 2MASS-detectable members of TWA is still likely incomplete, it is possible to use the spatial distribution of TWA members, combined with the sensitivity limits of 2MASS, to derive the maximum completeness of low-mass members that due to the 2MASS sensitivity limit.

This is especially important for TWA because its members span a wide range of distances ( $\sim 25\text{--}75$  pc). Such a correction will be most important for very low-mass and cool members with spectral types in the L spectral class, as will be demonstrated here. Such cool objects have very red  $J-K_S$  colors at young ages, which makes them more easily detected in the  $K_S$  band, despite the shallower  $K_S$ -band limiting 2MASS magnitude compared to  $J$  and  $H$ . For this reason, the determination of the completeness fraction carried out in this section will be based on the published sensitivity limits of 2MASS in the  $K_S$  band.

A photometric sequence in the  $K_S$  band must first be constructed for TWA members to perform this analysis. Such a sequence of absolute  $K_S$ -band magnitude as a function of spectral type is presented in Figure 7, using only high-likelihood candidates and bona fide members. Absolute magnitudes were corrected by adding a factor  $2.5 \log_{10} N$  for  $N$ -components equal-luminosity multiples. Equal luminosities were assumed when individual magnitude measurements were not available.

The magnitudes of TWA objects were interpolated on a regular grid in spectral type to obtain a smooth spectral type–absolute  $K_S$  magnitude sequence, to which a 7-order polynomial was fitted.

The  $K_S$ -band completeness fraction curve  $f_C(K_S)$  of 2MASS<sup>7</sup> was interpolated on a two-dimensional map  $\mathcal{K}_{i,j}$  of apparent  $K_S$ -band magnitudes, where the two dimensions correspond to a grid of distances  $\varpi_i$  (500 elements that range from 0.1 to 200 pc) and spectral types  $x_j$  (1000 elements that range from A0 to L8). This map of apparent  $K_S$ -band magnitudes can be described with the following equation:

$$\mathcal{K}_{i,j} = M_{K_S}(x_j) + 5 (\log_{10} \varpi_i - 1). \quad (5)$$

The spectral type dimension was subsequently mapped to most probable masses using the PDFs derived in Section 6 and displayed in Figure 6(c). The limiting distance at which TWA members can be de-

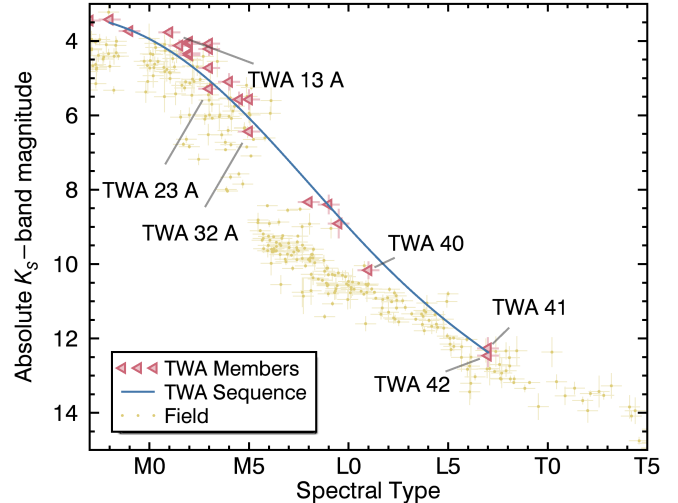


**Figure 7.** 2MASS  $K_S$ -band spectral type–absolute magnitude sequence (blue line) of high-likelihood and bona fide members of TWA (leftwards red triangles), corrected for unresolved companions. Field objects are represented with small yellow dots. See Section 7.1 for more details.

tected in 2MASS corresponds to the value of  $\varpi_i$  that yields a null completeness fraction  $f_C(\mathcal{K}_{i,j}) = 0$ . The solution to this constraint as a function of mass is displayed in Figure 8.

It is necessary to invoke a model of the TWA spatial distribution to determine the completeness limit of its members as a function of mass. The multivariate Gaussian spatial model developed in Section 5.2 was used to obtain the most up-to-date distance distribution of TWA members. A Monte Carlo simulation consisting in  $10^6$  random draws along this distribution was performed, and the distance to each of the  $10^6$  synthetic objects was calculated. A distance histogram was built from these to serve as a distance probability density distribution  $\mathcal{D}(\varpi_i)$ , which is displayed in Figure 9.

The completeness fraction as a function of mass  $f'_C(m_j)$  can then be obtained from the following expression:

$$f'_C(m_j) = \frac{\sum_i f_C(\mathcal{K}_{i,j}) \mathcal{D}(\varpi_i)}{\sum_i \mathcal{D}(\varpi_i)}. \quad (6)$$

This quantity is also displayed in Figure 8. It can be observed that more than 90% of TWA members with masses  $\geq 8.8 M_{\text{Jup}}$  should be detected in 2MASS, which correspond to temperatures of  $\gtrsim 1600$  K at the age of TWA, or to spectral types  $\lesssim \text{L3}$  (see Figure 6(a) and Filippazzo et al. 2015).

### 7.2. The Completeness of the Hipparcos Search for TWA members

The Hipparcos-based search for new TWA members presented in Section 2.4 can be used to determine a range of masses for which the sample completeness is

<sup>7</sup> Available at [http://www.ipac.caltech.edu/2mass/releases/allsky/doc/sec6\\_5a1.html](http://www.ipac.caltech.edu/2mass/releases/allsky/doc/sec6_5a1.html), Figure 5

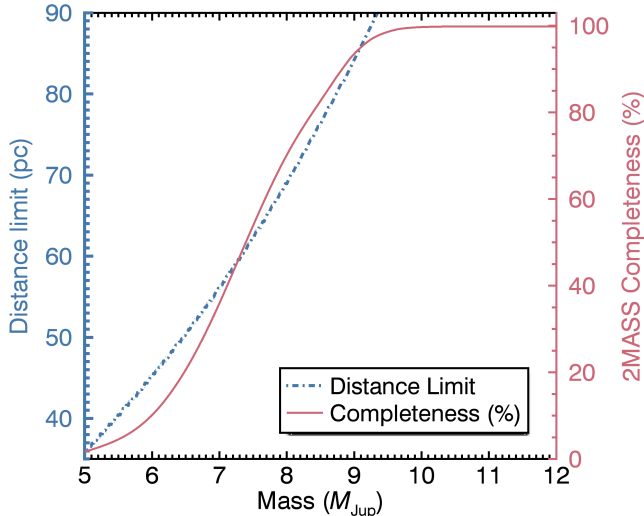


**Figure 8.** Limiting distance at which a TWA member of a given mass is detected in 2MASS (dash-dotted blue line) obtained from the photometric sequence of Figure 7 and the posterior mass distributions of Figure 6(d). The expected completeness fraction of TWA members, obtained from this limiting distance relation combined with the 2MASS  $K_S$ -band completeness limits and the BANYAN II spatial model of TWA, is displayed as a red line. See Section 7.1 for more details.

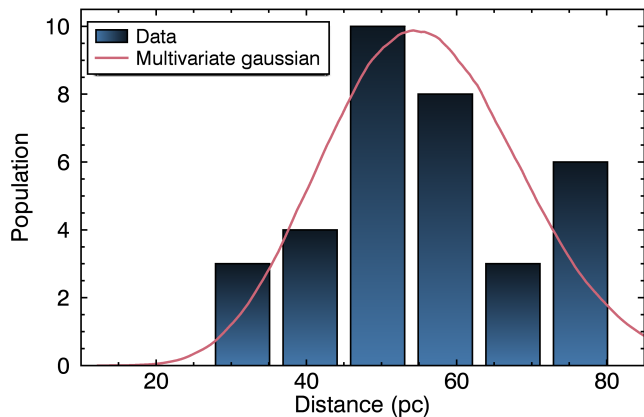


**Figure 9.** Distance histogram of TWA bona fide members and high-likelihood candidate members (dark blue bars), compared with a synthetic population drawn from a multivariate Gaussian PDF (red line). See Section 7.1 for more details.

largest and constant as a function of mass.

Although there is no published completeness curve as a function of magnitude for the Hipparcos survey, the Hipparcos input catalog was constructed to be complete for G5 or earlier stars that are brighter than  $V = 7.9 + 1.1 \sin |b|$ , where  $b$  is the Galactic latitude (Turon et al. 1992). In the case of later-type stars, this limiting magnitude is given by  $V = 7.3 + 1.1 \sin |b|$ . Averaging this limit over the spatial distribution of TWA members yields respective limiting magnitudes of  $V = 8.4$  and  $V = 7.8$  for early- and late-type stars.

A completeness curve for Hipparcos was determined using a Monte Carlo simulation:  $10^4$  synthetic objects were drawn from the spatial distribution of TWA presented in Equation (3) of Section 5.2 at each point of a  $10^3$  log-uniform array of masses, and the Choi et al. (2016) solar-metallicity isochrones at the age of TWA were used to determine their absolute  $V$ -band magnitudes and effective temperatures. The  $XYZ$  coordinates of each synthetic star were used to determine their distances, galactic latitudes, and relative  $V$ -band magnitudes. The G5 spectral type threshold that is used to select the appropriate magnitude limit corresponds to a temperature of 5500 K at the age of TWA (Pecaut & Mamajek 2013); the appropriate Hipparcos magnitude limit was used for each synthetic star to compute the fraction of stars that were detected in Hipparcos, while making the conservative assumption that no stars below the magnitude limits of Turon et al. (1992) were detected.

This Monte Carlo simulation yielded a minimal completeness curve as a function of mass for the TWA members detectable in Hipparcos, which is presented in Figure 10. This figure demonstrates that only TWA members with masses above  $\sim 1.43 M_{\odot}$  have been detected with confidence in Hipparcos. At the age of TWA, this mass corresponds to a temperature of  $\sim 5800$  K, or to the spectral type G2. Only two TWA members (TWA 11; A0 and TWA 43; A2) fall in this Hipparcos-complete regime. Hence, the Hipparcos survey does not provide a significant sample of bona fide TWA members to measure its IMF parameters in a regime of uniform completeness.

## 8. THE INITIAL MASS FUNCTION OF TW HYA

In this section, a continuous and empirical IMF of TWA is constructed. The Salpeter and log-normal functional forms are then fitted to this IMF using an MCMC statistical method that is independent on binning and accounts for small number statistics.

### 8.1. A Spatial Model of TWA

A model for the spatial extent of TWA must be considered to express the IMF as a space density rather than a number of stars. Such a model is available as part of the BANYAN II tool (Gagné et al. 2014c), however it does not benefit from recent updates to the list of high-likelihood members of TWA (see Section 5). For this reason, an updated spatial model of TWA is developed here.

To do this, a 3 dimensional version of the multivariate gaussian model of TWA that was described in Equation (3) was used, where only the spatial dimensions  $XYZ$  were conserved. The density  $n_{\text{max}}$  of objects at

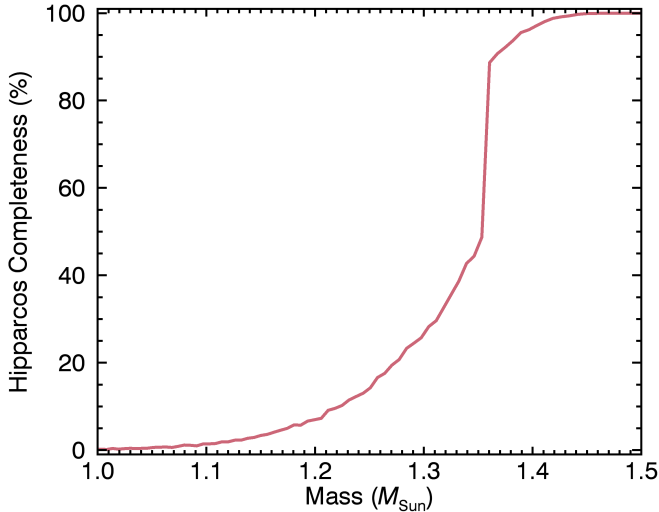


**Figure 10.** Sample completeness as a function of mass for TWA candidate members that are expected to be safely detected by the Hipparcos survey. The discontinuity at  $\sim 1.35 M_{\odot}$  is due to a break in the Hipparcos detection limit for stars later than G5. Only members with masses above  $\sim 1.43 M_{\odot}$  are all expected to be safely detected by Hipparcos. See Section 7.2 for more details.

the core of TWA then follows:

$$n_{\max} = N_{\text{tot}}/V_{\text{eff}}, \quad (7)$$

$$V_{\text{eff}} = (2\pi)^{3/2} \sqrt{|\Sigma|}, \quad (8)$$

where  $V_{\text{eff}}$  is referred to in this work as the *effective volume* of TWA. In the equation above, the covariance matrix  $\Sigma$  is a  $3 \times 3$  matrix that contains only the spatial coordinates.

The Galactic coordinates  $XYZ$  and measurement errors were calculated for all 31 high-likelihood and bona fide systems listed in Table 12. In the cases where a trigonometric distance was not available, the BANYAN II kinematic distance was used. The covariance matrix  $\Sigma$  and mean position  $\mathbf{X}_0$  were calculated in a Monte Carlo simulation with  $10^6$  cases that are normally distributed along measurements and errors of the  $XYZ$  positions of TWA members. This yielded an effective volume of  $V_{\text{eff}} = 6200_{-630}^{+690} \text{ pc}^3$ . The IMF of TWA can thus be divided by this volume to obtain a space density IMF.

**Table 11.** Best-Fitting IMF Parameters

Sample Name	$M_{\text{tot}}$ ( $M_{\odot}$ )	Salpeter			Log-normal					
		$\alpha$	$\phi_0$ ( $\text{pc}^{-3}$ )	$\rho(\alpha, \phi_0)$	$m_c$ ( $M_{\odot}$ )	$\sigma$ (dex)	$\phi_t$ ( $\text{pc}^{-3}$ )	$\rho(m_c, \sigma)$	$\rho(m_c, \phi_t)$	$\rho(\sigma, \phi_t)$
<b>Bona Fide Members and High-Likelihood Candidate Members</b>										
Primaries + Companions	$19.0_{-0.6}^{+0.4}$	$2.23_{-0.45}^{+1.05}$	$3.55_{-1.74}^{+0.64}$	-0.96	$0.21_{-0.06}^{+0.11}$	$0.76_{-0.13}^{+0.18}$	$9.8_{-1.4}^{+1.5}$	0.29	0.85	0.55
Primaries only	$12.6 \pm 0.3$	$1.92_{-0.45}^{+1.15}$	$2.15_{-1.02}^{+0.47}$	-0.90	$0.19_{-0.06}^{+0.14}$	$0.88_{-0.19}^{+0.25}$	$6.1_{-1.0}^{+1.1}$	0.35	0.84	0.51
<b>All Candidate Members Except Low-Likelihood</b>										
Primaries + Companions	$20.8_{-0.4}^{+0.3}$	...	...	...	$0.08 \pm 0.02$	$0.70_{-0.09}^{+0.12}$	$15.6_{-1.8}^{+2.2}$	0.74	0.86	0.71
Primaries only	$14.2_{-0.3}^{+0.5}$	...	...	...	$0.05 \pm 0.02$	$0.63 \pm 0.12$	$11.3_{-1.2}^{+1.8}$	0.72	0.83	0.70

NOTE—Results in the table section corresponding to all candidate members are not reported for samples that contain only high-likelihood candidates and bona fide members. See Section 8 for more details.

## 8.2. The Construction of a Continuous IMF

The mass probability functions that were derived in this work for individual TWA members (see Section 6) can be summed together to obtain a continuous version of the observed TWA IMF. Each candidate member’s mass PDF was weighted by  $1 - C_B$ , where  $C_B$  is the BANYAN II probability that a contaminant from the field imitates the properties of a given candidate member (see Section 5 of Gagné et al. 2014c for a detailed discussion), to account for the expected rate of false positives by assigning more weight to the more likely candidate members.

Four distinct IMFs were constructed for TWA, using a

variety of input data sets. The first class of two data sets includes only high-likelihood candidate members and bona fide members of TWA, whereas the second class of data sets also includes all candidate members (but excludes low-likelihood candidate members). The two subclasses are divided as follows: (1) primary and companion components of multiple systems are included (and counted as separate objects); and (2) only primaries of multiple systems (or isolated objects) are counted. The total masses of these four samples were also calculated and are listed Table 11. Calculating the total mass of multiple objects necessitates a special convolution-like combination of the individual PDFs, which is detailed in Appendix B. A total mass of  $19.0_{-0.6}^{+0.4} M_{\odot}$  was ob-

tained for the current census of TWA high-likelihood and bona fide members.

The compilation of TWA companions used to derive the companion IMF is likely incomplete and results in a compilation of heterogeneous literature searches for companions. It should therefore serve only as a rough estimation until a systematic search for TWA member companions is carried out.

Accounting for the effect of small number statistics in the calculation of the IMF requires to make the assumption that the formation of  $N$  stars in a given range of masses  $[m_0, m_1]$  is a random process in which every star formation event is independent of the previous ones to account for the effect of small number statistics in the calculation of the IMF. It follows that the PDF for the space density of objects  $n$  is described by a Poisson distribution  $\mathcal{P}(n|\lambda)$  parametrized with the mean number of star formation events  $\lambda$ , that is obtained from integrating the IMF  $\phi$  over this mass range:

$$\lambda = \int_{\log_{10} m_0}^{\log_{10} m_1} \phi(\log_{10} m) d \log_{10} m, \quad (9)$$

$$\mathcal{P}(n|\lambda) = \frac{e^{-\lambda} \lambda^n V_{\text{eff}}}{\Gamma(nV_{\text{eff}} + 1)}, \quad (10)$$

where  $\Gamma(x)$  is the Euler Gamma function.

The parameter  $\lambda$  can also be seen as the mean number of stars  $n$  that would be formed in the mass range  $[m_0, m_1]$  after a large number of simulations for the star formation of TWA members. The problem then consists of determining  $P(\lambda|n)$ , the PDF that describes the probable value of  $\lambda$  given the measured space density  $n$ . This can be obtained using Bayes' formula:

$$P(\lambda|n) = \frac{\mathcal{P}(n|\lambda)\pi(\lambda)}{P_n(n)}, \quad (11)$$

where  $\pi(\lambda)$  is the prior distribution on the parameter  $\lambda$ , and:

$$P_n(n) = \int_0^\infty \mathcal{P}(n|\lambda)\pi(\lambda) d\lambda. \quad (12)$$

The Jeffrey's non-informative prior (Jeffreys 1961) was chosen for  $\pi(\lambda)$ , which ensures in the case of 1-parameter PDFs that no prior knowledge on the value of this parameter is injected in the problem. This choice of a non-informative prior also ensures that the results will be independent under coordinate changes. The Jeffrey's prior of the Poisson distribution is given by Jaynes (1968):

$$\pi(\lambda) = \lambda^{-1/2}. \quad (13)$$

It follows that:

$$P_n(n) = \frac{\Gamma(nV_{\text{eff}} + 1/2)}{\Gamma(nV_{\text{eff}} + 1)}, \quad (14)$$

$$P(\lambda|n) = \frac{e^{-\lambda} \lambda^n V_{\text{eff}}^{-1/2}}{\Gamma(nV_{\text{eff}} + 1/2)}. \quad (15)$$

Hence, the value for the the cumulative IMF  $\Phi$  within a given range of masses follows the PDF described by Equation (15), which is a continuous analog of the Poisson distribution  $\mathcal{P}(k|\lambda)$  centered at  $k - 1/2$ , where the roles of the variable  $k$  and the parameter  $\lambda$  have been swapped.

The resulting IMF PDFs are displayed in Figure 11, along with binned versions that include Poisson error bars. It can be noted that there is an unexpectedly large number of candidate members with masses in the range 0.04–0.1  $M_\odot$ . Since this effect is not observed in the high-likelihood/bona fide members IMF, it could be caused by a larger number of contaminants at fainter magnitudes. This is similar to the relatively high fraction of M-type contaminants that were uncovered in Section 4, and would be consistent with the possibility that the large number of brown dwarfs in Upper Scorpius (Lodieu et al. 2007) could be artificial.

### 8.3. IMF Markov Chain Monte Carlo Fitting

The DREAM(ZS) Markov Chain Monte Carlo algorithm (ter Braak & Vrugt 2008) was used to determine the best parameters that fit the measured TWA IMFs. Initial parameter estimates for  $\phi_t$ ,  $\sigma$  and  $m_c$  were chosen by adjusting an error function to the cumulative IMF with a Levenberg-Marquardt least-squares fit (using the *mpfitfun.pro* IDL routine). In the case of a Salpeter functional form, the initial value for  $\alpha$  was set to the Salpeter slope  $\alpha = 2.35$ , and that of  $\phi_0$  was chosen as the value of the adjusted error function at  $m = 1 M_\odot$ . These initial parameter choices did not affect the posterior PDFs.

The DREAM(ZS) algorithm requires building an array of parameters for an initial set of synthetic samples; this was done by randomly selecting parameter values for 10D samples, where  $D$  is the number of parameters (2 when fitting a Salpeter form or 3 when fitting a log-normal form). These random values were centered around the initial parameter estimates with a scatter of one tenth of the initial estimates.

In all cases, we used  $2D + 1$  chains, a conservative  $10^3$  samples for the burn-in phase, and let the MCMC run for a total of  $10^5$  samples, with a thinning interval  $K = 10$ . The jumping scale factor  $\gamma$  of the algorithm was set to eight times the default value of  $2.38/\sqrt{2D}$  suggested by ter Braak & Vrugt (2008), to obtain mean acceptance rates below  $\sim 90\%$ . The Snooker update probability was set to the default value of 10%, and the

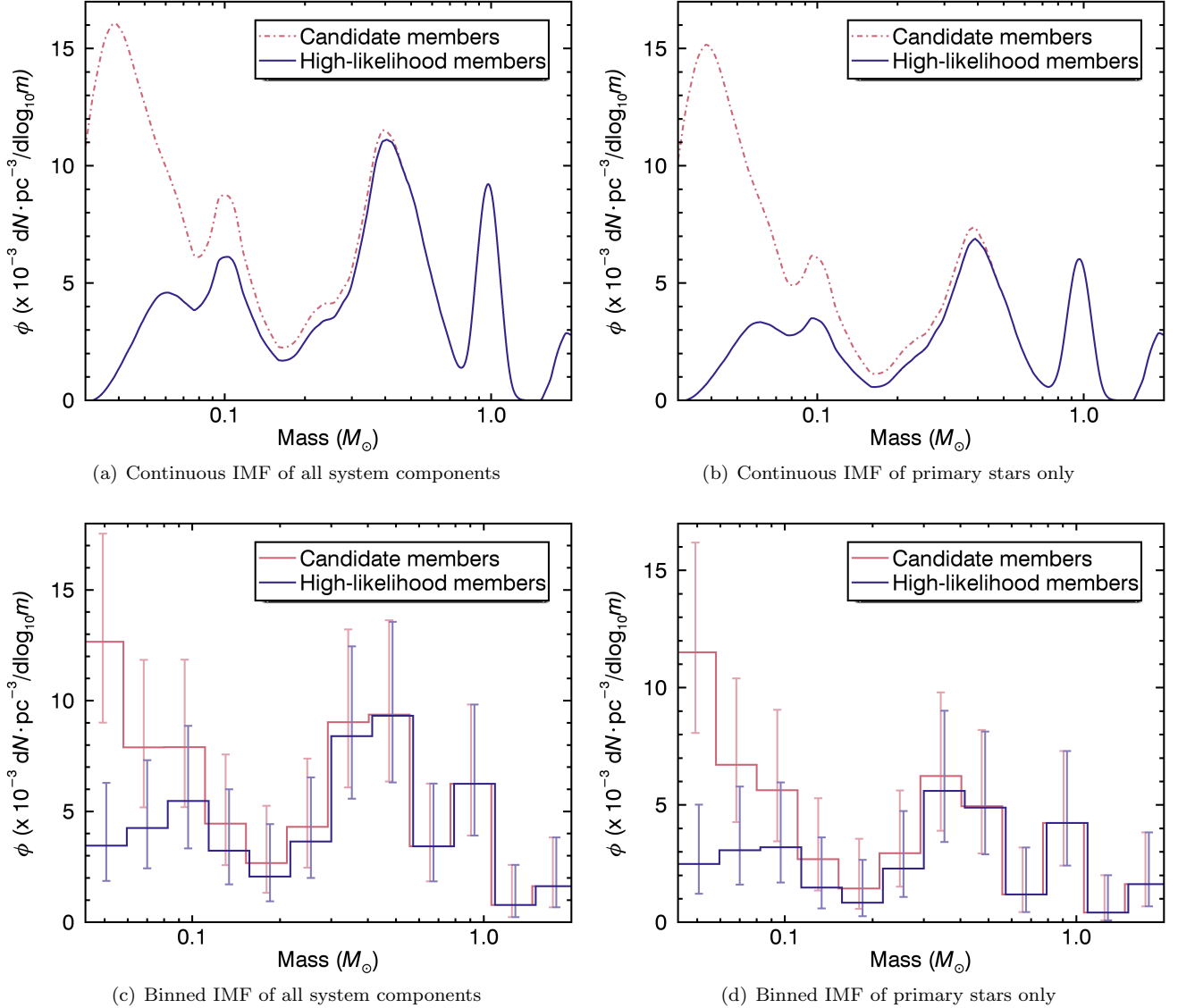


**Figure 11.** Panels a and b: Continuous IMFs of TWA candidate members (red dot-dashed line) and high-likelihood and bona fide members (blue line), for all system components (Panel a) and primary stars only (Panel b).

Panels c and d: Binned versions of the IMFs that include Poisson error bars and uncertainties on the volume of TWA. Bins of  $\Delta \log M_{\odot} = 0.13$  were used, with the same color scheme as Panels a and b. Histogram bars were shifted slightly to the left and right (by  $\pm 6 \times 10^{-3} M_{\odot}$ ) for visibility. See Section 8 for more details.

jumping scale factor during a Snooker update was set to  $\gamma_s = \sqrt{D}\gamma$ . The value of  $\gamma$  was set to unity once every 10 iterations, as suggested by [ter Braak & Vrugt \(2008\)](#). The improvement suggested by [Allers et al. \(2016\)](#) was used, where  $\gamma$  is inflated by a uniform random small number that is bound between  $-0.05$  and  $0.05$ . During Snooker updates, the value of  $\gamma_s$  was allowed to randomly vary by a factor  $1.3^{\pm 1}$ , which corresponds to the same fractional random scatter that was used by [ter Braak & Vrugt \(2008\)](#) with their value of  $\gamma_s$ .

The fits were performed directly on the cumulative IMFs to avoid the necessity of binning in accounting for small number statistics. The cumulative distribution

function of the Salpeter IMF has the form:

$$\Phi(\log_{10} m) = \frac{\phi_0}{(1-\alpha)\ln 10} (m_0^{1-\alpha} - m^{1-\alpha}), \quad (16)$$

where  $m_0$  is the lower mass bound, and the cumulative distribution function of the log-normal distribution has the form:

$$\Phi(\log_{10} m) = \frac{\phi_t}{2} \operatorname{erfc} \left( \frac{\log_{10} m - \log_{10} m_c}{\sigma\sqrt{2}} \right), \quad (17)$$

where  $\operatorname{erfc} x$  is the conjugate error function.

There is an additional complication in fitting a model to a cumulative distribution function. Using the classical approach of minimizing  $\chi^2$  would be mathematically



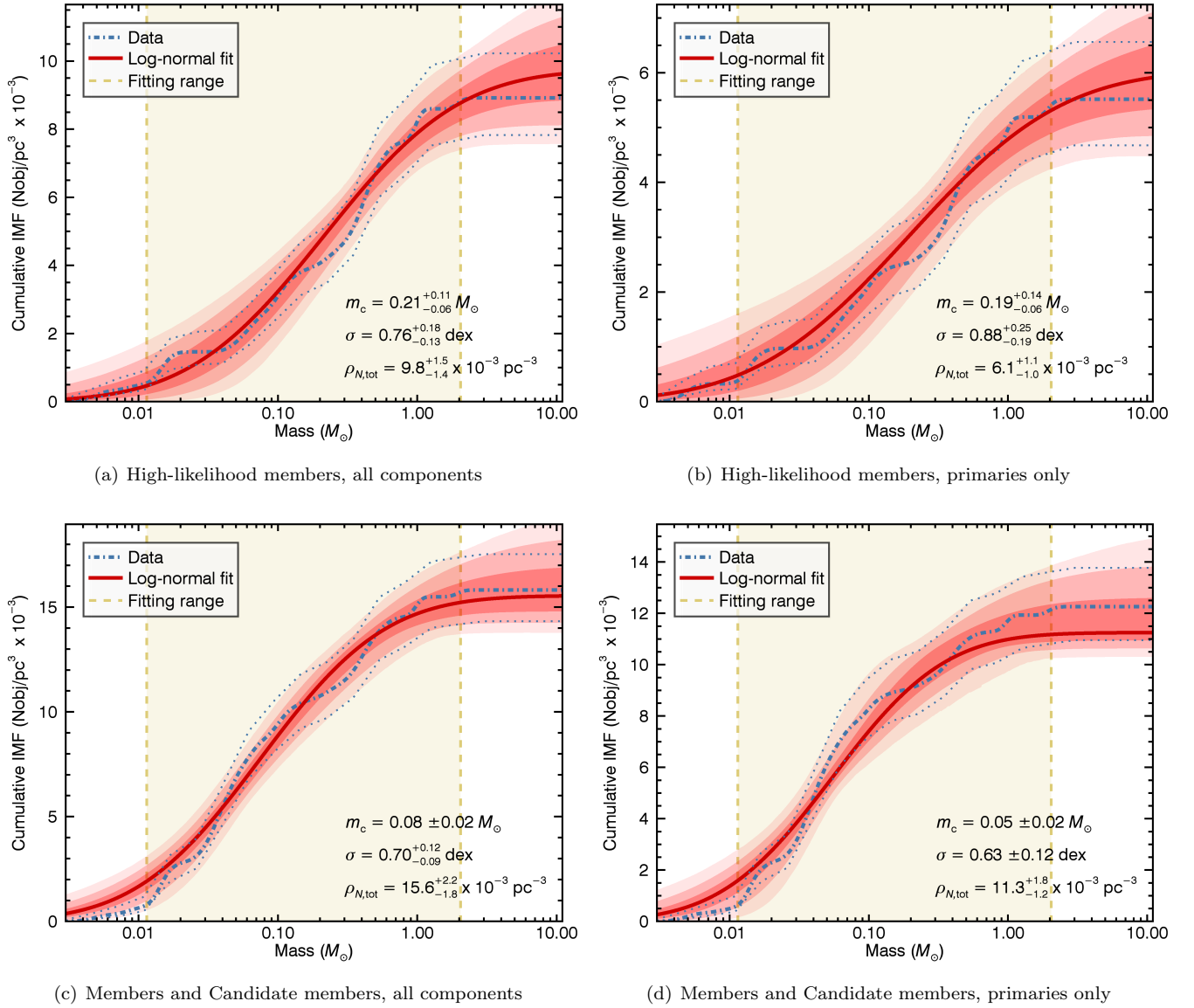


**Figure 12.** Fitted log-normal cumulative IMFs (thick red line) to the observed un-binned TWA cumulative IMFs (blue dash-dotted line). The thin blue dotted lines represent the  $\pm 1\sigma$  range due to small number statistics based on a Poisson distribution as well as errors on the TWA effective volume estimate. The yellow region represents the mass range used to perform the fit, and the red shaded regions indicate 1-3 $\sigma$  random draws from the MCMC solutions. See Section 8 for more details.

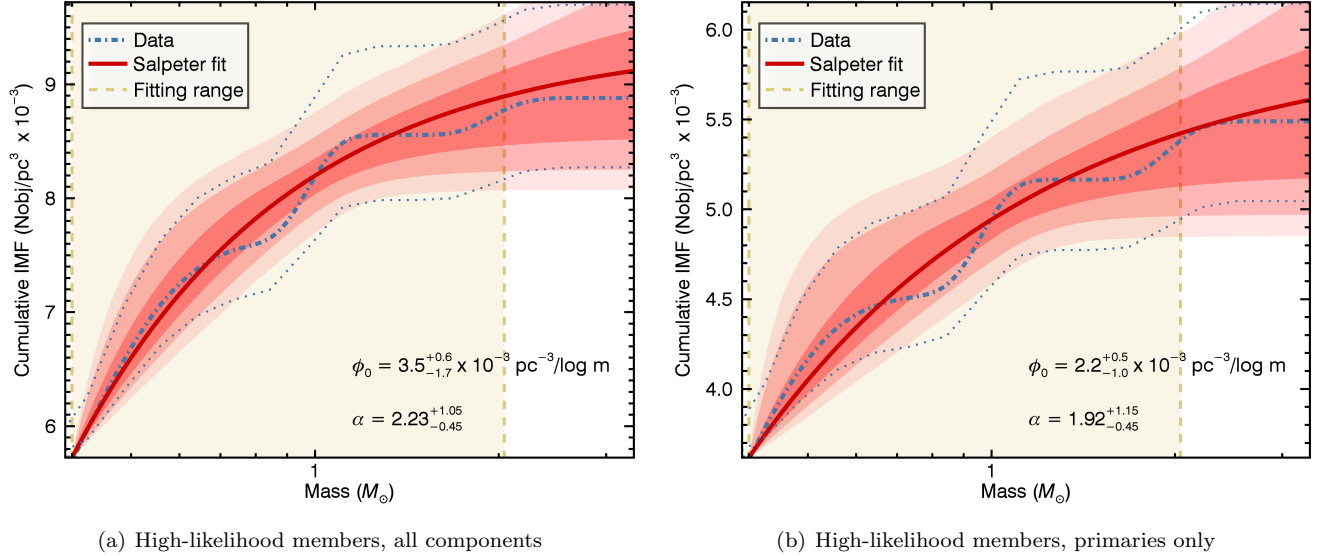


**Figure 13.** Fitted Salpeter cumulative IMFs to observed un-binned TWA cumulative IMFs. Colors and curves are similar to those of Figure 12. The cumulative integral of the IMFs used for the Salpeter fits have a lower bound of  $0.4 M_{\odot}$ . See Section 8 for more details.

inconsistent, as can be illustrated by the fact that the results would depend on the sampling of the cumulative IMF (e.g., a denser sampling would artificially yield smaller error bars on the best-fitting IMF parameters). The question that must be asked at a given step of the MCMC solver is the following: *What is the probability that the observed IMF was drawn from a given modelled cumulative IMF?* One way to answer this question, as suggested by Bastian et al. (2010), is to use a two-sided Kolmogorov-Smirnov (K-S) test (Kolmogorov 1933), which uses the maximal distance between two cumulative distribution functions to quantify the probability that their difference is significant.

In addition to the K-S test, a Poisson likelihood can be used to ensure that the value of the parameter  $\phi_0$  or  $N_{\text{tot}}$  is consistent with the observed total number of TWA members. As a consequence, the likelihood function that the MCMC algorithm will explore in the Salpeter case can be written as:

$$\mathcal{L}(\mathcal{D}|\phi_0, \alpha) = \mathcal{K}_S(\mathcal{D}|\alpha) \mathcal{P}(N_{\text{obs}}|\phi_{\text{tot}} V_{\text{eff}}), \quad (18)$$

where  $\mathcal{D}$  represents the data (the observed IMF),  $N_{\text{obs}}$  is the observed total number of TWA objects,  $\phi_{\text{tot}}$  is the total space density of objects (integrated over all masses) predicted from the model IMF,  $\mathcal{K}_S(\mathcal{D}|\alpha)$  is the probability returned by the K-S test given the data and model IMF, and  $\mathcal{P}(k|\lambda)$  is a Poisson distribution. In the log-normal case,  $\phi_0$  is replaced with  $\phi_t$  and  $\alpha$  is replaced with  $\{m_c, \sigma\}$  in the equation above.

The prior PDFs  $\pi_1(\phi_0, \alpha)$  and  $\pi_2(\phi_t, m_c, \sigma)$  were chosen such that no information is injected in the algorithm. In the present case where the likelihood depends on more

than one parameter, the Jeffrey’s priors do not correspond to the non-informative case, and the more general “reference priors” must be used instead (e.g., see Bernardo 1979). This choice of priors also ensures (1) that the problem is invariant under change of parameter variables, and (2) that the available data maximizes the difference between the prior and posterior distributions.

The determination of the reference prior associated with a likelihood is generally complicated to calculate, which is especially true in the present situation since the likelihood function includes a Kolmogorov-Smirnov test. Berger et al. (2009) presented a way to circumvent this with a numerical algorithm to compute the reference priors on a grid of parameters. The reference priors for the present problem were derived separately for the Salpeter and log-normal IMFs, and are discussed in more detail in Appendix C. Their applications did not significantly affect the resulting shapes of the posterior distributions.

#### 8.4. IMF Results

The MCMC fitting algorithm described above was applied on the four distinct sets of data that were previously mentioned. On each of these data sets, two fitting steps were performed: a log-normal IMF as described in Equation (2) was first fitted in the mass range  $12 M_{\text{Jup}} - 2 M_{\odot}$  and a Salpeter IMF as described in Equation (1) was then fitted in the mass range  $0.1 - 2.0 M_{\odot}$ . For the Salpeter fitting range, there were no candidate members in the TWA sample that were not also high-likelihood candidates or bona fide members, thus making the “members” or “candidates” IMFs identical. In this case, only a fit to the high-likelihood and bona fide members is thus reported.

A visual inspection of the chains revealed that the burn-in phase remained well within  $10^3$  samples in all cases. The autocorrelation length of the parameter chains were found to be in the range of 1–28 samples, meaning that the number of independent samples were in the range  $\sim 3\,500$ – $10\,000$ . Acceptance fractions in the range  $\sim 28$ – $75\%$  were obtained, depending on the data samples that were fit. The central parameter values reported in Table 11 were chosen as the peak locations of the marginalized PDFs, and the asymmetrical error bars were chosen as the regions that encompass 34% of the total area under its curve on each side.

The resulting cumulative IMFs are displayed in Figures 12 and 13 and the best-fitting parameters are listed in Table 11 along with their error bars and the Pearson correlation coefficients  $\rho(x, y)$  of two given parameters  $x$  and  $y$ . In most cases, correlations between the fitted parameters are significant. The error bars on the volume of TWA were added in quadrature to those of the space density parameters  $\phi_0$  and  $\phi_t$ . The best-fitting IMF curves are displayed in Figure 14.

All posterior PDFs are unimodal, but are not always well represented by Gaussian distributions, even if asymmetrical error bars are used. The marginalized PDFs for  $\alpha$  (Salpeter fit) in particular are heavy-tailed, with residual kurtosis values in the range  $\kappa \simeq 2$ – $16$ . This is also true to a lesser extent for the central mass ( $\kappa \simeq 0.1$ – $2.5$ ) and the characteristic width ( $\kappa \simeq 0.3$ – $2$ ) of the log-normal fits. All other cases have  $0 < \kappa < 1$ .

The Kullback-Leibler divergence  $D_{\text{KL}}(P||G)$  between the true PDF  $P$  and an asymmetrical Gaussian PDF  $G$  (see Kullback & Leibler 1951) was calculated to characterize how much information is lost when representing the true posterior PDFs using asymmetrical Gaussians with the values provided in Table 11. This divergence characterizes the entropy increase when representing  $P$  with  $G$ . This value was then compared with the Shannon entropy (Shannon & Weaver 1949)  $H$  of the true PDF, to obtain the fractional amount of entropy  $f_E$  that is gained when representing  $P$  with  $G$ , where  $f_E = D_{\text{KL}}/H$ . Low values of  $f_E < 6\%$  were obtained for all parameters except  $\alpha$  (Salpeter), meaning that the loss of information is small when approximating their posterior PDFs with asymmetrical Gaussians. In the case of  $\alpha$ , fractional entropy gains were found to be in the range 7–52%.

A Salpeter slope of  $\alpha = 2.2_{-0.5}^{+1.1}$  is obtained in the generic case of high-likelihood and bona fide members, where multiple system components are treated as separate objects. This value is similar to the Salpeter slope of field stars ( $\alpha = 2.35$ ; Salpeter 1955), despite the exclusion of 2– $10 M_\odot$  objects in the present analysis – including this mass range is impossible since there are no such known members of TWA. It is possible that the

Salpeter slope derived here is biased towards a shallower (lower) value due to the incompleteness of  $< F6$  stars in the current TWA sample.

The log-normal fit for the same case scenario yields a central mass of  $m_c = 0.21_{-0.06}^{+0.11} M_\odot$  and a characteristic width of  $0.8_{-0.1}^{+0.2}$  dex. The central mass derived here is consistent with typical values obtained for the field ( $m_c = 0.15$ – $0.25 M_\odot$ ; Chabrier 2005), and is smaller than the previous estimation of the TWA IMF ( $0.4$ – $0.6 M_\odot$ ; Looper 2011), which was carried out when fewer TWA brown dwarf members were known. Including candidate members in the IMF calculations drives the central mass to a much lower value of  $m_c = 0.08 \pm 0.02 M_\odot$ , slightly below the brown dwarf/low-mass star boundary. This is related to the previously mentioned large number of TWA candidate members in the  $0.04$ – $0.1 M_\odot$  range, which are possibly due to significant contamination from interlopers unrelated to TWA in the sample. It can therefore be expected that the true central mass of TWA members will be located between these two values, and may still agree with IMF determinations based on field stars.

The characteristic widths that are obtained here are high compared to most determinations based on the field or other young associations ( $0.3$ – $0.55$  dex; Bochanski et al. 2011; Jeffries 2012), whether candidate members are included in the analysis or not. This may indicate that completing the census of low-mass members of TWA might not remove this discrepancy, however this is not definitive as the completeness of low-mass stars of the current sample of TWA candidates and members is not known. Such a large characteristic width is consistent with the observation that the IMF of the current TWA census is flatter than that of the field or other young associations (Looper 2011).

In comparison to these previous determinations of the TWA IMF, the *primaries only* and *primaries + companions* case scenarios display similar log-normal shape parameters. This should however be seen as a tentative result since the binary fraction of very low-mass objects in TWA is largely unexplored. It is therefore subject to change when future surveys identify additional low-mass companions of TWA members.

## 9. THE SPACE DENSITY OF ISOLATED PLANETARY-MASS OBJECTS IN TW HYA

The recent discovery of two isolated high-likelihood candidate members of TWA with estimated masses in the range  $\sim 5$ – $7 M_{\text{Jup}}$  prompts an estimation of their total population. Since such objects are located near the 2MASS detection limit, only those at the nearest end of TWA should have been discovered to date. Adopting a Poisson probability distribution described by Equation (15), one can estimate  $\lambda$ , the value of the mea-

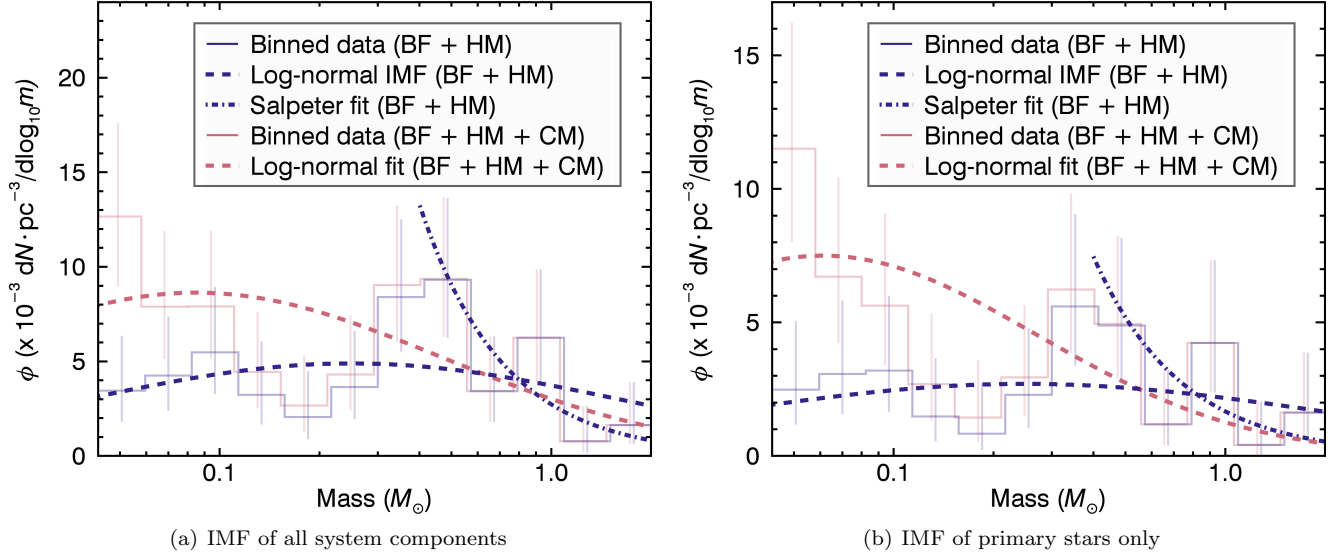


**Figure 14.** Best log-normal and Salpeter fits compared to the observed binned IMFs of TWA objects, for the four input samples described in the text. *BF+HM* indicates bona fide members and high-likelihood candidate members only, whereas *CM* indicates all currently known candidate members. Binned versions of the empirical IMFs are displayed here to make the comparison easier because Poisson error bars cannot be determined for a continuous un-binned IMF. See Section 8 for more details.

sured IMF integrated over this specific mass range. This yields an estimate of  $\lambda = 1.5^{+2.0}_{-0.7}$  objects. At a completeness limit of  $\sim 15\%$  (obtained from the statistical expectation of the relation displayed in Figure 8 over the mean mass PDF of TWA 41 and TWA 42), this corresponds to an estimated total of  $10^{+13}_{-5}$  similar isolated objects in TWA. The mass estimates of these objects are strongly model-dependent and rely on a hot-start formation mechanism, but it can be noted that this predicted population is not model-dependent if viewed as that of TWA members with absolute magnitudes  $K_S \sim 12.2$ – $12.5$ . This expected population is based on the assumption that TWA 41 and TWA 42 are members of TWA. Only trigonometric distances remain to be measured for this to be confirmed, and the case for their membership is strengthened by their spectrophotometric distances (accounting for their young age) that are consistent with their TWA kinematic distances.

Using the effective volume of TWA that was estimated in Section 8 ( $V_{\text{eff}} = 6200^{+690}_{-630} \text{ pc}^3$ ), this population of  $\sim 5$ – $7 M_{\text{Jup}}$  objects can be translated to a space density around the core of TWA. This calculation yields a space density of  $1.7^{+2.1}_{-0.8} \times 10^{-3} \text{ objects pc}^{-3}$ . This is remarkably high in comparison to the space density of field stars ( $93 \pm 20 \times 10^{-3} \text{ stars pc}^{-3}$ ; Chabrier 2005), as it would account for one such isolated planetary-mass object for every  $24^{+42}_{-9}$  main-sequence stars in the field. This is not simply due to TWA being denser than the field: this estimate corresponds to one expected  $\sim 5$ – $7 M_{\text{Jup}}$  TWA object for every  $1.9^{+3.1}_{-0.6}$  currently known main sequence ( $\geq 75 M_{\text{Jup}}$ ) member of TWA.

This estimated fraction of planetary-mass to stellar

TWA members is larger than recent estimates based on the lowest-mass candidate members of the Tucana-Horologium Association (THA). Gagné et al. (2015d) estimated this fraction at one  $12.5$ – $14.0 M_{\text{Jup}}$  object per  $17.5^{+6.6}_{-5.0}$  main-sequence member of THA. Using the Bayesian formalism presented here, we revise this to one low-mass object per  $16.6^{+4.8}_{-3.2} \times 10^{-3} \text{ objects pc}^{-3}$  main-sequence THA member. This estimate remains high in comparison to predictions based on a log-normal IMF of TWA. Such an estimation for TWA, based on the *primary + companions* IMF of high-likelihood and bona fide members (Section 8), would predict a total of only  $0.5^{+0.4}_{-0.2} \sim 5$ – $7 M_{\text{Jup}}$  objects in the whole TWA association.

It is possible to make a prediction for the field space density of  $\sim 5$ – $7 M_{\text{Jup}}$  objects by assuming that the low-mass end of the field IMF is identical to that of TWA. This was done by assuming that the field is well represented by a fiducial log-normal IMF anchored on the stellar space density of Chabrier (2005), and anchoring it in turn on the stellar population of TWA. Since TWA has a notable lack of massive, early-type stars (no A3–G9 high-likelihood candidates or members are currently known), the field IMF was anchored on K0–K9 members of TWA, corresponding to a mass range of  $\sim 0.7$ – $1.5 M_{\odot}$ . This calculation based on TWA yields a predicted space density of  $26^{+29}_{-15} \times 10^{-3} \text{ objects pc}^{-3}$  for field  $\sim 5$ – $7 M_{\text{Jup}}$  objects, most of which would be faint, Y-type dwarfs ( $\lesssim 300 \text{ K}$ ; Luhman 2014). This estimate should be seen as an upper limit because it is likely that there are still K dwarfs that are missing in the current TWA census. We avoided anchoring this estimation on the two A-type

members of TWA (A0 and A2) because these spectral types span a small range of masses ( $1.84\text{--}2.00 M_{\odot}$ ) at the age of TWA (see Figure 6(c)). A similar calculation based on the low-mass members of THA would predict a lower space density of  $4.6_{-1.2}^{+2.0} \times 10^{-3}$  objects  $\text{pc}^{-3}$  for objects at the deuterium-burning limit ( $12.5\text{--}14.0 M_{\text{Jup}}$ ), which would correspond to early Y-type dwarfs ( $\sim 300\text{--}400\text{ K}$ ; Cushing et al. 2011) at the age of the field.

A calculation similar to the one carried out in Section 8 yields an effective volume of  $15200_{-700}^{+900} \text{pc}^3$  for THA. This allows an estimation of the THA density of stars ( $23.1_{-1.7}^{+1.8} \times 10^{-3}$  objects  $\text{pc}^{-3}$ ) and objects at the deuterium-burning limit ( $1.3 \pm 0.4 \times 10^{-3}$  objects  $\text{pc}^{-3}$ ). This demonstrates that THA is denser than TWA (the latter has a core stellar density of  $7.2_{-1.2}^{+1.4} \times 10^{-3}$  objects  $\text{pc}^{-3}$ ), but still much sparser than the population of field stars.

The recent discovery of WISE J085510.83–071442.5 (W0855 hereafter; Luhman 2014), which is an isolated  $\sim 3\text{--}10 M_{\text{Jup}}$  object unrelated to TWA and located at a distance of  $2.23 \pm 0.04 \text{pc}$  (Luhman & Esplin 2016), also hints at the possibility that isolated objects in the planetary-mass regime may be more numerous in the field than predictions from a fiducial log-normal IMF. Deriving the space density PDF associated with one such object in a spherical volume with a radius of  $2.31 \pm 0.08 \text{pc}$  while accounting for Poisson statistics yields a space density estimate of  $25_{-17}^{+30} \times 10^{-3}$  objects  $\text{pc}^{-3}$  for objects similar to W0855. This estimate is associated with large error bars because it is based on only one object, however even the 99.7% ( $3\sigma$ ) interval of this PDF would be consistent with a minimal space density of  $3.3 \times 10^{-4}$  objects  $\text{pc}^{-3}$ .

The results of Scholz et al. (2012) indicate that there may be as few as one  $5\text{--}15 M_{\text{Jup}}$  object for every 20–50 stars in the young ( $\sim 1 \text{Myr}$ ) association NGC 1333, in strong contradiction with other results mentioned above. Similar but less constraining results have been obtained by Muzic et al. (2015) for the  $\sim 2 \text{Myr}$ -old Chamaeleon I region, and by Comerón (2011) and Muzic et al. (2015) for the  $\sim 1 \text{Myr}$ -old Lupus 3 region. Results by Marsh et al. (2010) yielded estimates of planetary-mass to main-sequence population ratios in the  $\sim 1 \text{Myr}$   $\rho$  Oph cloud core region that are more in line with our findings for TWA (see Figure 15). Detailed studies of completed young moving group censuses in the Solar neighborhood will be needed to assess whether young moving groups have fractions of isolated planetary-mass objects that are fundamentally different from NGC 1333.

In Figure 15, space densities per logarithmic mass intervals from different works are compared with a typical log-normal IMF anchored on the stellar space density of Chabrier (2005). This figure demonstrates how the current planetary-mass space-density estimates of THA

and TWA are higher than the predictions from a typical log-normal IMF anchored on the space density of main-sequence stars in the field, even though the stellar densities of both associations are much sparser than those of field stars. Predictions for the field space densities of planetary-mass (mostly Y-type) dwarfs are also displayed from the data available for both associations.

## 10. SUMMARY AND CONCLUSIONS

New optical and near-infrared spectra were presented for several candidate members of TWA, in addition to 17 new radial velocity measurements. These new data allowed us to secure four new high-likelihood candidate members (2MASS J10284580–2830374 or TWA 34; 2MASS J12074836–3900043 or TWA 40; 2MASS J11472421–2040204 or TWA 41; and 2MASS J12175920–3734433 or TWA 44; i.e., objects with only a radial velocity, parallax or signs of youth left to measure) and three new bona fide members (TWA 28, TWA 29 and TWA 33).

The updated census of TWA objects contains 13 high-likelihood candidate members (11 systems) and 42 bona fide members (23 systems) with spectral types in the range A0–L7 and estimated masses in the range  $\sim 5 M_{\text{Jup}}\text{--}2 M_{\odot}$ . A determination of the initial mass function of TWA is presented using this updated census and a statistically robust method. A log-normal distribution was found to reproduce well the observed IMF of TWA, with a characteristic width that is larger than typical values for the field and other young associations. These results are however possibly biased by the unknown completeness in the current sample of TWA candidates and members, which was constructed from a heterogeneous set of surveys. It is possible that a significant incompleteness in the low-mass star regime could entirely explain the unusually flat IMF.

The recent discoveries of two new, isolated  $\sim 5\text{--}7 M_{\text{Jup}}$  high-likelihood members of TWA at the nearby end ( $\sim 29$  and  $\sim 31 \text{pc}$ ) of its spatial structure are indicative that several more such members might remain to be discovered. We argue that only the nearest of these objects have been discovered yet because of the limited sensitivity of 2MASS, and that accounting for the spatial structure of TWA and Poisson statistics based on these two detections, a total of  $10_{-5}^{+13}$  TWA members with similar properties could be expected.

This is much higher than what would be expected based on a log-normal IMF that is anchored on the higher-mass population of TWA. This possible overdensity of objects in the planetary-mass regime is surprising, but consistent with recent estimates for the space density of objects at the deuterium-burning limit in THA (Gagné et al. 2015d), the recent discovery of a cold, planetary-mass Y dwarf at only 2 pc from the Sun



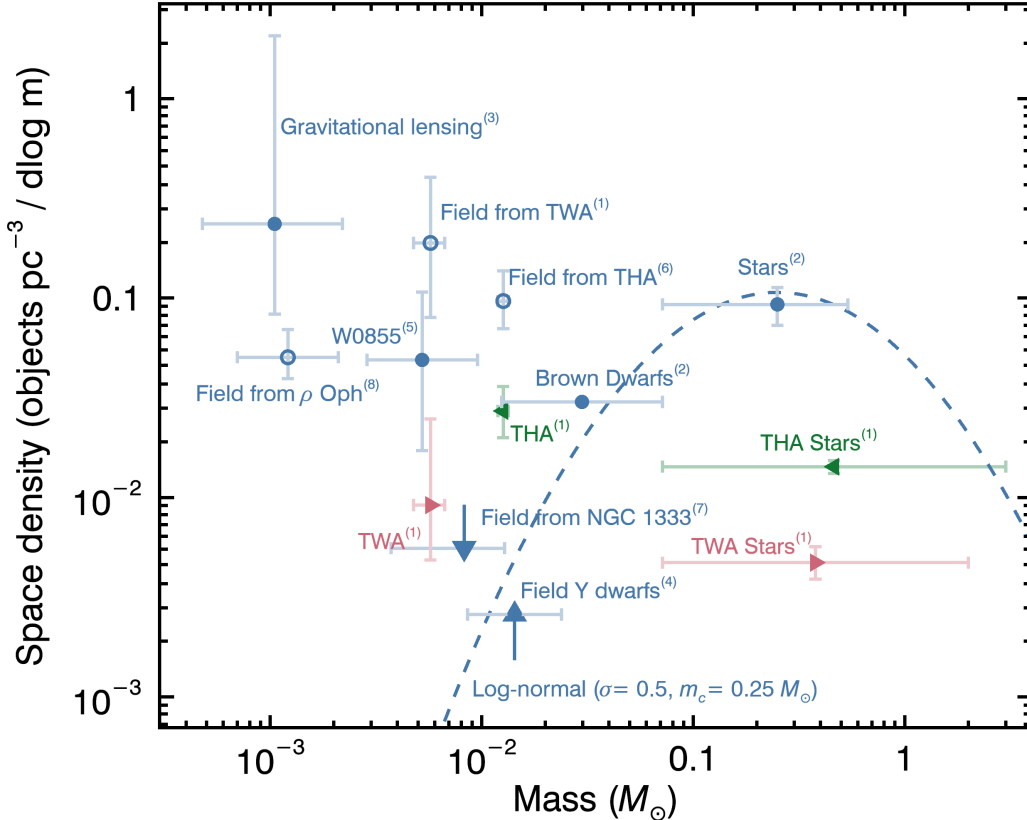


**Figure 15.** Estimates of space densities per unit logarithmic mass from various works, compared to a fiducial log-normal IMF ( $\sigma = 0.5$ ,  $m_c = 0.25 M_\odot$ ) anchored on the space density of stars (blue dashed line). All blue circles represent estimates for field objects; filled circles are direct measurements, and open circles are predictions for the field based on the IMFs of TWA and THA anchored on the stellar space density estimated by [Chabrier \(2005\)](#). “Field from TWA” indicates the estimated field space density based on the ratio of low-mass to main-sequence stars in TWA and the [Chabrier \(2005\)](#) space density of main-sequence stars. The space density of Y dwarfs (blue upwards triangle) is a lower limit, the space density translated to the field from NGC 1333 (blue downwards triangle) is an upper limit, and the predicted field space density based on TWA should be seen as an upper limit, due to the incomplete census of low-mass stars in TWA. Red rightwards triangles are estimates for TWA and green leftwards triangles are estimates for THA. References in this figure are as follows: (1) This paper; (2) [Chabrier 2005](#); (3) [Sumi et al. 2011](#); (4) [Kirkpatrick et al. 2011](#); (5) [Luhman 2014](#); (6) [Gagné et al. 2015d](#); (7) [Scholz et al. 2012](#); (8) [Marsh et al. 2010](#). See Section 9 for more details.

([Luhman 2014](#)), as well as results from micro-lensing surveys ([Sumi et al. 2011](#)).

More studies will be needed to further assess the apparent discrepancy between the aforementioned results and those of [Scholz et al. \(2012\)](#) for the NGC 1333 association, which seems to have less than one  $5\text{--}15 M_{\text{Jup}}$  object for every 20–50 stars. For example, the James Webb Space Telescope will open the doors to a detailed study of a large number of more distant young clusters, which their IMFs to be characterized with a high significance down to  $\sim 1 M_{\text{Jup}}$ . The *Gaia* mission will also allow completing the stellar census of TWA and other young moving groups, which will allow determining a more precise ratio of their BDs or planetary-mass objects to stellar members.

Our results indicate that many isolated planetary-mass members of TWA might still be hiding in deep large-area surveys such as VHS and AllWISE. It will

however be challenging to identify them due to the relatively short temporal baseline between these surveys ( $\sim 1$  yr), which makes it impossible to derive proper motions at the  $\sim 10 \text{ mas yr}^{-1}$  precision using the survey data alone. Future surveys such as LSST ([Ivezić et al. 2008](#)) and MaxWISE ([Faherty et al. 2015](#)) will be able to reveal the population of TWA members well into the planetary-mass regime at distances up to 80 pc.

The authors would like to thank the anonymous referee for comments and suggestions that significantly improved the quality of this manuscript, as well as Tri L. Astraatmadja for help with the *Gaia* DR1, and Robert Simcoe for help with the FIRE data reduction. We thank Sarah Schmidt, Isabelle Baraffe, Gilles Chabrier, Peter Plavchan, Niall Deacon, Brendan Bowler, Michael Betancourt and Thierry Bazier-Matte for useful comments. We thank Kelle Cruz, Haley Fica, Victoria

Ditomasso, Alan Munazza and Carolina Galindo for help with the observing. We thank Katelyn N. Allers and Michael C. Liu for sharing data. We thank the Gemini queue mode observers for data that was included in this work: Eder Martioli, Robert Bassett, K. Scott, Kathy Roth, Vinicius Placco, James Turner, Pablo Prado, Rachel Mason, Tom Geballe, Peter Pesev, German Gimeno, Mischa Schirmer, Eduardo Marin, Erich Wenderoth, David A. Krogsrud, Andrew Cardwell, Joanna E. Thomas-Osip, André-Nicolas Chené, Percy L. Gomez. This work has benefitted from the *Best practices for reporting the results of MCMC analyses* document, created by Peter K. G. Williams and located at <https://github.com/pkgw/mcmc-reporting>.

This work was supported in part through grants from the Natural Science and Engineering Research Council of Canada. *EEM* acknowledges support from National Science Foundation (NSF) award *AST-1313029* and the NASA NExSS program, and *SL* acknowledges support from NSF grant *AST 09-08419*. This research has benefitted from the SpeX Prism Spectral Libraries, maintained by Adam Burgasser at <http://pono.ucsd.edu/~adam/browndwarfs/spexprism>. This document has benefitted from technical report SRON/EPS/TN/09-002 prepared by Paul Tol on color blind-friendly color schemes. This research made use of: the SIMBAD database and Vizier catalog access tool, operated at the Centre de Données astronomiques de Strasbourg, France (Ochsenbein et al. 2000); data products from the Two Micron All Sky Survey (*2MASS*; Skrutskie et al. 2006; Kirkpatrick et al. 2003), which is a joint project of the University of Massachusetts and the Infrared Processing and Analysis Center (IPAC)/California Institute of Technology (Caltech), funded by the National Aeronautics and Space Administration (NASA) and the National Science Foundation (Skrutskie et al. 2006); data products from the *Wide-field Infrared Survey Explorer* (*WISE*; Wright et al. 2010), which is a joint project of the University of California, Los Angeles, and the Jet Propulsion Laboratory (JPL)/Caltech, funded by NASA; the VISTA Hemisphere Survey, ESO Program, 179.A-2010 (PI: McMahon); the NASA/IPAC Infrared Science Archive (IRSA), which is operated by JPL, Caltech, under contract with NASA; and the Infrared Telescope Facility (IRTF), which is operated by the University of Hawaii under Cooperative Agreement NNX-08AE38A with NASA, Science Mission Directorate, Planetary Astronomy Program. This work has made use of data from the European Space Agency (ESA) mission *Gaia* (<http://www.cosmos.esa.int/gaia>), processed by the *Gaia* Data Processing and Analysis Consortium (DPAC, <http://www.cosmos.esa.int/web/gaia/dpac/consortium>). Funding for the DPAC has been provided by national institutions, in

particular the institutions participating in the *Gaia* Multilateral Agreement. Part of this research was carried out at the JPL, Caltech, under a contract with NASA.

This paper includes data gathered with the 6.5 meter Magellan Telescopes located at Las Campanas Observatory, Chile (CNTAC program CN2013A-135). Based on observations obtained as part of the VISTA Hemisphere Survey, ESO Program, 179.A-2010 (PI: McMahon). Based on observations obtained at the Gemini Observatory through programs number GN-2013A-Q-106, GN-2014A-Q-94, GS-2012B-Q-70, GS-2013A-Q-66, GS-2014A-Q-55, GS-2015A-Q-85 and GS-2015A-Q-60. The Gemini Observatory is operated by the Association of Universities for Research in Astronomy, Inc., under a cooperative agreement with the National Science Foundation (NSF) on behalf of the Gemini partnership: the NSF (United States), the National Research Council (Canada), CONICYT (Chile), the Australian Research Council (Australia), Ministério da Ciência, Tecnologia e Inovação (Brazil) and Ministerio de Ciencia, Tecnología e Innovación Productiva (Argentina). All data were acquired through the Canadian Astronomy Data Center. This material is based upon work supported by AURA through the National Science Foundation under AURA Cooperative Agreement AST 0132798 as amended. This publication uses observations obtained at IRTF through program number 2015B091. The authors recognize and acknowledge the very significant cultural role and reverence that the summit of Mauna Kea has always had within the indigenous Hawaiian community. We are most fortunate to have the opportunity to conduct observations from this mountain.

*JG* wrote the manuscript, generated figures, tables and led most of the analysis; obtained and reduced the Flamingos-2 data; obtained the GMOS data; obtained parts of the SpeX and FIRE data; reduced the SpeX data and parts of the FIRE data; and led the BASS-Ultracool survey. *JKF* obtained parts of the FIRE and SpeX data; reduced parts of the FIRE data; provided help with observing and writing; and ideas in designing the BASS-Ultracool survey; *EEM* performed the isochrone analysis of the Hipparcos candidates, wrote most of Section 2.4 and performed the related analysis, and generated Figure 1; *RD* led the kinematic reanalysis of Hipparcos data; *JCF* calculated bolometric luminosities and effective temperatures for substellar objects; *AJW* and *JKD* provided parallax data and ideas for the IMF analysis; *LM* obtained, reduced and analyzed ESPADONS data and performed the identification of TWA candidates from SUPERBLINK-South; *DL* and *ÉA* provided useful comments and help with parts of the observing; *AJB* and *DL* provided SpeX data and additional information on some TWA members; *YB* ob-

served parts of the FIRE data; *AB* led the TWA 37 WISE excess analysis; *SL* led the SUPERBLINK-South survey; *CB* and *GA* reduced and analyzed the GMOS data; and *SC* observed parts of the SpeX data.

*Facility:* Gemini-South (Flamingos-2); Gemini-South (GMOS); Gemini-North (GMOS); IRTF (SpeX); Magellan:Baade (FIRE)

*Software:* IDL by Harris Geospatial, Notability by Ginger Labs, Texpad by Valletta Ventures LLP

Table 12. Kinematic Properties of Candidates and Members of TWA

2MASS Designation	Other Names	RA J2000	DEC J2000	$\mu_{\alpha} \cos \delta$ (mas yr <sup>-1</sup> )	$\mu_{\delta}$ (mas yr <sup>-1</sup> )	RV (km s <sup>-1</sup> )	Distance (pc)	Refer- ences <sup>a</sup>
<b>Bona Fide Members of TW Hydrae</b>								
10120908-3124451	TWA 39 AB	10:12:09.089	-31:24:45.19	-74.8 ± 1.1	-9.4 ± 1.0	14.6 ± 0.6	53.9 ± 5.1	1,2,3,2
10423011-3340162	TWA 7	10:42:30.113	-33:40:16.21	-114.4 ± 0.8	-19.1 ± 0.8	11.9 ± 0.4	34.5 ± 2.5	4,5,6,5
11015191-3442170	TWA 1	11:01:51.917	-34:42:17.00	-68.2 ± 0.1	-13.9 ± 0.1	12.4 ± 0.5	59.5 ± 1.0	7,8,6,8
11020983-3430355	TWA 28	11:02:09.833	-34:30:35.53	-65.2 ± 5.6	-15.6 ± 6.1	9 ± 3	56.4 ± 1.6	9,10,10,11
11084400-2804504	TWA 43; HIP 54477; HR 4334	11:08:44.002	-28:04:50.44	-72.8 ± 0.4	-22.2 ± 0.5	16 ± 5	55.7 ± 1.6	12,13,14,13
11091380-3001398	TWA 2 AB	11:09:13.807	-30:01:39.85	-91.1 ± 0.8	-21.0 ± 0.8	10.98 ± 0.03	46.6 ± 2.8	7,15,6,15
11210549-3845163	TWA 12	11:21:05.498	-38:45:16.34	-68.3 ± 2.7	-12.1 ± 1.5	10.9 ± 0.3	64.1 ± 2.9	16,15,6,15
11211723-3446454	TWA 13 A	11:21:17.135	-34:46:45.77	-66.4 ± 2.4	-12.5 ± 1.8	10.8 ± 0.4	55.6 ± 2.2	16,15,6,15
11211745-3446497	TWA 13 B	11:21:17.359	-34:46:50.03	-68.0 ± 3.1	-11.0 ± 2.7	11.5 ± 0.4	59.7 ± 2.6	16,15,6,15
11220530-2446393	TWA 4 AB	11:22:05.287	-24:46:39.78	-85.4 ± 1.7	-33.1 ± 2.1	12.8 ± 0.1	44.9 ± 4.7	7,13,17,13
11315526-3436272	TWA 5 AB	11:31:55.262	-34:36:27.24	-82.2 ± 1.6	-19.7 ± 0.6	13 ± 2	48.3 ± 1.5	7,8,18,8
11324116-2652090	TWA 8 B	11:32:41.165	-26:52:09.04	-72.3 ± 0.3	-20.9 ± 0.5	8.9 ± 0.3	46.1 ± 5.1	4,2,18,19
11324124-2651559	TWA 8 A	11:32:41.246	-26:51:55.95	-72.6 ± 0.3	-24.3 ± 0.5	8.1 ± 0.4	47.0 ± 2.2	4,2,18,2
11321822-3018316	TWA 30 B	11:32:18.223	-30:18:31.65	-84.4 ± 5.6	-19.5 ± 7.4	12 ± 3	...	20,10,20,
11321831-3019518	TWA 30 A	11:32:18.317	-30:19:51.81	-89.6 ± 1.3	-25.8 ± 1.4	12 ± 2	43.8 ± 4.9	21,21,21,19
11393382-3040002	TWA 33	11:39:33.826	-30:40:00.29	-79.9 ± 6.3	-30.0 ± 6.8	5.8 ± 0.7	51.3 ± 4.4	22,10,10,19
11395113-3159214	TWA 26	11:39:51.139	-31:59:21.50	-93.3 ± 0.5	-27.5 ± 0.5	12 ± 2	42.0 ± 4.5	23,5,24,15
11482373-3728485	TWA 9 B	11:48:23.731	-37:28:48.53	-51.0 ± 0.6	-18.1 ± 0.6	11.5 ± 0.9	...	4,5,6,
11482422-3728491	TWA 9 A	11:48:24.226	-37:28:49.15	-53.0 ± 0.2	-18.4 ± 0.1	10.4 ± 0.6	75.7 ± 1.7	4,8,6,8
12072738-3247002	TWA 23 AB	12:07:27.384	-32:47:00.27	-70.4 ± 1.4	-29.7 ± 1.1	10.9 ± 0.1	53.9 ± 1.4	25,26,6,15
12073346-3932539	TWA 27 AB	12:07:33.468	-39:32:53.00	-62.7 ± 1.7	-22.8 ± 2.7	11 ± 2	52.8 ± 1.0	23,27,24,2
12153072-3948426	TWA 25	12:15:30.722	-39:48:42.61	-76.5 ± 0.7	-26.7 ± 1.3	7.0 ± 0.6	51.8 ± 1.0	25,8,6,8
12265135-3316124	TWA 32 AB	12:26:51.355	-33:16:12.47	-55.3 ± 0.6	-28.0 ± 2.8	7.2 ± 0.3	66.1 ± 2.9	18,19,28,19
12313807-4558593	TWA 20 AB	12:31:38.074	-45:58:59.38	-63.5 ± 1.1	-27.8 ± 1.1	8 ± 4	77.3 ± 3.6	29,26,12,15
12345629-4538075	TWA 16 AB	12:34:56.297	-45:38:07.57	-49.2 ± 1.6	-21.2 ± 0.8	8.7 ± 0.4	78.1 ± 3.1	30,15,6,15
12350424-4136385	TWA 10	12:35:04.250	-41:36:38.58	-64.6 ± 0.4	-30.3 ± 0.4	6.3 ± 0.2	59.0 ± 2.5	4,5,6,19
12354893-3950245	TWA 11 C	12:35:48.938	-39:50:24.55	-45.1 ± 2.4	-20.1 ± 2.3	...	69.0 ± 2.4	31,15,,15
12360055-3952156	TWA 11 B	12:36:00.554	-39:52:15.69	...	...	9 ± 1	...	4,,32,
12360103-3952102	TWA 11 A; HR 4796B	12:36:01.034	-39:52:10.21	-53.3 ± 3.0	-21.2 ± 4.0	7 ± 1	72.8 ± 1.7	4,15,33,13
12451416-4429077	TWA 29	12:45:14.160	-44:29:07.72	-45.6 ± 6.2	-21.8 ± 7.1	8 ± 3	79 ± 13	34,10,10,15
<b>High-Likelihood Candidate Members of TW Hydrae</b>								
10284580-2830374	TWA 34	10:28:45.809	-28:30:37.46	-65.5 ± 4.1	-11.1 ± 4.1	12.4 ± 0.3	...	22,22,10,
11102788-3731520	TWA 3 A	11:10:27.767	-37:31:51.79	-107.3 ± 0.9	-18.0 ± 1.1	11.8 ± 0.5	...	7,35,3,
...	TWA 3 AbB	...	...	...	...	10.1 ± 0.5	...	7,,3,
...	TWA 3 B	...	...	...	...	9.8 ± 0.6	...	7,,3,
11193254-1137466	TWA 42	11:19:32.544	-11:37:46.70	-145 ± 15	-72 ± 16	9 ± 3	...	36,37,37,
11472421-2040204	TWA 41	11:47:24.214	-20:40:20.44	-122 ± 11	-74 ± 12	7 ± 3	...	38,10,10,
11592786-4510192	TWA 45	11:59:27.866	-45:10:19.22	-46.7 ± 6.3	-18.9 ± 2.1	...	77.3 ± 5.9	19,19,,19
12002750-3405371	TWA 35	12:00:27.506	-34:05:37.17	-51.5 ± 5.7	-22.7 ± 6.1	11 ± 2	...	39,10,40,
12023799-3328402	TWA 36	12:02:37.997	-33:28:40.24	-65.0 ± 6.1	-21.9 ± 6.2	6 ± 2	...	41,10,40,
12074836-3900043	TWA 40	12:07:48.362	-39:00:04.40	-66.9 ± 7.0	-31.2 ± 6.9	6 ± 3	...	42,10,10,
12175920-3734433	TWA 44	12:17:59.206	-37:34:43.31	-54.6 ± 5.9	-23.8 ± 6.3	5 ± 3	...	41,10,10,
12354615-4115531	TWA 46	12:35:46.154	-41:15:53.16	-58.6 ± 1.6	-24.8 ± 2.2	...	48.2 ± 1.8	19,19,,19
12371238-4021480	TWA 47	12:37:12.384	-40:21:48.10	-63.7 ± 1.1	-29.1 ± 1.1	11 ± 2	...	43,26,43,
<b>Candidate Members of TW Hydrae</b>								
09400251-2229251	...	09:40:02.513	-22:29:25.13	-59.6 ± 5.5	-22.6 ± 5.7	...	...	41,10,,
09532126-1014205	...	09:53:21.269	-10:14:20.57	-72.8 ± 6.3	-67.7 ± 6.3	...	...	41,10,,
10023100-2814280	...	10:02:31.006	-28:14:28.00	-74.8 ± 5.4	-21.7 ± 5.6	...	...	41,10,,
10103260-2832250	...	10:10:32.606	-28:32:25.06	-64.4 ± 6.0	-17.1 ± 6.3	...	...	10,10,,
10331650-3517001	...	10:33:16.502	-35:17:00.11	-57.5 ± 5.6	-7.5 ± 6.3	...	...	10,10,,
10380178-2154225	...	10:38:01.783	-21:54:22.56	-111.9 ± 6.4	-21.6 ± 6.1	...	...	41,10,,
10541299-3016450	...	10:54:12.991	-30:16:45.02	-65.0 ± 6.7	-14.2 ± 6.5	...	...	10,10,,
10585054-2346206	...	10:58:50.546	-23:46:20.66	-86.1 ± 2.2	-20.0 ± 4.8	8.2 ± 0.2	...	41,44,10,
11034950-3409445	...	11:03:49.507	-34:09:44.58	-50.1 ± 7.7	-14.0 ± 7.9	...	...	41,10,,
11035165-3711483	...	11:03:51.655	-37:11:48.33	-76.4 ± 5.7	1.0 ± 6.3	...	...	41,10,,
11064461-3715115	...	11:06:44.616	-37:15:11.53	-45.9 ± 5.7	-4.9 ± 6.4	...	...	45,10,,
11112820-2655027	TWA 37	11:11:28.202	-26:55:02.71	-87.4 ± 5.9	-29.7 ± 6.0	...	...	45,10,,
11131034-1504005	...	11:13:10.346	-15:04:00.53	-104.9 ± 6.6	-34.3 ± 6.4	...	...	41,10,,
11150259-3759251	...	11:15:02.597	-37:59:25.12	-48.6 ± 6.2	-9.2 ± 6.9	...	...	41,10,,

Table 12 continued

GAGNÉ ET AL.  
Table 12 (*continued*)

2MASS Designation	Other Names	RA J2000	DEC J2000	$\mu_{\alpha} \cos \delta$ (mas yr <sup>-1</sup> )	$\mu_{\delta}$ (mas yr <sup>-1</sup> )	RV (km s <sup>-1</sup> )	Distance (pc)	Refer- ences <sup>a</sup>
11152992-2954436	...	11:15:29.928	-29:54:43.61	-48.6 ± 6.3	-24.5 ± 6.1	13.3 ± 0.2	...	41,10,10,
11160937-3601063	...	11:16:09.374	-36:01:06.30	-71.0 ± 5.6	-21.2 ± 6.9	...	...	41,10,,
11271382-3735076	...	11:27:13.819	-37:35:07.62	-65 ± 13	1 ± 17	...	...	41,10,,
11283294-2924353	...	11:28:32.950	-29:24:35.37	-116.0 ± 6.7	-18.0 ± 7.4	...	...	41,10,,
11353003-1947062	...	11:35:30.031	-19:47:06.25	-126.6 ± 6.7	-55.5 ± 5.8	...	...	41,10,,
11382538-3841525	...	11:38:25.385	-38:41:52.50	-64.0 ± 6.0	-11.1 ± 6.2	...	...	41,10,,
11430143-3927002	...	11:43:01.435	-39:27:00.26	-61.8 ± 6.6	-5.1 ± 6.9	...	...	41,10,,
11443970-3455026	...	11:44:39.708	-34:55:02.64	-88.2 ± 6.7	-9.7 ± 6.2	...	...	41,10,,
11480096-2836488	...	11:48:00.962	-28:36:48.90	-87 ± 11	-14 ± 10	6 ± 3	...	41,10,10,
11501755-3407074	...	11:50:17.556	-34:07:07.49	-141.6 ± 8.9	-54.0 ± 7.1	...	...	41,10,,
11510246-3611457	...	11:51:02.470	-36:11:45.75	-150.8 ± 9.3	-55.1 ± 7.2	...	...	41,10,,
11561415-3917217	...	11:56:14.153	-39:17:21.71	-74.8 ± 6.3	-33.7 ± 6.4	...	...	41,10,,
12012242-4103432	...	12:01:22.428	-41:03:43.30	-46.7 ± 5.9	-6.2 ± 6.6	...	...	41,10,,
12035905-3821402	TWA 38	12:03:59.059	-38:21:40.29	-51.9 ± 6.0	-22.8 ± 6.5	...	...	45,10,,
12072486-3608359	...	12:07:24.869	-36:08:35.92	-57.6 ± 6.1	-8.6 ± 7.1	...	...	41,10,,
12093096-3820290	...	12:09:30.960	-38:20:29.08	-38.9 ± 5.9	-7.8 ± 6.6	...	...	41,10,,
12120009-3519434	...	12:12:00.098	-35:19:43.47	-39.1 ± 5.8	-12.3 ± 7.0	...	...	41,10,,
12134001-3723362	...	12:13:40.015	-37:23:36.23	-46.8 ± 5.9	-9.6 ± 6.3	...	...	41,10,,
12173617-2846082	...	12:17:36.178	-28:46:08.27	-97.0 ± 6.7	-25.6 ± 6.7	...	...	41,10,,
12193723-3132237	...	12:19:37.231	-31:32:23.80	-65.1 ± 6.4	-45.5 ± 6.5	...	...	41,10,,
12384389-2705384	...	12:38:43.894	-27:05:38.48	-56.9 ± 6.5	-27.5 ± 7.2	...	...	41,10,,
12414195-3625573	...	12:41:41.954	-36:25:57.40	-63.5 ± 6.2	-34.6 ± 6.5	...	...	41,10,,
12471536-3252233	...	12:47:15.365	-32:52:23.35	-66.2 ± 7.5	-20.0 ± 7.0	...	...	41,10,,
12474428-3816464	...	12:47:44.290	-38:16:46.40	-35.8 ± 5.9	-21.2 ± 6.5	...	...	42,10,,
12532702-3504151	...	12:53:27.029	-35:04:15.16	-50.1 ± 5.8	-21.3 ± 6.2	...	...	10,10,,
12574941-4111373	...	12:57:49.418	-41:11:37.37	-40.5 ± 5.6	-22.3 ± 6.4	...	...	41,10,,
13075615-4159202	...	13:07:56.153	-41:59:20.20	-84.6 ± 7.7	-42.1 ± 7.7	...	...	41,10,,
13110859-3725022	...	13:11:08.594	-37:25:02.27	-61.6 ± 6.3	-25.1 ± 6.6	...	...	41,10,,
13153357-3425084	...	13:15:33.578	-34:25:08.41	-65.4 ± 6.3	-32.4 ± 6.5	...	...	41,10,,
13191194-3600082	...	13:19:11.947	-36:00:08.21	-58.1 ± 6.2	-32.0 ± 7.3	...	...	41,10,,
<b>Low-Likelihood Candidate Members of TW Hydrae</b>								
08561384-1342242	...	08:56:13.848	-13:42:24.23	-58.8 ± 5.8	-19.8 ± 5.8	...	...	39,10,,
09395647-2946286	...	09:39:56.477	-29:46:28.62	-60.6 ± 6.3	7.2 ± 6.7	...	...	41,10,,
10211908+0804268	...	10:21:19.085	08:04:26.89	-131.3 ± 8.1	-95.8 ± 9.5	...	...	10,10,,
10563080-3028137	...	10:56:30.802	-30:28:13.79	-76.6 ± 6.5	3.9 ± 7.7	...	...	41,10,,
10582800-1046304	NLTT 25869	10:58:28.003	-10:46:30.46	-196.2 ± 8.0	-79.5 ± 6.2	...	...	41,10,,
11023986-2507113	...	11:02:39.862	-25:07:11.34	-75.7 ± 6.5	-15.7 ± 7.4	17.3 ± 0.3	...	41,10,10,
11153797-2552192	...	11:15:37.975	-25:52:19.28	-70.5 ± 6.8	-7.0 ± 6.2	...	...	41,10,,
11382693-3843138	...	11:38:26.935	-38:43:13.86	-63.7 ± 6.0	-7.9 ± 6.2	18.7 ± 0.4	...	41,10,10,
12021801-3110348	...	12:02:18.012	-31:10:34.85	-98.6 ± 7.6	-27.0 ± 7.0	...	...	10,10,,
12162481-2742007	...	12:16:24.818	-27:42:00.75	-77.5 ± 6.7	-31.2 ± 6.5	...	...	10,10,,
12271545-0636458	...	12:27:15.456	-06:36:45.89	-121.4 ± 7.5	-64.8 ± 6.5	...	...	39,10,,
12333935-3040139	...	12:33:39.358	-30:40:13.93	-58.5 ± 6.7	-13.9 ± 6.7	...	...	41,10,,
12454194-3903106	...	12:45:41.947	-39:03:10.68	-73.1 ± 7.3	-22.3 ± 7.4	...	...	10,10,,
12471067-3632150	...	12:47:10.678	-36:32:15.05	-39.0 ± 5.7	-12.9 ± 7.1	...	...	41,10,,
13155594-3403418	...	13:15:55.944	-34:03:41.87	-52.9 ± 6.1	-24.8 ± 6.4	...	...	41,10,,
<b>Likely Contaminants from Centaurus Crux</b>								
10134260-2759586	...	10:13:42.600	-27:59:58.61	-61.8 ± 6.6	-33.9 ± 6.2	...	...	23,10,,
10182870-3150029	TWA 6 AB	10:18:28.702	-31:50:02.92	-55.6 ± 0.9	-19.5 ± 0.6	21 ± 2	63.9 ± 1.3	4,8,17,8
10212570-2830427	...	10:21:25.706	-28:30:42.76	-55 ± 11	-35 ± 12	...	...	41,10,,
10252092-4241539	...	10:25:20.921	-42:41:53.94	-46.8 ± 1.2	-2.2 ± 1.2	17.6 ± 0.5	108 ± 15	46,46,3,19
10260210-4105537	...	10:26:02.110	-41:05:53.72	-45.3 ± 1.4	-2.5 ± 1.4	...	...	28,26,,
10292874-3823394	...	10:29:28.740	-38:23:39.42	-61.4 ± 5.6	16.7 ± 6.2	...	...	41,10,,
10394605-3510139	...	10:39:46.054	-35:10:13.94	-47.5 ± 5.6	-9.7 ± 7.0	...	...	41,10,,
10443052-3730554	...	10:44:30.530	-37:30:55.43	-47.7 ± 5.5	14.7 ± 6.2	...	...	41,10,,
10455263-2819303	...	10:45:52.630	-28:19:30.32	-41.0 ± 3.0	-17.0 ± 4.0	...	...	45,47,,
10492026-2440101	...	10:49:20.266	-24:40:10.11	-53.3 ± 5.9	-44.2 ± 6.2	...	...	41,10,,
10492579-3527125	...	10:49:25.790	-35:27:12.55	-41.1 ± 5.6	-16.6 ± 6.3	...	...	10,10,,
10514507-3226337	...	10:51:45.072	-32:26:33.76	-51.1 ± 5.7	-28.7 ± 6.3	...	...	10,10,,
10571669-3512548	...	10:57:16.699	-35:12:54.81	-36.5 ± 5.6	-5.9 ± 6.3	...	...	41,10,,
11035873-4156475	...	11:03:58.740	-41:56:47.59	-30.9 ± 5.8	-14.3 ± 7.8	...	...	41,10,,
11062620-4019330	...	11:06:26.201	-40:19:33.05	-91.4 ± 5.6	16.0 ± 6.1	...	...	41,10,,
11130416-4516056	...	11:13:04.164	-45:16:05.66	-41.0 ± 3.2	4.0 ± 3.0	...	...	48,48,,

*Table 12 continued*



Table 12 (*continued*)

2MASS Designation	Other Names	RA J2000	DEC J2000	$\mu_{\alpha} \cos \delta$ (mas yr <sup>-1</sup> )	$\mu_{\delta}$ (mas yr <sup>-1</sup> )	RV (km s <sup>-1</sup> )	Distance (pc)	Refer- ences <sup>a</sup>
11132622-4523427	TWA 14 AB	11:13:26.227	-45:23:42.77	-43.9 ± 1.4	-7.4 ± 1.4	16 ± 2	96 ± 11	30,26,18,15
11191302-4342401	...	11:19:13.027	-43:42:40.17	-43.3 ± 5.5	2.6 ± 6.3	...	...	41,10,,
11204706-2738056	...	11:20:47.062	-27:38:05.60	-40.9 ± 6.3	-27.4 ± 7.5	...	...	41,10,,
11385038-3830011	...	11:38:50.381	-38:30:01.20	-55.3 ± 6.0	6.6 ± 6.3	...	...	41,10,,
11394506-3729069	...	11:39:45.060	-37:29:06.94	-38.4 ± 5.7	-19.5 ± 6.3	...	...	41,10,,
11443034-3820341	...	11:44:30.348	-38:20:34.15	-68.9 ± 6.7	4.0 ± 6.8	...	...	41,10,,
11455177-5520456	...	11:45:51.780	-55:20:45.67	-99.6 ± 2.0	-5.9 ± 1.4	16.0 ± 0.4	42.6 ± 0.8	46,8,6,8
11472454-4953029	TWA 19 AB	11:47:24.542	-49:53:02.94	-34.8 ± 0.1	-9.8 ± 0.1	14 ± 2	110.4 ± 3.2	49,8,17,8
11511119-4132064	...	11:51:11.194	-41:32:06.44	-67.7 ± 6.5	12.7 ± 6.8	...	...	41,10,,
11554920-4303109	...	11:55:49.210	-43:03:10.95	-52.5 ± 6.1	10.7 ± 6.8	...	...	41,10,,
12011772-3712329	...	12:01:17.726	-37:12:32.91	-33.5 ± 5.6	-13.7 ± 6.3	...	...	41,10,,
12071089-3230537	TWA 31	12:07:10.894	-32:30:53.72	-38.8 ± 0.2	-21.6 ± 0.2	10.5 ± 0.4	79.9 ± 3.3	18,19,50,19
12094184-5854450	TWA 24 AB	12:09:41.849	-58:54:45.09	-37.6 ± 0.9	-10.4 ± 0.6	11.9 ± 0.9	107.0 ± 4.0	25,8,51,8
12105770-3708100	...	12:10:57.708	-37:08:10.07	-64.2 ± 6.3	-46.9 ± 7.5	...	...	41,10,,
12174683-3804157	...	12:17:46.831	-38:04:15.73	-56.7 ± 6.0	-0.4 ± 6.3	...	...	41,10,,
12333140-3641407	...	12:33:31.404	-36:41:40.78	-53.1 ± 5.7	-46.0 ± 6.4	...	...	10,10,,
12342064-4815135	TWA 15 A	12:34:20.650	-48:15:13.51	-37.5 ± 2.4	-10.4 ± 2.0	11 ± 2	117 ± 22	30,15,18,15
12342047-4815195	TWA 15 B	12:34:20.474	-48:15:19.52	-36.5 ± 2.9	-9.9 ± 2.8	10 ± 2	110 ± 21	30,15,29,15
12421948-3805064	...	12:42:19.486	-38:05:06.48	-78.5 ± 6.3	-7.4 ± 6.1	...	...	10,10,,
12482006-4237338	HD 111265	12:48:20.059	-42:37:33.81	-49.4 ± 1.3	-11.2 ± 0.5	6 ± 2	123.9 ± 5.2	29,8,29,8
12520989-4948280	...	12:52:09.893	-49:48:28.08	-38.0 ± 2.0	-17.0 ± 2.0	...	...	45,47,,
12522053-4515542	...	12:52:20.534	-45:15:54.24	-37.9 ± 5.4	-26.9 ± 6.5	...	...	41,10,,
12535039-4211215	...	12:53:50.393	-42:11:21.58	-46.1 ± 8.5	-9.0 ± 9.5	...	...	41,10,,
12574463-3635431	...	12:57:44.638	-36:35:43.12	-64.3 ± 7.6	-15.4 ± 7.4	...	...	41,10,,
13204539-4611377	TWA 17 AB	13:20:45.391	-46:11:37.74	-22.0 ± 1.2	-18.4 ± 2.6	10 ± 4	157 ± 13	30,19,52,19
13213722-4421518	TWA 18	13:21:37.224	-44:21:51.84	-24.0 ± 0.7	-20.4 ± 1.7	7 ± 3	162 ± 37	30,19,29,19
13412668-4341522	...	13:41:26.688	-43:41:52.26	-107.0 ± 3.0	-60.8 ± 3.0	3.1 ± 0.2	...	46,46,3,
13481593-3642228	...	13:48:15.936	-36:42:22.81	-61.2 ± 6.1	-41.9 ± 6.5	...	...	10,10,,
<b>Candidate Members of Carina</b>								
10131476-5230540	TWA 21	10:13:14.762	-52:30:54.05	-62.0 ± 1.0	9.7 ± 0.6	17.5 ± 0.8	52.4 ± 0.7	25,8,25,8
10282500-3959230	...	10:28:25.010	-39:59:23.00	-144.4 ± 6.1	1.4 ± 6.1	20 ± 2	...	41,10,40,
<b>Member of <math>\beta</math> Pictoris</b>								
10172689-5354265	TWA 22 AB	10:17:26.892	-53:54:26.52	-175.8 ± 0.8	-21.3 ± 0.8	15 ± 2	17.5 ± 0.2	25,53,53,53
<b>Rejected candidates</b>								
08141769+0253199	...	08:14:17.700	02:53:19.99	-30.1 ± 6.8	-54.9 ± 7.5	...	...	10,10,,
08144321+2336045	...	08:14:43.219	23:36:04.53	-53.4 ± 5.5	-135.3 ± 6.9	...	...	41,10,,
08254335-0029110	...	08:25:43.351	-00:29:11.01	-40.3 ± 6.9	-40.4 ± 7.5	17 ± 3	...	39,10,10,
09292857-4431563	HIP 46535	09:29:28.570	-44:31:56.37	-105.87 ± 0.03	14.53 ± 0.03	24.3 ± 0.5	38.1 ± 0.5	49,8,54,8
09353126-2802552	...	09:35:31.270	-28:02:55.25	-49.4 ± 0.6	-57.4 ± 0.7	0 ± 3	...	46,46,52,
09471986-4003098	XACT 10	09:47:19.860	-40:03:09.83	-44.5 ± 0.8	16.1 ± 0.4	14 ± 2	101.2 ± 2.6	29,8,52,8
09512673-2220196	...	09:51:26.731	-22:20:19.68	-45.8 ± 5.5	-23.8 ± 5.7	...	...	10,10,,
09553336-0208403	...	09:55:33.365	-02:08:40.37	-124 ± 15	-106 ± 16	-20 ± 4	...	10,10,10,
09590842-2239345	TYC 6604-118-1	09:59:08.429	-22:39:34.54	-62.6 ± 1.8	-12.3 ± 0.7	27 ± 2	62.2 ± 1.9	49,8,17,8
10104667-3447531	TYC 7178-1493-1	10:10:46.675	-34:47:53.13	-72.4 ± 1.0	-17.3 ± 0.6	48 ± 3	154 ± 10	49,8,17,8
10144705-3728151	...	10:14:47.054	-37:28:15.18	-57.6 ± 5.5	7.2 ± 6.2	...	...	41,10,,
10190109-2646336	...	10:19:01.097	-26:46:33.60	-77.1 ± 6.0	-28.3 ± 6.2	-3.1 ± 0.3	...	41,10,10,
10220449-3233270	TYC 7188-0575-1	10:22:04.490	-32:33:27.01	-119.5 ± 0.9	-21.9 ± 0.6	43 ± 2	111.6 ± 5.7	49,8,17,8
10221800-1032156	HIP 50796	10:22:18.005	-10:32:15.64	-78.9 ± 3.2	-22.8 ± 2.7	24.9 ± 0.1	38.8 ± 5.5	49,13,55,13
10432828-2903513	HIP 52462	10:43:28.284	-29:03:51.35	-215.57 ± 0.03	-49.88 ± 0.04	22.9 ± 0.2	21.7 ± 0.1	49,8,56,8
10473117-2220528	HIP 52787	10:47:31.171	-22:20:52.82	-124.57 ± 0.06	-28.23 ± 0.04	23 ± 2	33.8 ± 0.4	49,8,57,8
10513331-1916530	...	10:51:33.319	-19:16:53.01	-93.8 ± 6.7	-29.6 ± 6.6	...	...	41,10,,
10542303-1507082	...	10:54:23.035	-15:07:08.26	-105.4 ± 7.7	-70.2 ± 7.4	...	...	41,10,,
10563080+0723184	HIP 53486	10:56:30.804	07:23:18.46	-256.9 ± 0.1	-77.4 ± 0.1	5.54 ± 0.01	17.3 ± 0.1	49,8,58,8
11063147-4201251	...	11:06:31.476	-42:01:25.10	-101.6 ± 7.9	-0.3 ± 7.7	...	...	10,10,,
11112984-2713320	...	11:11:29.844	-27:13:32.01	-63.1 ± 5.8	-32.9 ± 6.1	...	...	41,10,,
11195251-3917150	...	11:19:52.512	-39:17:15.02	-65.7 ± 6.0	-20.3 ± 6.3	...	...	10,10,,
11254754-4410267	...	11:25:47.549	-44:10:26.76	-83.9 ± 2.6	-57.0 ± 7.7	20.9 ± 0.8	...	28,26,3,
11423628-3859108	...	11:42:36.281	-38:59:10.88	-68.5 ± 6.6	-33.6 ± 7.0	...	...	41,10,,
11424808-3548577	HIP 57129	11:42:48.084	-35:48:57.76	-52.1 ± 1.9	-25.7 ± 1.2	29.1 ± 0.8	85 ± 14	49,13,59,13
11443846-4925025	HIP 57269	11:44:38.462	-49:25:02.59	-137.8 ± 1.5	-45.3 ± 1.6	17.2 ± 0.4	48.6 ± 5.0	49,13,33,13
11504110-2356075	...	11:50:41.102	-23:56:07.52	-109.8 ± 2.3	-6.7 ± 4.1	...	...	10,44,,
11532691-3015414	...	11:53:26.911	-30:15:41.46	-79.7 ± 1.6	-6.3 ± 2.8	...	...	10,44,,

Table 12 *continued*

Table 12 (*continued*)

2MASS Designation	Other Names	RA J2000	DEC J2000	$\mu_{\alpha} \cos \delta$ (mas yr <sup>-1</sup> )	$\mu_{\delta}$ (mas yr <sup>-1</sup> )	RV (km s <sup>-1</sup> )	Distance (pc)	Refer- ences <sup>a</sup>
11571557-4022292	...	11:57:15.571	-40:22:29.24	-39.8 ± 5.6	13.9 ± 6.3	...	...	41,10,,
12000160-1731308	...	12:00:01.603	-17:31:30.80	-71.5 ± 1.8	-29.7 ± 2.2	-0.1 ± 0.8	...	10,44,10,
12041256+0514128	...	12:04:12.569	05:14:12.84	-199.6 ± 8.8	-146.0 ± 7.4	...	...	10,10,,
12073145-3310222	...	12:07:31.457	-33:10:22.27	-62.7 ± 1.8	-32.3 ± 1.4	-9.0 ± 0.2	...	48,48,10,
12090628-3247453	...	12:09:06.286	-32:47:45.37	-68.1 ± 2.0	-40.2 ± 2.7	...	...	48,48,,
12100648-4910505	HIP 59315	12:10:06.482	-49:10:50.57	-148.1 ± 0.1	-60.4 ± 0.1	16.2 ± 0.2	37.2 ± 0.3	49,8,33,8
12113180-3416537	...	12:11:31.807	-34:16:53.78	-110.2 ± 7.2	-33.4 ± 6.2	...	...	10,10,,
12194846-3232059	...	12:19:48.461	-32:32:05.96	-70.2 ± 7.7	-15.9 ± 8.3	...	...	10,10,,
12220574-4159572	...	12:22:05.746	-41:59:57.25	-33.9 ± 6.5	17.0 ± 6.4	...	...	41,10,,
12214223-4012050	...	12:21:42.235	-40:12:05.07	-38 ± 13	-6 ± 18	...	...	41,10,,
12214852-3652349	...	12:21:48.521	-36:52:34.93	-57.1 ± 6.0	-3.3 ± 6.3	...	...	10,10,,
12282569-3955014	...	12:28:25.692	-39:55:01.44	-89.3 ± 6.5	-25.8 ± 6.2	...	...	10,10,,
12310489-3801065	...	12:31:04.894	-38:01:06.58	-69.0 ± 6.6	-4.2 ± 6.7	...	...	41,10,,
12451035-1443029	...	12:45:10.354	-14:43:02.00	-78.5 ± 6.3	-7.4 ± 6.1	...	...	10,10,,
12563961-2718455	...	12:56:39.612	-27:18:45.58	-75.6 ± 8.6	-62.1 ± 9.8	-19 ± 4	...	41,10,10,
13112902-4252418	...	13:11:29.026	-42:52:41.84	-29.6 ± 0.9	-19.9 ± 0.7	...	79.8 ± 6.0	19,19,,19
13265348-5022270	...	13:26:53.484	-50:22:27.05	-24.7 ± 7.0	-17.0 ± 7.0	...	...	45,47,,
14112131-2119503	...	14:11:21.314	-21:19:50.33	-85.5 ± 6.6	-75.4 ± 6.6	-1 ± 3	...	10,10,60,
14252913-4113323	SCR 1425-4113 AB	14:25:29.131	-41:13:32.38	-46.8 ± 2.1	-49.2 ± 1.7	-1 ± 1	66.9 ± 4.3	2,2,2,2
18440971+7129178	1RXS J1844+7129 A	18:44:09.710	71:29:17.84	-71 ± 12	160 ± 12	-19 ± 3	...	61,62,61,
18441019+7129175	1RXS J1844+7129 B	18:44:10.200	71:29:17.57	...	...	-17 ± 2	...	61,,61,

<sup>a</sup> Four references separated by commas are given for TWA membership, proper motion, radial velocity and trigonometric distance, respectively. The references listed for TWA membership are the first ones to have suggested that a given object is a possible member of TWA; in some cases membership was subsequently rejected.

<sup>b</sup> Radial velocity variable star. The radial velocity value reported here is the average of two measurements from Torres et al. (2006b) and Malo et al. (2014).

NOTE—See Section 5 for more details.

**References**—(1) Riedel 2012; (2) Riedel et al. 2014; (3) Malo et al. 2014; (4) Webb et al. 1999; (5) Ducourant et al. 2014a; (6) Elliott et al. 2014; (7) Kastner et al. 1997; (8) Lindgren et al. 2016; (9) Scholz et al. 2005; (10) this paper; (11) Teixeira et al. 2008; (12) Mamajek 2005; (13) van Leeuwen 2007b; (14) Kharchenko et al. 2007; (15) Weinberger et al. 2013; (16) Sterzik et al. 1999; (17) Torres et al. 2006b; (18) Shkolnik et al. 2011; (19) Donaldson et al. 2016; (20)Looper et al. 2010a; (21) Looper et al. 2010b; (22) Schneider et al. 2012b; (23) Gizis 2002; (24) Mohanty et al. 2003; (25) Song et al. 2003; (26) Zacharias et al. 2013; (27) Gizis et al. 2007; (28) Rodriguez et al. 2011; (29) Reid 2003; (30) Zuckerman et al. 2001b; (31) Kastner et al. 2008; (32) Torres et al. 2003; (33) Gontcharov 2006a; (34) Looper et al. 2007; (35) Finch et al. 2010; (36) Kellogg et al. 2015; (37) Kellogg et al. 2016; (38) Schneider et al. 2016; (39) Gagné et al. 2015d; (40) Murphy et al. 2015; (41) Gagné et al. 2015b; (42) Gagné et al. 2014a; (43) Riedel et al. 2016; (44) Qi et al. 2015; (45) Looper 2011; (46) Malo et al. 2013; (47) Messina et al. 2010; (48) Elliott et al. 2016; (49) Makarov & Fabricius 2001; (50) Schneider et al. 2012a; (51) Fernández et al. 2008; (52) Kordopatis et al. 2013; (53) Torres et al. 2009; (54) Holmberg et al. 2007; (55) Pourbaix et al. 2004; (56) Gontcharov 2006b; (57) Jenkins et al. 2011; (58) Soubiran et al. 2013; (59) de Bruijne & Eilers 2012; (60) Faherty et al. 2016a; (61) Shkolnik et al. 2012; (62) Roeser et al. 2010.

Table 13. Spectrophotometric Properties of Candidates and Members of TWA

2MASS Designation	Spectral Type <sup>a</sup>			2MASS <sup>b</sup>			AllWISE <sup>b</sup>	
	Optical	NIR	Ref. <sup>c</sup>	<i>J</i>	<i>H</i>	<i>K<sub>S</sub></i>	<i>W1</i>	<i>W2</i>
<b>Bona Fide Members of TW Hydrae</b>								
10120908-3124451 A	M4 Ve	...	1,	[9.60 ± 0.00]	[9.01 ± 0.04]	[8.75 ± 0.03]	[8.51 ± 0.03]	[8.25 ± 0.02]
10120908-3124451 B	[M4 Ve]	...	1,	[9.60 ± 0.00]	[9.01 ± 0.04]	[8.75 ± 0.03]	[8.51 ± 0.03]	[8.25 ± 0.02]
10423011-3340162	M3 IVe	M4 pec	2,3	7.79 ± 0.01	7.13 ± 0.03	6.90 ± 0.02	6.79 ± 0.04	6.66 ± 0.02
11015191-3442170	K8 IVe	M3 e pec	2,3	8.22 ± 0.02	7.56 ± 0.04	7.30 ± 0.02	7.01 ± 0.05	6.88 ± 0.02
11020983-3430355	M8.5 $\gamma$	M9 $\gamma$	4,5	13.03 ± 0.02	12.36 ± 0.02	11.89 ± 0.02	11.45 ± 0.02	10.81 ± 0.02
11084400-2804504	A2 Vn	...	6,	5.31 ± 0.03	5.35 ± 0.03	5.24 ± 0.02	5.2 ± 0.2	5.04 ± 0.06
11091380-3001398 A	M1.5 IVe	...	2,	[8.38 ± 0.03]	[7.68 ± 0.04]	[7.46 ± 0.02]	[7.41 ± 0.07]	[7.24 ± 0.02]
11091380-3001398 B	M2	...	7,	[8.38 ± 0.03]	[7.68 ± 0.04]	[7.46 ± 0.02]	[7.41 ± 0.07]	[7.24 ± 0.02]
11210549-3845163	M2 IVe	...	2,	9.00 ± 0.03	8.33 ± 0.03	8.05 ± 0.03	8.05 ± 0.02	7.95 ± 0.02
11211723-3446454	M1 Ve	...	8,	8.43 ± 0.04	7.73 ± 0.06	7.49 ± 0.04	8.34 ± 0.09	8.26 ± 0.03
11211745-3446497	[M1 Ve]	...	8,	8.43 ± 0.04	7.68 ± 0.05	7.46 ± 0.03	8.34 ± 0.09	8.26 ± 0.03
11220530-2446393 Aa	K6 IVe	...	2,	[7.90 ± 0.01]	[7.26 ± 0.02]	[7.09 ± 0.01]	[7.0 ± 0.2]	[6.85 ± 0.06]
11220530-2446393 Ab	[K6 IVe]	...	2,	[7.90 ± 0.01]	[7.26 ± 0.02]	[7.09 ± 0.01]	[7.0 ± 0.2]	[6.85 ± 0.06]
11220530-2446393 Ba	K7	...	9,	[7.90 ± 0.01]	[7.26 ± 0.02]	[7.09 ± 0.01]	[7.0 ± 0.2]	[6.85 ± 0.06]
11220530-2446393 Bb	M1	...	9,	[7.90 ± 0.01]	[7.26 ± 0.02]	[7.09 ± 0.01]	[7.0 ± 0.2]	[6.85 ± 0.06]
11315526-3436272 Aa	M2 IVe	...	2,	[8.42 ± 0.02]	[7.74 ± 0.03]	[7.50 ± 0.02]	[7.41 ± 0.07]	[7.20 ± 0.02]
11315526-3436272 Ab	[M2 IVe]	...	2,	[8.42 ± 0.02]	[7.74 ± 0.03]	[7.50 ± 0.02]	[7.41 ± 0.07]	[7.20 ± 0.02]
11315526-3436272 B	M8.5	M8 $\gamma$	10,5	...	...	...	...	...
11324116-2652090	M5 Ve	M6 $\gamma$	1,5	9.84 ± 0.02	9.28 ± 0.02	9.01 ± 0.02	8.93 ± 0.08	8.65 ± 0.05

Table 13 continued

Table 13 (*continued*)

2MASS Designation	Spectral Type <sup>a</sup>		Ref. <sup>c</sup>	2MASS <sup>b</sup>			ALLWISE <sup>b</sup>	
	Optical	NIR		<i>J</i>	<i>H</i>	<i>K<sub>S</sub></i>	<i>W1</i>	<i>W2</i>
11324124–2651559	M3 IVe	...	2,	8.34 ± 0.02	7.66 ± 0.04	7.43 ± 0.01	7.28 ± 0.04	7.21 ± 0.02
11321822–3018316	M4	...	11,	15.35 ± 0.05	14.53 ± 0.05	13.72 ± 0.04	12.44 ± 0.02	10.69 ± 0.02
11321831–3019518	M5 Ve	M5 pec	11,11	9.64 ± 0.02	9.03 ± 0.02	8.77 ± 0.02	8.82 ± 0.02	8.44 ± 0.02
11393382–3040002	M4.5 e	...	12,	9.98 ± 0.02	9.41 ± 0.02	9.12 ± 0.02	8.82 ± 0.02	8.46 ± 0.02
11395113–3159214	M9 $\gamma$	M9 $\gamma$	13,5	12.69 ± 0.02	12.00 ± 0.02	11.50 ± 0.02	11.17 ± 0.02	10.82 ± 0.02
11482373–3728485	M1	...	7,	9.98 ± 0.03	9.38 ± 0.02	9.15 ± 0.02	9.00 ± 0.06	8.83 ± 0.04
11482422–3728491	K7 IVe	...	2,	8.68 ± 0.03	8.03 ± 0.04	7.85 ± 0.03	7.67 ± 0.04	7.68 ± 0.02
12072738–3247002 Aa	M3 Ve	...	14,	[9.81 ± 0.02]	[9.22 ± 0.04]	[8.94 ± 0.03]	[8.80 ± 0.03]	[8.68 ± 0.02]
12072738–3247002 Ab	M3 Ve	...	14,	[9.81 ± 0.02]	[9.22 ± 0.04]	[8.94 ± 0.03]	[8.80 ± 0.03]	[8.68 ± 0.02]
12073346–3932539 A	M8 pec	M8 $\gamma$	15,5	12.99 ± 0.02	12.39 ± 0.03	11.94 ± 0.02	11.57 ± 0.02	11.02 ± 0.02
12073346–3932539 b	...	L3 $\gamma$ pec	,5	20.0 ± 0.2	18.1 ± 0.2	16.9 ± 0.1	...	...
12153072–3948426	K9 IV-Ve	...	2,	8.17 ± 0.03	7.50 ± 0.04	7.31 ± 0.01	7.21 ± 0.04	7.21 ± 0.02
12265135–3316124 A	M5	M5.5 $\gamma$	16,17	[11.44 ± 0.02]	[10.87 ± 0.03]	[10.54 ± 0.02]	[10.32 ± 0.02]	[9.96 ± 0.02]
12265135–3316124 B	[M5]	[M5.5 $\gamma$ ]	16,17	[11.44 ± 0.02]	[10.87 ± 0.03]	[10.54 ± 0.02]	[10.32 ± 0.02]	[9.96 ± 0.02]
12313807–4558593 A	M3 IVe	...	2,	[10.08 ± 0.03]	[9.45 ± 0.06]	[9.16 ± 0.03]	[9.09 ± 0.02]	[8.95 ± 0.02]
12313807–4558593 B	[M3 IVe]	...	2,	[10.08 ± 0.03]	[9.45 ± 0.06]	[9.16 ± 0.03]	[9.09 ± 0.02]	[8.95 ± 0.02]
12345629–4538075 A	M2 IVe	...	2,	[9.75 ± 0.02]	[9.08 ± 0.04]	[8.84 ± 0.02]	[8.69 ± 0.03]	[8.61 ± 0.02]
12345629–4538075 B	[M2 IVe]	...	2,	[9.75 ± 0.02]	[9.08 ± 0.04]	[8.84 ± 0.02]	[8.69 ± 0.03]	[8.61 ± 0.02]
12350424–4136385	M2 Ve	...	18,	9.12 ± 0.02	8.48 ± 0.04	8.19 ± 0.03	8.10 ± 0.02	7.97 ± 0.02
12354893–3950245	M4.5	M5 $\gamma$	19,5	9.79 ± 0.02	9.22 ± 0.02	8.94 ± 0.02	8.81 ± 0.02	8.60 ± 0.02
12360055–3952156	M2 Ve	...	12,	9.15 ± 0.02	8.53 ± 0.04	8.35 ± 0.02	7.68 ± 0.06	6.11 ± 0.01
12360103–3952102	A0	...	20,	5.78 ± 0.01	5.79 ± 0.03	5.77 ± 0.02	5.37 ± 0.04	5.40 ± 0.03
12451416–4429077	M9.5 $\gamma$	M9.5 $\gamma$	21,5	14.52 ± 0.03	13.80 ± 0.03	13.37 ± 0.04	12.99 ± 0.02	12.65 ± 0.02
<b>High-Likelihood Candidate Members of TW Hydrae</b>								
10284580–2830374	M5 $\gamma$ e	M6 $\gamma$	5,17	10.95 ± 0.02	10.41 ± 0.02	10.03 ± 0.02	9.48 ± 0.02	8.99 ± 0.02
11102788–3731520 Aa	M4 IVe	M4 pec	2,3	[8.84 ± 0.01]	[8.23 ± 0.02]	[7.97 ± 0.01]	[7.78 ± 0.09]	[7.37 ± 0.03]
11102788–3731520 Ab	[M4 IVe]	[M4 pec]	2,3	[8.84 ± 0.01]	[8.23 ± 0.02]	[7.97 ± 0.01]	[7.78 ± 0.09]	[7.37 ± 0.03]
11102788–3731520 B	M4 IVe	M4 pec	2,3	[8.84 ± 0.01]	[8.23 ± 0.02]	[7.97 ± 0.01]	[7.78 ± 0.09]	[7.37 ± 0.03]
11193254–1137466	...	L7 pec(red)	,22	17.33 ± 0.03 <sup>d</sup>	15.84 ± 0.02 <sup>d</sup>	14.75 ± 0.01 <sup>d</sup>	13.55 ± 0.03	12.88 ± 0.03
11472421–2040204	...	L7 pec(red)	,5	17.44 ± 0.03 <sup>e</sup>	15.8 ± 0.1 <sup>e</sup>	14.87 ± 0.01 <sup>e</sup>	13.72 ± 0.03	13.09 ± 0.03
11592786–4510192	M4.5	...	16,	9.93 ± 0.02	9.35 ± 0.03	9.06 ± 0.02	8.92 ± 0.02	8.72 ± 0.02
12002750–3405371	M4.5	M4	23,17	9.61 ± 0.02	8.98 ± 0.03	8.72 ± 0.02	8.57 ± 0.02	8.33 ± 0.02
12023799–3328402	M5	...	23,	10.69 ± 0.02	10.12 ± 0.02	9.85 ± 0.02	9.68 ± 0.02	9.45 ± 0.02
12074836–3900043	L0 $\gamma$	L1 $\gamma$	24,24	15.49 ± 0.06	14.61 ± 0.05	14.04 ± 0.06	13.64 ± 0.02	13.20 ± 0.03
12175920–3734433	M5 $\gamma$ e	...	5,	11.57 ± 0.02	10.99 ± 0.02	10.72 ± 0.02	10.54 ± 0.02	10.30 ± 0.02
12354615–4115531	M3	...	25,	10.07 ± 0.03	9.47 ± 0.02	9.23 ± 0.02	9.06 ± 0.02	8.89 ± 0.02
12371238–4021480	M2.5 Ve	...	26,	9.47 ± 0.02	8.81 ± 0.02	8.52 ± 0.02	8.42 ± 0.02	8.27 ± 0.02
<b>Candidate Members of TW Hydrae</b>								
09400251–2229251	...	(M4.5)	,5	11.15 ± 0.02	10.60 ± 0.02	10.27 ± 0.02	10.11 ± 0.02	9.94 ± 0.02
09532126–1014205	L0	M9 $\beta$	27,17	13.47 ± 0.03	12.64 ± 0.03	12.14 ± 0.02	11.77 ± 0.02	11.41 ± 0.02
10023100–2814280 A	M4	...	28,	[10.64 ± 0.02]	[10.07 ± 0.02]	[9.78 ± 0.02]	[9.60 ± 0.02]	[9.42 ± 0.02]
10023100–2814280 B	M6	...	28,	[10.64 ± 0.02]	[10.07 ± 0.02]	[9.78 ± 0.02]	[9.60 ± 0.02]	[9.42 ± 0.02]
10103260–2832250	...	(M6.5)	,5	13.39 ± 0.03	12.75 ± 0.02	12.43 ± 0.03	12.16 ± 0.02	11.99 ± 0.02
10331650–3517001	...	(M6)	,5	13.10 ± 0.03	12.52 ± 0.03	12.22 ± 0.03	12.05 ± 0.02	11.85 ± 0.02
10380178–2154225	...	(M5.5)	,5	11.81 ± 0.02	11.25 ± 0.02	10.98 ± 0.03	10.77 ± 0.02	10.58 ± 0.02
10541299–3016450	...	(M7)	,5	14.14 ± 0.03	13.54 ± 0.03	13.22 ± 0.04	12.95 ± 0.03	12.71 ± 0.03
10585054–2346206	M6 $\gamma$ e	...	5,	10.30 ± 0.03	9.71 ± 0.02	9.43 ± 0.02	9.21 ± 0.02	8.97 ± 0.02
11034950–3409445	...	M9 $\beta$	,5	15.70 ± 0.06	15.02 ± 0.06	14.53 ± 0.08	14.23 ± 0.03	13.93 ± 0.04
11035165–3711483	...	(M5.5)	,5	12.42 ± 0.02	11.84 ± 0.02	11.54 ± 0.02	11.34 ± 0.02	11.11 ± 0.02
11064461–3715115	M9	M9 $\gamma$	3,17	14.49 ± 0.03	13.85 ± 0.03	13.34 ± 0.04	13.09 ± 0.02	12.76 ± 0.03
11112820–2655027	M6 $\gamma$ e	M6 $\gamma$	5,3	10.33 ± 0.02	9.81 ± 0.02	9.45 ± 0.02	9.24 ± 0.02	8.97 ± 0.02
11131034–1504005	...	(M6)	,5	12.36 ± 0.03	11.76 ± 0.03	11.40 ± 0.02	11.17 ± 0.02	11.00 ± 0.02
11150259–3759251	...	(M8.5)	,5	15.36 ± 0.05	14.59 ± 0.05	14.11 ± 0.06	13.84 ± 0.03	13.56 ± 0.03
11152992–2954436	M4 e	...	5,	12.37 ± 0.02	11.81 ± 0.03	11.53 ± 0.02	11.36 ± 0.02	11.18 ± 0.02
11160937–3601063	...	(M5.5)	,5	13.00 ± 0.02	12.35 ± 0.03	12.04 ± 0.02	11.86 ± 0.02	11.70 ± 0.02
11271382–3735076	...	L0 $\delta$	,17	16.47 ± 0.10	15.6 ± 0.1	15.2 ± 0.2	14.42 ± 0.03	14.03 ± 0.04
11283294–2924353	...	(M5)	,5	11.60 ± 0.03	11.03 ± 0.02	10.73 ± 0.02	10.59 ± 0.02	10.39 ± 0.02
11353003–1947062	...	(M6)	,5	12.21 ± 0.02	11.63 ± 0.02	11.32 ± 0.02	11.15 ± 0.02	10.96 ± 0.02
11382538–3841525	...	(M4)	,5	11.64 ± 0.02	11.08 ± 0.03	10.77 ± 0.02	10.63 ± 0.02	10.45 ± 0.02
11430143–3927002	...	(M5.5)	,5	12.83 ± 0.02	12.26 ± 0.02	11.97 ± 0.02	11.76 ± 0.02	11.59 ± 0.02
11443970–3455026	...	(M5.5)	,5	12.59 ± 0.02	12.02 ± 0.03	11.71 ± 0.02	11.55 ± 0.02	11.36 ± 0.02
11480096–2836488	...	L3 $\beta$	,5	16.11 ± 0.08	15.19 ± 0.08	14.56 ± 0.08	14.16 ± 0.03	13.85 ± 0.04
11501755–3407074	...	(M5)	,5	11.19 ± 0.02	10.65 ± 0.02	10.35 ± 0.02	10.14 ± 0.02	9.95 ± 0.02

Table 13 *continued*

GAGNÉ ET AL.  
Table 13 (*continued*)

2MASS Designation	Spectral Type <sup>a</sup>		Ref. <sup>c</sup>	2MASS <sup>b</sup>			AllWISE <sup>b</sup>	
	Optical	NIR		<i>J</i>	<i>H</i>	<i>K<sub>S</sub></i>	W1	W2
11510246-3611457	...	(M5.5)	,5	11.21 ± 0.02	10.61 ± 0.03	10.32 ± 0.02	10.11 ± 0.02	9.93 ± 0.02
11561415-3917217	...	(M6)	,5	13.07 ± 0.02	12.44 ± 0.03	12.14 ± 0.03	11.90 ± 0.02	11.69 ± 0.02
12012242-4103432	...	(M5.5)	,5	13.23 ± 0.02	12.70 ± 0.03	12.40 ± 0.03	12.24 ± 0.02	12.06 ± 0.02
12035905-3821402	...	M8 $\gamma$	,3	13.77 ± 0.03	13.12 ± 0.03	12.69 ± 0.03	12.42 ± 0.02	12.11 ± 0.02
12072486-3608359	...	(M6)	,5	13.48 ± 0.03	12.92 ± 0.03	12.57 ± 0.03	12.40 ± 0.02	12.18 ± 0.02
12093096-3820290	...	(M6.5)	,5	14.31 ± 0.03	13.70 ± 0.04	13.33 ± 0.03	13.12 ± 0.02	12.90 ± 0.03
12120009-3519434	...	(M5)	,5	12.95 ± 0.02	12.37 ± 0.02	12.10 ± 0.02	11.94 ± 0.02	11.72 ± 0.02
12134001-3723362	...	(M5)	,5	12.92 ± 0.03	12.31 ± 0.03	12.00 ± 0.02	11.80 ± 0.02	11.60 ± 0.02
12173617-2846082	...	(M6)	,5	12.77 ± 0.02	12.24 ± 0.03	11.90 ± 0.02	11.74 ± 0.02	11.54 ± 0.02
12193723-3132237	...	(M5.5)	,5	12.64 ± 0.02	12.03 ± 0.02	11.73 ± 0.03	11.57 ± 0.02	11.39 ± 0.02
12384389-2705384	...	(M6)	,5	13.25 ± 0.02	12.64 ± 0.02	12.35 ± 0.03	12.13 ± 0.02	11.90 ± 0.02
12414195-3625573	...	(M4.5)	,5	11.81 ± 0.02	11.27 ± 0.02	10.97 ± 0.02	10.81 ± 0.02	10.64 ± 0.02
12471536-3252233	...	(M5.5)	,5	13.05 ± 0.03	12.51 ± 0.02	12.20 ± 0.03	11.96 ± 0.02	11.76 ± 0.02
12474428-3816464	...	M9 $\gamma$	,24	14.78 ± 0.03	14.10 ± 0.04	13.57 ± 0.04	13.12 ± 0.02	12.53 ± 0.02
12532702-3504151	M3 e	...	5,	10.26 ± 0.02	9.64 ± 0.02	9.39 ± 0.02	9.27 ± 0.02	9.13 ± 0.02
12574941-4111373	...	M6 $\gamma$	,17	13.02 ± 0.02	12.46 ± 0.03	12.09 ± 0.03	11.88 ± 0.02	11.64 ± 0.02
13075615-4159202	...	(M6)	,5	13.09 ± 0.02	12.51 ± 0.02	12.18 ± 0.02	12.04 ± 0.02	11.87 ± 0.02
13110859-3725022	...	(M6)	,5	13.61 ± 0.03	13.08 ± 0.03	12.73 ± 0.03	12.56 ± 0.02	12.35 ± 0.02
13153357-3425084	...	(M6)	,29	13.36 ± 0.02	12.78 ± 0.02	12.48 ± 0.02	12.26 ± 0.02	12.03 ± 0.02
13191194-3600082	...	(M5.5)	,29	13.41 ± 0.02	12.77 ± 0.02	12.49 ± 0.03	12.31 ± 0.02	12.10 ± 0.02
<b>Low-Likelihood Candidate Members of TW Hydrae</b>								
08561384-1342242	...	M8.5 $\gamma$	,17	13.60 ± 0.02	12.98 ± 0.03	12.49 ± 0.02	12.17 ± 0.02	11.64 ± 0.02
09395647-2946286	...	(M5)	,5	11.76 ± 0.02	11.21 ± 0.02	10.93 ± 0.02	10.77 ± 0.02	10.58 ± 0.02
10211908+0804268	...	(M5)	,5	10.79 ± 0.02	10.23 ± 0.02	9.93 ± 0.02	9.74 ± 0.02	9.56 ± 0.02
10563080-3028137	...	(M4.5)	,5	11.66 ± 0.02	11.09 ± 0.02	10.82 ± 0.02	10.63 ± 0.02	10.45 ± 0.02
10582800-1046304	M4	...	30,	9.51 ± 0.02	8.97 ± 0.02	8.64 ± 0.02	8.46 ± 0.02	8.27 ± 0.02
11023986-2507113	M4 e	...	5,	11.29 ± 0.03	10.74 ± 0.03	10.44 ± 0.02	10.27 ± 0.02	10.08 ± 0.02
11153797-2552192	...	(M5.5)	,5	12.33 ± 0.02	11.77 ± 0.03	11.46 ± 0.02	11.27 ± 0.03	11.07 ± 0.02
11382693-3843138	M5 e	...	5,	12.13 ± 0.02	11.55 ± 0.02	11.25 ± 0.02	11.09 ± 0.02	10.88 ± 0.02
12021801-3110348	...	(M9.5)	,5	14.91 ± 0.04	14.19 ± 0.03	13.84 ± 0.05	13.62 ± 0.03	13.41 ± 0.03
12162481-2742007	...	(M8.8)	,5	14.84 ± 0.04	14.25 ± 0.04	13.85 ± 0.05	13.66 ± 0.03	13.43 ± 0.03
12271545-0636458	M9	M8.5 $\beta$	31,17	14.19 ± 0.03	13.39 ± 0.03	12.88 ± 0.03	12.53 ± 0.02	12.28 ± 0.02
12333935-3040139	...	(M7.5)	,5	14.64 ± 0.04	14.05 ± 0.04	13.64 ± 0.04	13.22 ± 0.03	12.89 ± 0.03
12454194-3903106	...	(M9.5)	,5	15.46 ± 0.05	14.84 ± 0.05	14.41 ± 0.07	14.22 ± 0.03	13.95 ± 0.04
12471067-3632150	...	(M5)	,5	12.91 ± 0.02	12.35 ± 0.02	12.07 ± 0.02	11.89 ± 0.02	11.69 ± 0.02
13155594-3403418	...	(M5.5)	,29	13.10 ± 0.03	12.54 ± 0.03	12.22 ± 0.02	12.02 ± 0.02	11.82 ± 0.02
<b>Likely Contaminants from Lower Centaurus Crux</b>								
10134260-2759586	M5	...	15,	12.26 ± 0.03	11.63 ± 0.02	11.25 ± 0.02	11.07 ± 0.02	10.90 ± 0.02
10182870-3150029 A	M0 e	M2 pec	18,3	[9.62 ± 0.03]	[8.93 ± 0.03]	[8.79 ± 0.01]	[8.58 ± 0.02]	[8.55 ± 0.02]
10182870-3150029 B	[M0 e]	[M2 pec]	18,3	[9.62 ± 0.03]	[8.93 ± 0.03]	[8.79 ± 0.01]	[8.58 ± 0.02]	[8.55 ± 0.02]
10212570-2830427	...	L5 $\beta$	,5	16.9 ± 0.2	15.9 ± 0.1	15.0 ± 0.1	14.18 ± 0.03	13.73 ± 0.04
10252092-4241539	M1	...	25,	9.50 ± 0.03	8.81 ± 0.02	8.59 ± 0.02	8.50 ± 0.02	8.45 ± 0.02
10260210-4105537	M0.5	...	25,	9.18 ± 0.02	8.49 ± 0.05	8.27 ± 0.03	8.15 ± 0.02	8.06 ± 0.02
10292874-3823394	...	(M6)	,5	12.94 ± 0.03	12.35 ± 0.03	12.04 ± 0.02	11.85 ± 0.02	11.65 ± 0.02
10394605-3510139	...	(M5)	,5	12.43 ± 0.03	11.87 ± 0.03	11.58 ± 0.02	11.38 ± 0.02	11.19 ± 0.02
10443052-3730554	...	(M5.5)	,5	12.93 ± 0.02	12.34 ± 0.03	12.05 ± 0.02	11.87 ± 0.02	11.68 ± 0.02
10455263-2819303	M5.5 $\gamma$ e	M6 $\gamma$	5,17	12.82 ± 0.02	12.31 ± 0.02	11.94 ± 0.03	11.72 ± 0.02	11.44 ± 0.02
10492026-2440101	...	(M5.5)	,5	12.29 ± 0.02	11.74 ± 0.02	11.46 ± 0.02	11.30 ± 0.02	11.08 ± 0.02
10492579-3527125	...	(M6)	,5	13.42 ± 0.03	12.83 ± 0.03	12.56 ± 0.02	12.37 ± 0.02	12.20 ± 0.02
10514507-3226337	...	(M6)	,5	13.30 ± 0.03	12.75 ± 0.03	12.45 ± 0.03	12.23 ± 0.02	12.03 ± 0.02
10571669-3512548	...	(M6)	,5	13.41 ± 0.03	12.78 ± 0.03	12.44 ± 0.03	12.18 ± 0.02	11.92 ± 0.02
11035873-4156475	...	(M6)	,5	13.54 ± 0.02	13.03 ± 0.03	12.58 ± 0.03	12.38 ± 0.02	12.11 ± 0.02
11062620-4019330	...	(M5.5)	,5	12.45 ± 0.02	11.88 ± 0.02	11.61 ± 0.02	11.42 ± 0.02	11.24 ± 0.02
11130416-4516056	M0	...	32,	12.56 ± 0.03	11.93 ± 0.03	11.72 ± 0.03	11.59 ± 0.02	11.55 ± 0.02
11132622-4523427 A	M0.5	...	14,	[10.17 ± 0.03]	[9.48 ± 0.04]	[9.25 ± 0.03]	[9.12 ± 0.02]	[9.02 ± 0.02]
11132622-4523427 B	M1	...	25,	[10.17 ± 0.03]	[9.48 ± 0.04]	[9.25 ± 0.03]	[9.12 ± 0.02]	[9.02 ± 0.02]
11191302-4342401	...	(M5)	,5	13.02 ± 0.03	12.45 ± 0.02	12.14 ± 0.02	11.98 ± 0.02	11.79 ± 0.02
11204706-2738056	...	(M4.5)	,5	11.82 ± 0.02	11.22 ± 0.02	10.93 ± 0.03	10.76 ± 0.02	10.55 ± 0.02
11385038-3830011	...	(M5.5)	,5	12.98 ± 0.02	12.42 ± 0.03	12.10 ± 0.02	11.90 ± 0.02	11.71 ± 0.02
11394506-3729069	...	(M5)	,5	12.90 ± 0.02	12.32 ± 0.03	12.02 ± 0.02	11.84 ± 0.02	11.60 ± 0.02
11443034-3820341	...	(M4.5)	,5	12.03 ± 0.02	11.45 ± 0.02	11.17 ± 0.02	11.02 ± 0.02	10.82 ± 0.02
11455177-5520456	K5 e	...	18,	8.02 ± 0.03	7.41 ± 0.03	7.27 ± 0.03	7.07 ± 0.05	7.16 ± 0.02
11472064-4953042 A	K7 e	...	33,	[9.90 ± 0.02]	[9.23 ± 0.04]	[9.03 ± 0.03]	[8.95 ± 0.02]	[8.91 ± 0.02]

*Table 13 continued*

Table 13 (*continued*)

2MASS Designation	Spectral Type <sup>a</sup>		Ref. <sup>c</sup>	2MASS <sup>b</sup>			AllWISE <sup>b</sup>	
	Optical	NIR		<i>J</i>	<i>H</i>	<i>K<sub>S</sub></i>	W1	W2
11472064-4953042 B	[K7 e]	...	33,	[9.90 ± 0.02]	[9.23 ± 0.04]	[9.03 ± 0.03]	[8.95 ± 0.02]	[8.91 ± 0.02]
11472454-4953029	G5	...	33,	7.89 ± 0.02	7.57 ± 0.05	7.51 ± 0.03	7.39 ± 0.03	7.45 ± 0.02
11511119-4132064	...	(M6)	,5	13.34 ± 0.03	12.75 ± 0.02	12.45 ± 0.03	12.27 ± 0.02	12.08 ± 0.02
11554920-4303109	...	(M4.5)	,5	12.24 ± 0.02	11.71 ± 0.02	11.42 ± 0.02	11.28 ± 0.02	11.09 ± 0.02
12011772-3712329	...	(M5)	,5	12.75 ± 0.02	12.22 ± 0.02	11.94 ± 0.03	11.76 ± 0.02	11.53 ± 0.02
12071089-3230537	M4 e	M6 $\gamma$	14,3	13.05 ± 0.02	12.49 ± 0.02	12.11 ± 0.02	11.73 ± 0.02	11.22 ± 0.02
12094181-5854420	[K0 IVe]	...	34,	8.45 ± 0.03	7.95 ± 0.03	7.83 ± 0.08	8.25 ± 0.03	8.30 ± 0.02
12094184-5854450	K0 IVe	...	34,	8.32 ± 0.02	7.81 ± 0.02	7.66 ± 0.02	8.25 ± 0.03	8.30 ± 0.02
12105770-3708100	...	(M7.5)	,5	14.24 ± 0.03	13.65 ± 0.03	13.29 ± 0.04	13.01 ± 0.02	12.78 ± 0.03
12174683-3804157	...	(M5)	,5	12.90 ± 0.02	12.32 ± 0.03	11.96 ± 0.02	11.78 ± 0.02	11.57 ± 0.02
12333140-3641407	...	(M3.5)	,5	9.62 ± 0.02	9.03 ± 0.02	8.74 ± 0.02	8.60 ± 0.02	8.48 ± 0.02
12342064-4815135	M1.5 Ve	M3	33,35	10.56 ± 0.03	9.94 ± 0.02	9.67 ± 0.02	9.42 ± 0.02	9.25 ± 0.02
12342047-4815195	M2 Ve	M3.5	33,35	10.49 ± 0.04	9.83 ± 0.03	9.56 ± 0.04	9.42 ± 0.02	9.25 ± 0.02
12421948-3805064 A	M3 e	...	5,	[12.29 ± 0.04]	[11.62 ± 0.04]	[11.42 ± 0.04]	[11.06 ± 0.02]	[10.89 ± 0.02]
12421948-3805064 B	M3 e	...	5,	[12.29 ± 0.04]	[11.62 ± 0.04]	[11.42 ± 0.04]	[11.06 ± 0.02]	[10.89 ± 0.02]
12482006-4237338	G0 V	...	36,	8.99 ± 0.03	8.72 ± 0.05	8.67 ± 0.02	8.62 ± 0.02	8.65 ± 0.02
12520989-4948280	M9	M8 $\gamma$	3,3	13.76 ± 0.02	13.15 ± 0.02	12.72 ± 0.03	12.51 ± 0.02	12.22 ± 0.02
12522053-4515542	...	(M5)	,5	13.11 ± 0.03	12.54 ± 0.03	12.24 ± 0.03	12.09 ± 0.02	11.90 ± 0.02
12535039-4211215	...	M9.5 $\gamma$	,17	16.0 ± 0.1	15.3 ± 0.1	14.7 ± 0.1	14.28 ± 0.03	13.93 ± 0.03
12574463-3635431	...	M7 $\beta$	,17	14.58 ± 0.03	13.91 ± 0.04	13.61 ± 0.04	13.31 ± 0.02	13.07 ± 0.03
13204539-4611377 A	K5	...	33,	[10.56 ± 0.02]	[9.94 ± 0.02]	[9.77 ± 0.02]	[9.66 ± 0.02]	[9.63 ± 0.02]
13204539-4611377 B	[K5]	...	33,	[10.56 ± 0.02]	[9.94 ± 0.02]	[9.77 ± 0.02]	[9.66 ± 0.02]	[9.63 ± 0.02]
13213722-4421518	M0.5	...	37,	8.85 ± 0.02	9.08 ± 0.02	9.74 ± 0.02	8.74 ± 0.02	8.67 ± 0.02
13412668-4341522	M3.5	...	25,	10.75 ± 0.02	10.13 ± 0.02	9.87 ± 0.02	9.71 ± 0.02	9.54 ± 0.02
13481593-3642228	...	(M5)	,5	12.21 ± 0.03	11.62 ± 0.02	11.29 ± 0.02	11.12 ± 0.02	10.93 ± 0.02
<b>Candidate Members of Carina</b>								
10131476-5230540	K3 IV(e)	K3	2,3	7.87 ± 0.01	7.35 ± 0.03	7.19 ± 0.01	7.01 ± 0.05	7.18 ± 0.02
10282500-3959230	M5	...	23,	10.87 ± 0.02	10.35 ± 0.02	10.02 ± 0.02	9.82 ± 0.02	9.62 ± 0.02
<b>Member of <math>\beta</math> Pictoris</b>								
10172689-5354265 A	M6 Ve	M5	38,39	[9.31 ± 0.01]	[8.84 ± 0.04]	[8.44 ± 0.01]	[8.25 ± 0.02]	[8.02 ± 0.02]
10172689-5354265 B	[M6 Ve]	[M5]	38,39	[9.31 ± 0.01]	[8.84 ± 0.04]	[8.44 ± 0.01]	[8.25 ± 0.02]	[8.02 ± 0.02]
<b>Rejected candidates</b>								
08141769+0253199	M5 e	...	5,	11.52 ± 0.02	10.97 ± 0.02	10.67 ± 0.03	10.47 ± 0.02	10.25 ± 0.02
08144321+2336045	M4 e	...	5,	10.94 ± 0.02	10.40 ± 0.02	10.08 ± 0.03	9.93 ± 0.02	9.73 ± 0.02
08254335-0029110	...	L0.5	,17	15.45 ± 0.06	14.58 ± 0.04	13.98 ± 0.06	13.55 ± 0.03	13.24 ± 0.03
09292857-4431563	F7 V	...	36,	6.04 ± 0.03	5.81 ± 0.05	5.74 ± 0.02	5.7 ± 0.1	5.60 ± 0.04
09353126-2802552	K6 Ve	...	18,	8.51 ± 0.01	7.88 ± 0.04	7.69 ± 0.01	7.62 ± 0.03	7.65 ± 0.02
09471986-4003098	K0 V	...	18,	9.41 ± 0.02	8.98 ± 0.03	8.88 ± 0.02	8.79 ± 0.02	8.81 ± 0.02
09512673-2220196 A	M5	...	5,	[12.63 ± 0.03]	[12.07 ± 0.03]	[11.69 ± 0.03]	[11.50 ± 0.02]	[11.36 ± 0.02]
09512673-2220196 B	M5	...	5,	[12.63 ± 0.03]	[12.07 ± 0.03]	[11.69 ± 0.03]	[11.50 ± 0.02]	[11.36 ± 0.02]
09553336-0208403	...	L7 pec(red)	,5	17.14 ± 0.02 <sup>d</sup>	15.96 ± 0.01 <sup>d</sup>	15.01 ± 0.01 <sup>d</sup>	13.93 ± 0.03	13.39 ± 0.03
09590842-2239345	K2 Ve	...	18,	8.03 ± 0.02	7.49 ± 0.04	7.39 ± 0.02	7.23 ± 0.04	7.34 ± 0.02
10104667-3447531	G8: V:	...	18,	9.94 ± 0.03	9.48 ± 0.02	9.35 ± 0.02	9.30 ± 0.02	9.32 ± 0.02
10144705-3728151 A	M3 pec	...	5,	[13.45 ± 0.04]	[12.90 ± 0.04]	[12.58 ± 0.04]	[12.25 ± 0.02]	[12.06 ± 0.02]
10144705-3728151 B	M3 pec	...	5,	[13.45 ± 0.04]	[12.90 ± 0.04]	[12.58 ± 0.04]	[12.25 ± 0.02]	[12.06 ± 0.02]
10190109-2646336	M5 e	(M5.5)	5,5	11.93 ± 0.02	11.34 ± 0.02	11.06 ± 0.02	10.87 ± 0.02	10.66 ± 0.02
10220449-3233270	K0 V:e	...	18,	7.91 ± 0.03	7.39 ± 0.04	7.20 ± 0.02	6.98 ± 0.05	7.10 ± 0.02
10221800-1032156	K5 V	...	40,	8.40 ± 0.02	7.79 ± 0.03	7.66 ± 0.03	7.46 ± 0.03	7.51 ± 0.02
10432828-2903513	K1 V	...	20,	6.18 ± 0.02	5.77 ± 0.05	5.66 ± 0.02	5.6 ± 0.2	5.51 ± 0.05
10473117-2220528	K1 V	...	41,	6.96 ± 0.02	6.56 ± 0.03	6.51 ± 0.02	6.43 ± 0.09	6.40 ± 0.03
10513331-1916530	...	M9 pec	,17	14.69 ± 0.03	13.95 ± 0.03	13.43 ± 0.04	13.10 ± 0.03	12.82 ± 0.03
10542303-1507082	M5.5 e	...	5,	11.10 ± 0.02	10.57 ± 0.02	10.26 ± 0.02	10.04 ± 0.02	9.82 ± 0.02
10563080+0723184	K2.5 V	...	42,	5.74 ± 0.02	5.35 ± 0.03	5.20 ± 0.02	5.2 ± 0.2	5.05 ± 0.07
11063147-4201251	...	M8	,5	15.27 ± 0.06	14.44 ± 0.07	14.09 ± 0.08	13.87 ± 0.03	13.65 ± 0.03
11112984-2713320	M4.5 e	...	5,	11.80 ± 0.02	11.21 ± 0.02	10.90 ± 0.02	10.70 ± 0.02	10.50 ± 0.02
11195251-3917150 A	M2	...	5,	[13.88 ± 0.04]	[13.33 ± 0.05]	[12.99 ± 0.04]	[12.64 ± 0.02]	[12.49 ± 0.02]
11195251-3917150 B	M2	...	5,	[13.88 ± 0.04]	[13.33 ± 0.05]	[12.99 ± 0.04]	[12.64 ± 0.02]	[12.49 ± 0.02]
11254754-4410267	M4	...	25,	10.34 ± 0.03	9.75 ± 0.02	9.48 ± 0.02	9.33 ± 0.02	9.14 ± 0.02
11423628-3859108	< M0	...	5,	12.46 ± 0.02	11.89 ± 0.02	11.59 ± 0.02	11.43 ± 0.02	11.25 ± 0.02
11424808-3548577	F5 + F8	...	43,	[8.84 ± 0.02]	[8.58 ± 0.03]	[8.44 ± 0.02]	[8.44 ± 0.03]	[8.49 ± 0.02]
11443846-4925025	K1 V	...	18,	[7.87 ± 0.02]	[7.39 ± 0.03]	[7.23 ± 0.02]	[6.91 ± 0.07]	[7.01 ± 0.02]
11504110-2356075	M6 e	...	5,	12.27 ± 0.02	11.65 ± 0.02	11.28 ± 0.02	11.11 ± 0.02	10.91 ± 0.02

Table 13 *continued*



GAGNÉ ET AL.  
Table 13 (*continued*)

2MASS Designation	Spectral Type <sup>a</sup>		Ref. <sup>c</sup>	2MASS <sup>b</sup>			AllWISE <sup>b</sup>	
	Optical	NIR		<i>J</i>	<i>H</i>	<i>K<sub>S</sub></i>	W1	W2
11532691–3015414	M4.5 e	...	5,	12.31 ± 0.03	11.76 ± 0.03	11.42 ± 0.02	11.26 ± 0.02	11.05 ± 0.02
11571557–4022292	...	(M5)	,29	13.20 ± 0.03	12.49 ± 0.03	12.16 ± 0.02	12.02 ± 0.02	11.83 ± 0.02
12000160–1731308	M4 γ e	...	5,	9.40 ± 0.02	8.69 ± 0.04	8.47 ± 0.03	8.38 ± 0.02	8.19 ± 0.02
12041256+0514128	M5 e	...	5,	10.22 ± 0.02	9.64 ± 0.02	9.32 ± 0.02	9.11 ± 0.02	8.90 ± 0.02
12073145–3310222	K9	...	32,	11.85 ± 0.02	11.19 ± 0.03	11.01 ± 0.02	10.92 ± 0.02	10.89 ± 0.02
12090628–3247453	M1	...	32,	12.80 ± 0.03	12.24 ± 0.02	11.98 ± 0.02	11.86 ± 0.02	11.75 ± 0.02
12100648–4910505	G5 V	...	18,	6.92 ± 0.03	6.59 ± 0.03	6.49 ± 0.02	6.45 ± 0.07	6.42 ± 0.02
12113180–3416537	M2	...	5,	9.45 ± 0.02	8.81 ± 0.04	8.52 ± 0.02	8.40 ± 0.02	8.39 ± 0.02
12194846–3232059	...	M7	,5	15.66 ± 0.06	14.97 ± 0.06	14.59 ± 0.08	14.38 ± 0.03	14.16 ± 0.04
12220574–4159572	...	(M5.5)	,29	13.09 ± 0.02	12.52 ± 0.03	12.23 ± 0.03	11.87 ± 0.02	11.74 ± 0.02
12214223–4012050	...	< M0	,17	16.5 ± 0.1	15.6 ± 0.1	15.0 ± 0.1	14.45 ± 0.03	14.21 ± 0.04
12214852–3652349 A	M4 e	...	5,	[12.95 ± 0.03]	[12.34 ± 0.04]	[11.98 ± 0.02]	[11.83 ± 0.02]	[11.66 ± 0.02]
12214852–3652349 B	M4 e	...	5,	[12.95 ± 0.03]	[12.34 ± 0.04]	[11.98 ± 0.02]	[11.83 ± 0.02]	[11.66 ± 0.02]
12282569–3955014 A	M4 e	...	5,	[11.91 ± 0.03]	[11.30 ± 0.05]	[10.90 ± 0.03]	[10.65 ± 0.02]	[10.48 ± 0.02]
12282569–3955014 B	M3.5 e	...	5,	[11.91 ± 0.03]	[11.30 ± 0.05]	[10.90 ± 0.03]	[10.65 ± 0.02]	[10.48 ± 0.02]
12310489–3801065	...	M8 pec	,17	14.68 ± 0.04	14.09 ± 0.05	13.53 ± 0.04	13.37 ± 0.02	13.15 ± 0.03
12451035–1443029	...	< M0	,5	15.51 ± 0.06	14.94 ± 0.06	14.7 ± 0.1	16.65 ± 0.09	16.6 ± 0.3
12563961–2718455	...	L4 β	,5	16.4 ± 0.1	15.4 ± 0.1	14.71 ± 0.09	14.13 ± 0.03	13.74 ± 0.04
13112902–4252418	M1.5	...	16,	10.14 ± 0.03	9.42 ± 0.03	9.24 ± 0.03	9.15 ± 0.02	9.07 ± 0.02
13265348–5022270	M9	M9 pec	3,3	14.72 ± 0.04	13.98 ± 0.04	13.40 ± 0.04	12.92 ± 0.02	12.35 ± 0.02
14112131–2119503	M9 β	M8 β	31,17	12.44 ± 0.02	11.83 ± 0.03	11.33 ± 0.02	11.08 ± 0.02	10.82 ± 0.02
14252913–4113323 A	M2.5 Ve	...	1,	[9.30 ± 0.02]	[8.66 ± 0.03]	[8.37 ± 0.01]	[8.29 ± 0.03]	[8.11 ± 0.02]
14252913–4113323 B	[M2.5 Ve]	...	1,	[9.30 ± 0.02]	[8.66 ± 0.03]	[8.37 ± 0.01]	[8.29 ± 0.03]	[8.11 ± 0.02]
18440971+7129178	M4	...	44,	9.83 ± 0.05	9.23 ± 0.02	> 9.1	9.40 ± 0.02	9.18 ± 0.02
18441019+7129175	M4	...	44,	10.14 ± 0.04	9.46 ± 0.04	8.76 ± 0.01	...	...

<sup>a</sup> Spectral types between parentheses are photometric spectral types estimated from 2MASS and AllWISE photometry, whereas those between square brackets are obtained assuming equal-type companions (for binaries with brightness ratios close to unity).

<sup>b</sup> Values between square brackets are corrected for the known multiplicity level, assuming equal-brightness.

<sup>c</sup> Two references, separated by a comma, are given for the optical and NIR spectral types, respectively.

<sup>d</sup> Synthetic 2MASS photometry calculated from a NIR spectrum that is anchored on *J*-, *H*- and *K*-bands Vista Hemisphere Survey (VHS) photometry.

<sup>e</sup> Synthetic 2MASS photometry calculated from a NIR spectrum that is anchored on *J*- and *K*-bands Vista Hemisphere Survey (VHS) photometry.

NOTE—See Section 5 for more details.

**References**—(1) Riedel et al. 2014; (2) Pecaut & Mamajek 2013; (3) Looper 2011; (4) Scholz et al. 2005; (5) this paper; (6) Abt & Morrell 1995; (7) Webb et al. 1999; (8) Malo et al. 2014; (9) Torres et al. 2003; (10) Konopacky et al. 2007; (11) Looper et al. 2010a; (12) Schneider et al. 2012b; (13) Reid et al. 2008; (14) Shkolnik et al. 2011; (15) Gizis 2002; (16) Rodriguez et al. 2011; (17) Gagné et al. 2015d; (18) Torres et al. 2006b; (19) Kastner et al. 2008; (20) Houk 1982; (21) Looper et al. 2007; (22) Kellogg et al. 2016; (23) Murphy et al. 2015; (24) Gagné et al. 2014a; (25) Riaz et al. 2006; (26) Riedel et al. 2016; (27) Cruz et al. 2007; (28) Janson et al. 2012a; (29) Gagné et al. 2015b; (30) Rojas-Ayala et al. 2012; (31) Cruz et al. 2003; (32) Elliott et al. 2016; (33) Zuckerman et al. 2001b; (34) Mamajek et al. 2002; (35) Manara et al. 2013; (36) Houk 1978; (37) Reid 2003; (38) Malo et al. 2013; (39) Weis 1993; (40) Stocke et al. 1991; (41) Gray et al. 2006; (42) Gray et al. 2003; (43) Kharchenko et al. 2007; (44) Shkolnik et al. 2012.

**Table 14.** BANYAN II Probabilities for Candidates and Members of TWA

2MASS Designation	Other Names	BANYAN II Inputs <sup>a</sup>	Bayesian Probability (%)	Contamination Probability (%) <sup>b</sup>	Statistical Distance (pc)	Statistical RV (km s <sup>-1</sup> )
<b>Bona Fide Members of TW Hydrae</b>						
10120908-3124451	TWA 39 AB	μyrt	99.4	< 0.1	...	...
10423011-3340162	TWA 7	μyrt	99.9	< 0.1	...	...
11015191-3442170	TWA 1	μyrt	100.0	< 0.1	...	...
11020983-3430355	TWA 28	μyprt	99.9	< 0.1	...	...
11084400-2804504	TWA 43; HIP 54477; HR 4334	μyrt	98.7	< 0.1	...	...
11091380-3001398	TWA 2 AB	μyrt	100.0	< 0.1	...	...
11210549-3845163	TWA 12	μyrt	100.0	< 0.1	...	...
11211723-3446454	TWA 13 A	μyrt	100.0	< 0.1	...	...

*Table 14 continued*

Table 14 (*continued*)

2MASS Designation	Other Names	BANYAN II Inputs <sup>a</sup>	Bayesian Probability (%)	Contamination Probability (%) <sup>b</sup>	Statistical Distance (pc)	Statistical RV (km s <sup>-1</sup> )
11211745-3446497	TWA 13 B	$\mu yrt$	100.0	< 0.1	...	...
11220530-2446393	TWA 4 AB	$\mu yrt$	99.9	< 0.1	...	...
11315526-3436272	TWA 5 AB	$\mu yrt$	100.0	< 0.1	...	...
11324116-2652090	TWA 8 B	$\mu yprt$	99.8	< 0.1	...	...
11324124-2651559	TWA 8 A	$\mu yrt$	99.6	< 0.1	...	...
11321822-3018316	TWA 30 B	$\mu y$	100.0	< 0.1	47.0 ± 5.6	...
11321831-3019518	TWA 30 A	$\mu yprt$	100.0	< 0.1	...	...
11393382-3040002	TWA 33	$\mu yrt$	98.6	< 0.1	...	...
11395113-3159214	TWA 26	$\mu yprt$	100.0	< 0.1	...	...
11482373-3728485	TWA 9 B	$\mu y$	100.0	< 0.1	66.2 ± 7.2	...
11482422-3728491	TWA 9 A	$\mu yrt$	100.0	< 0.1	...	...
12072738-3247002	TWA 23 AB	$\mu yrt$	100.0	< 0.1	...	...
12073346-3932539	TWA 27 AB	$\mu yprt$	100.0	< 0.1	...	...
12153072-3948426	TWA 25	$\mu yrt$	100.0	< 0.1	...	...
12265135-3316124	TWA 32 AB	$\mu yprt$	99.6	< 0.1	...	...
12313807-4558593	TWA 20 AB	$\mu yrt$	99.7	< 0.1	...	...
12345629-4538075	TWA 16 AB	$\mu yrt$	99.9	< 0.1	...	...
12350424-4136385	TWA 10	$\mu yrt$	99.8	< 0.1	...	...
12354893-3950245	TWA 11 C	$\mu yt$	98.9	< 0.1	...	9.9 ± 1.5
12360103-3952102	TWA 11 A; HR 4796B	$\mu yrt$	99.9	< 0.1	...	...
12451416-4429077	TWA 29	$\mu yprt$	99.0	< 0.1	...	...
<b>High-Likelihood Candidate Members of TW Hydrae</b>						
10284580-2830374	TWA 34	$\mu ypr$	98.3	< 0.1	47.0 ± 5.6	...
11102788-3731520	TWA 3 AB	$\mu y$	99.9	< 0.1	40.2 <sup>+4.8</sup> <sub>-4.4</sub>	...
11193254-1137466	TWA 42	$\mu ypr$	95.2	< 0.1	28.9 ± 3.6	...
11472421-2040204	TWA 41	$\mu ypr$	96.9	< 0.1	33.3 <sup>+4.4</sup> <sub>-4.0</sub>	...
11592786-4510192	TWA 45	$\mu yt$	99.7	< 0.1	...	11.0 ± 1.7
12002750-3405371	TWA 35	$\mu y$	99.4	< 0.1	61.4 <sup>+7.2</sup> <sub>-6.8</sub>	...
12023799-3328402	TWA 36	$\mu ypr$	98.4	< 0.1	58.6 ± 6.4	...
12074836-3900043	TWA 40	$\mu ypr$	99.6	< 0.1	59.8 ± 5.6	...
12175920-3734433	TWA 44	$\mu ypr$	98.4	< 0.1	65.4 <sup>+8.0</sup> <sub>-7.6</sub>	...
12354615-4115531	TWA 46	$\mu yt$	96.7	< 0.1	...	10.3 ± 1.4
12371238-4021480	TWA 47	$\mu y$	99.8	< 0.1	62.6 ± 6.8	...
<b>Candidate Members of TW Hydrae</b>						
09400251-2229251	...	$\mu$	68.7	3.5	39.0 <sup>+5.2</sup> <sub>-4.8</sub>	15.6 ± 1.4
09532126-1014205	...	$\mu ypr$	81.1	< 0.1	29.3 ± 2.8	14.2 ± 1.3
10023100-2814280	...	$\mu$	93.4	1.8	39.4 ± 5.2	15.4 ± 1.4
10103260-2832250	...	$\mu pr$	83.7	1.9	45.8 ± 5.2	14.8 ± 1.5
10331650-3517001	...	$\mu pr$	93.9	1.1	54.2 <sup>+6.4</sup> <sub>-6.0</sub>	14.1 ± 1.5
10380178-2154225	...	$\mu pr$	46.8	5.1	36.6 ± 4.0	12.4 ± 1.4
10541299-3016450	...	$\mu pr$	82.6	1.7	54.2 <sup>+5.2</sup> <sub>-4.4</sub>	12.8 ± 1.5
10585054-2346206	...	$\mu ypr$	73.8	< 0.1	44.6 ± 4.8	...
11034950-3409445	...	$\mu ypr$	44.8	< 0.1	65.8 <sup>+6.8</sup> <sub>-7.6</sub>	12.6 ± 1.7
11035165-3711483	...	$\mu pr$	87.2	0.9	50.6 <sup>+6.4</sup> <sub>-6.0</sub>	12.7 ± 1.4
11064461-3715115	...	$\mu ypr$	94.6	< 0.1	62.6 <sup>+7.2</sup> <sub>-6.4</sub>	13.0 ± 1.5
11112820-2655027	TWA 37	$\mu ypr$	99.3	< 0.1	43.4 <sup>+5.2</sup> <sub>-4.8</sub>	11.7 ± 1.4
11131034-1504005	...	$\mu pr$	24.6	16.4	38.6 <sup>+4.0</sup> <sub>-3.6</sub>	9.7 ± 1.4
11150259-3759251	...	$\mu pr$	94.4	1.4	67.8 ± 6.0	12.6 ± 1.7

Table 14 *continued*

Table 14 (*continued*)

2MASS Designation	Other Names	BANYAN II Inputs <sup>a</sup>	Bayesian Probability (%)	Contamination Probability (%) <sup>b</sup>	Statistical Distance (pc)	Statistical RV (km s <sup>-1</sup> )
11152992-2954436	...	$\mu\gamma$	98.3	< 0.1	53.0 ± 6.4	...
11160937-3601063	...	$\mu\rho$	99.4	0.7	53.4 ± 6.0	12.1 ± 1.5
11271382-3735076	...	$\mu\gamma\rho$	91.8	< 0.1	61.8 <sup>+9.2</sup> <sub>-8.0</sub>	12.1 ± 2.1
11283294-2924353	...	$\mu\rho$	47.3	4.5	39.0 <sup>+4.8</sup> <sub>-4.4</sub>	10.3 ± 1.5
11353003-1947062	...	$\mu\rho$	52.7	15.0	33.8 ± 3.2	9.3 ± 1.4
11382538-3841525	...	$\mu$	99.4	0.6	59.8 ± 7.2	11.4 ± 1.5
11430143-3927002	...	$\mu\rho$	98.0	0.7	62.6 <sup>+7.6</sup> <sub>-6.8</sub>	11.4 ± 1.7
11443970-3455026	...	$\mu\rho$	75.3	1.5	49.8 ± 5.6	10.5 ± 1.5
11480096-2836488	...	$\mu\gamma\rho$	77.4	< 0.1	49.8 <sup>+6.0</sup> <sub>-5.2</sub>	...
11501755-3407074	...	$\mu\rho$	74.6	2.7	31.7 <sup>+4.0</sup> <sub>-3.2</sub>	10.0 ± 1.5
11510246-3611457	...	$\mu\rho$	62.1	2.9	30.1 <sup>+3.6</sup> <sub>-3.2</sub>	10.2 ± 1.5
11561415-3917217	...	$\mu\rho$	98.8	0.6	54.6 <sup>+6.4</sup> <sub>-5.6</sub>	10.5 ± 1.5
12012242-4103432	...	$\mu\rho$	95.5	1.6	73.4 <sup>+8.4</sup> <sub>-7.6</sub>	11.2 ± 1.7
12035905-3821402	TWA 38	$\mu\gamma\rho$	99.5	< 0.1	63.8 <sup>+6.8</sup> <sub>-6.4</sub>	10.6 ± 1.7
12072486-3608359	...	$\mu\rho$	87.1	1.8	65.0 <sup>+7.2</sup> <sub>-6.8</sub>	10.5 ± 1.7
12093096-3820290	...	$\mu\rho$	55.3	8.0	75.4 <sup>+8.0</sup> <sub>-7.6</sub>	11.0 ± 1.7
12120009-3519434	...	$\mu\rho$	45.2	8.9	69.8 <sup>+7.6</sup> <sub>-7.2</sub>	10.7 ± 1.7
12134001-3723362	...	$\mu\rho$	86.5	2.7	69.8 <sup>+8.0</sup> <sub>-7.6</sub>	10.6 ± 1.7
12173617-2846082	...	$\mu\rho$	23.7	10.9	46.2 ± 4.8	7.9 ± 1.7
12193723-3132237	...	$\mu\rho$	65.4	3.0	51.8 ± 5.6	9.5 ± 1.7
12384389-2705384	...	$\mu\rho$	20.0	12.2	57.8 <sup>+6.0</sup> <sub>-5.6</sub>	8.3 ± 2.0
12414195-3625573	...	$\mu$	94.3	1.3	59.0 <sup>+6.8</sup> <sub>-6.4</sub>	8.6 ± 1.8
12471536-3252233	...	$\mu\rho$	44.6	5.3	59.4 <sup>+6.4</sup> <sub>-6.0</sub>	8.2 ± 2.0
12474428-3816464	...	$\mu\gamma\rho$	49.4	< 0.1	67.8 ± 7.2	9.9 ± 1.8
12532702-3504151	...	$\mu$	56.2	4.6	67.0 <sup>+7.6</sup> <sub>-7.2</sub>	8.6 ± 1.8
12574941-4111373	...	$\mu\gamma\rho$	67.0	< 0.1	77.4 <sup>+8.8</sup> <sub>-8.4</sub>	9.0 ± 2.0
13075615-4159202	...	$\mu\rho$	44.7	2.5	51.8 <sup>+6.0</sup> <sub>-5.6</sub>	7.5 ± 2.0
13110859-3725022	...	$\mu\rho$	36.3	4.2	64.2 <sup>+6.8</sup> <sub>-6.4</sub>	7.6 ± 2.0
13153357-3425084	...	$\mu\rho$	24.7	7.1	59.0 ± 6.0	6.9 ± 2.0
13191194-3600082	...	$\mu\rho$	23.7	5.9	63.0 <sup>+6.8</sup> <sub>-6.4</sub>	7.2 ± 2.1
<b>Low-Likelihood Candidate Members of TW Hydrae</b>						
08561384-1342242	...	$\mu\gamma\rho$	4.9	< 0.1	36.6 ± 3.6	16.3 ± 1.4
09395647-2946286	...	$\mu\rho$	5.6	8.8	41.8 <sup>+5.6</sup> <sub>-5.2</sub>	15.9 ± 1.5
10211908+0804268	...	$\mu\rho$	8.3	47.1	26.9 ± 2.4	9.9 ± 1.3
10563080-3028137	...	$\mu$	15.1	3.6	47.4 ± 6.0	12.7 ± 1.5
10582800-1046304	NLTT 25869	$\mu$	7.2	46.7	22.9 <sup>+2.0</sup> <sub>-2.4</sub>	10.0 ± 1.1
11023986-2507113	...	$\mu\gamma\rho$	16.7	< 0.1	47.4 ± 5.2	...
11153797-2552192	...	$\mu\rho$	15.0	6.5	49.8 <sup>+5.6</sup> <sub>-5.2</sub>	11.3 ± 1.5
11382693-3843138	...	$\mu\gamma\rho$	7.4	< 0.1	59.8 ± 7.2	...
12021801-3110348	...	$\mu\rho$	2.6	12.6	54.6 ± 4.8	8.6 ± 1.7
12162481-2742007	...	$\mu\rho$	4.5	16.7	59.4 ± 4.4	8.1 ± 1.8
12271545-0636458	...	$\mu\gamma\rho$	1.5	0.6	35.0 ± 2.8	3.7 ± 1.7
12333935-3040139	...	$\mu\rho$	15.3	9.5	62.6 <sup>+6.0</sup> <sub>-5.2</sub>	8.8 ± 1.8
12454194-3903106	...	$\mu\rho$	5.9	6.5	71.4 <sup>+6.4</sup> <sub>-7.2</sub>	8.1 ± 2.0
12471067-3632150	...	$\mu\rho$	13.5	14.9	73.8 ± 8.0	9.6 ± 1.8
13155594-3403418	...	$\mu\rho$	10.8	10.4	65.0 <sup>+7.2</sup> <sub>-6.4</sub>	7.5 ± 2.1
<b>Likely Contaminants from Lower Centaurus Crux</b>						
10134260-2759586	...	$\mu\rho$	75.6	2.3	39.8 ± 5.2	14.8 ± 1.4

Table 14 *continued*

Table 14 (*continued*)

2MASS Designation	Other Names	BANYAN II Inputs <sup>a</sup>	Bayesian Probability (%)	Contamination Probability (%) <sup>b</sup>	Statistical Distance (pc)	Statistical RV (km s <sup>-1</sup> )
10182870-3150029	TWA 6 AB	$\mu yrt$	66.6	< 0.1	...	...
10212570-2830427	...	$\mu y p$	92.6	< 0.1	$43.4^{+6.4}_{-6.0}$	$13.5 \pm 1.7$
10252092-4241539	...	$\mu yrt$	0.0	15.0	...	...
10260210-4105537	...	$\mu y$	90.4	< 0.1	$59.4 \pm 7.6$	$14.8 \pm 1.4$
10292874-3823394	...	$\mu p$	3.0	5.3	$50.6^{+6.8}_{-6.4}$	$14.4 \pm 1.5$
10394605-3510139	...	$\mu p$	91.1	1.8	$55.4^{+6.8}_{-6.4}$	$13.8 \pm 1.5$
10443052-3730554	...	$\mu p$	1.3	8.4	$56.6 \pm 7.2$	$14.0 \pm 1.5$
10455263-2819303	...	$\mu y p$	42.8	< 0.1	$52.6 \pm 6.0$	$13.5 \pm 1.4$
10492026-2440101	...	$\mu p$	16.9	6.6	$42.2^{+5.2}_{-4.8}$	$13.5 \pm 1.4$
10492579-3527125	...	$\mu p$	65.2	3.6	$59.8 \pm 6.8$	$13.5 \pm 1.5$
10514507-3226337	...	$\mu p$	67.8	2.0	$53.0^{+6.4}_{-6.0}$	$13.4 \pm 1.5$
10571669-3512548	...	$\mu p$	38.1	9.7	$60.6 \pm 6.8$	$13.4 \pm 1.5$
11035873-4156475	...	$\mu p$	39.9	11.5	$68.2^{+8.0}_{-7.6}$	$13.1 \pm 1.5$
11062620-4019330	...	$\mu p$	3.5	91.1	$43.0^{+6.0}_{-5.6}$	$12.4 \pm 1.4$
11130416-4516056	...	$\mu$	60.1	5.5	$69.4 \pm 8.8$	$13.0 \pm 1.4$
11132622-4523427	TWA 14 AB	$\mu yrt$	87.8	< 0.1	...	...
11191302-4342401	...	$\mu p$	88.4	2.8	$70.2 \pm 8.4$	$13.0 \pm 1.5$
11204706-2738056	...	$\mu$	31.8	7.5	$53.0 \pm 6.4$	$12.1 \pm 1.5$
11385038-3830011	...	$\mu p$	24.6	2.6	$63.4^{+7.6}_{-7.2}$	$11.9 \pm 1.5$
11394506-3729069	...	$\mu p$	84.1	3.1	$67.4 \pm 7.6$	$11.9 \pm 1.7$
11443034-3820341	...	$\mu$	46.4	1.5	$57.8 \pm 7.2$	$11.3 \pm 1.7$
11455177-5520456	...	$\mu yrt$	43.1	0.4	...	...
11472454-4953029	TWA 19 AB	$\mu yrt$	54.7	< 0.1	...	...
11511119-4132064	...	$\mu p$	1.4	3.9	$61.4^{+8.0}_{-7.6}$	$11.4 \pm 1.5$
11554920-4303109	...	$\mu$	16.9	2.8	$69.4^{+9.2}_{-8.8}$	$11.7 \pm 1.7$
12011772-3712329	...	$\mu p$	41.2	12.1	$72.2 \pm 8.0$	$11.3 \pm 1.7$
12071089-3230537	TWA 31	$\mu yrt$	68.4	< 0.1	...	...
12094184-5854450	TWA 24 AB	$\mu yrt$	0.0	83.2	...	...
12105770-3708100	...	$\mu p$	40.5	2.0	$57.4^{+5.6}_{-5.2}$	$9.6 \pm 1.7$
12174683-3804157	...	$\mu p$	26.0	3.2	$65.8 \pm 8.0$	$10.3 \pm 1.7$
12333140-3641407	...	$\mu$	16.4	2.9	$59.0 \pm 6.8$	$9.3 \pm 1.7$
12342064-4815135	TWA 15 A	$\mu yrt$	75.7	< 0.1	...	...
12342047-4815195	TWA 15 B	$\mu yrt$	89.5	< 0.1	...	...
12421948-3805064	...	$\mu$	2.0	6.1	...	...
12482006-4237338	HD 111265	$\mu rt$	0.0	99.9	...	...
12520989-4948280	...	$\mu y p$	36.7	< 0.1	$90.6 \pm 10.0$	$9.6 \pm 1.5$
12522053-4515542	...	$\mu p$	49.2	4.8	$81.4^{+9.2}_{-8.8}$	$9.3 \pm 1.8$
12535039-4211215	...	$\mu y p$	58.9	< 0.1	$80.2 \pm 7.6$	$9.7 \pm 2.1$
12574463-3635431	...	$\mu y p$	26.9	< 0.1	$65.8^{+6.8}_{-6.0}$	$8.2 \pm 2.0$
13204539-4611377	TWA 17 AB	$\mu yrt$	0.0	98.0	...	...
13213722-4421518	TWA 18	$\mu yrt$	0.0	47.0	...	...
13412668-4341522	...	$\mu y p$	7.7	< 0.1	$39.4^{+3.2}_{-3.6}$	...
13481593-3642228	...	$\mu p$	1.6	12.8	$57.0 \pm 6.0$	$5.8 \pm 2.2$
<b>Candidate Members of Carina</b>						
10131476-5230540	TWA 21	$\mu yrt$	98.2	< 0.1	...	...
10282500-3959230	...	$\mu p r$	51.4	2.7	$28.9^{+4.0}_{-3.6}$	...
<b>Member of <math>\beta</math> Pictoris</b>						
10172689-5354265	TWA 22 AB	$\mu yprt$	99.7	0.2	...	...

Table 14 *continued*

Table 14 (*continued*)

2MASS Designation	Other Names	BANYAN II Inputs <sup>a</sup>	Bayesian Probability (%)	Contamination Probability (%) <sup>b</sup>	Statistical Distance (pc)	Statistical RV (km s <sup>-1</sup> )
<b>Rejected candidates</b>						
08141769+0253199	...	$\mu\rho$	...	...	...	...
08144321+2336045	...	$\mu$	...	...	...	...
08254335-0029110	...	$\mu\rho r$	...	...	...	...
09292857-4431563	HIP 46535	$\mu r t$	...	...	...	...
09353126-2802552	...	$\mu y r$	...	...	$12.5 \pm 3.6$	...
09471986-4003098	XACT 10	$\mu r t$	...	...	...	...
09512673-2220196	...	$\mu\rho$	...	...	...	...
09553336-0208403	...	$\mu y r r$	...	...	$41.4 \pm 4.0$	...
09590842-2239345	TYC 6604-118-1	$\mu y r t$	...	...	...	...
10104667-3447531	TYC 7178-1493-1	$\mu r t$	...	...	...	...
10144705-3728151	...	$\mu$	...	...	...	...
10190109-2646336	...	$\mu\rho r$	...	...	$63.4 \pm 5.2$	...
10220449-3233270	TYC 7188-0575-1	$\mu r t$	...	...	...	...
10221800-1032156	HIP 50796	$\mu r t$	...	...	...	...
10432828-2903513	HIP 52462	$\mu r t$	...	...	...	...
10473117-2220528	HIP 52787	$\mu r t$	...	...	...	...
10513331-1916530	...	$\mu\rho$	...	...	...	...
10542303-1507082	...	$\mu\rho$	...	...	...	...
10563080+0723184	HIP 53486	$\mu r t$	...	...	...	...
11063147-4201251	...	$\mu\rho$	...	...	...	...
11112984-2713320	...	$\mu$	...	...	...	...
11195251-3917150	...	$\mu$	...	...	...	...
11254754-4410267	...	$\mu x$	...	...	...	...
11423628-3859108	...	$\mu$	...	...	...	...
11424808-3548577	HIP 57129	$\mu r t$	...	...	...	...
11443846-4925025	HIP 57269	$\mu r t$	...	...	...	...
11504110-2356075	...	$\mu\rho$	...	...	...	...
11532691-3015414	...	$\mu$	...	...	...	...
11571557-4022292	...	$\mu\rho$	...	...	$71.4^{+9.6}_{-9.2}$	$12.1 \pm 1.7$
12000160-1731308	...	$\mu y r$	...	...	$55.4 \pm 4.8$	...
12041256+0514128	...	$\mu\rho$	...	...	...	...
12073145-3310222	...	$\mu x$	...	...	$83.0 \pm 5.6$	...
12090628-3247453	...	$\mu$	...	...	...	...
12100648-4910505	HIP 59315	$\mu r t$	...	...	...	...
12113180-3416537	...	$\mu$	...	...	...	...
12194846-3232059	...	$\mu\rho$	...	...	...	...
12220574-4159572	...	$\mu\rho$	...	...	$78.6^{+10.4}_{-10.0}$	$11.7 \pm 1.8$
12214223-4012050	...	$\mu$	...	...	...	...
12214852-3652349	...	$\mu$	...	...	...	...
12282569-3955014	...	$\mu$	...	...	...	...
12310489-3801065	...	$\mu\rho$	...	...	...	...
12451035-1443029	...	$\mu$	...	...	$44.6^{+4.8}_{-5.2}$	$3.7 \pm 2.0$
12563961-2718455	...	$\mu y r r$	...	...	$60.2^{+5.2}_{-5.6}$	...
13112902-4252418	...	$\mu y t$	...	...	...	$9.7 \pm 1.5$
13265348-5022270	...	$\mu y r$	...	...	$70.2^{+8.4}_{-8.0}$	$10.0 \pm 1.8$
14112131-2119503	...	$\mu y r r$	...	...	$37.0 \pm 3.6$	...
14252913-4113323	SCR 1425-4113 AB	$\mu y r t$	...	...	...	...
18440971+7129178	1RXS J1844+7129 AB	$\mu y r$	...	...	$16.9^{+2.4}_{-2.0}$	...

Table 14 *continued*



Table 14 (*continued*)

2MASS Designation	Other Names	BANYAN II Inputs <sup>a</sup>	Bayesian Probability (%)	Contamination Probability (%) <sup>b</sup>	Statistical Distance (pc)	Statistical RV (km s <sup>-1</sup> )
----------------------	----------------	----------------------------------	-----------------------------	---	------------------------------	---

<sup>a</sup> All observables that were included in BANYAN II to derive membership probabilities;  $\mu$ : proper motion,  $y$ : signs of youth (i.e., age securely younger than  $\sim 1$  Gyr),  $p$ : 2MASS and AllWISE photometry,  $r$ : radial velocity,  $t$ : trigonometric distance. Photometric measurements were not used for  $\geq L5$ -type objects, because the young photometric sequences used in BANYAN II are not well calibrated at these late spectral types.

<sup>b</sup> Probability that a synthetic object drawn from a field Galactic model obtains an equal or higher Bayesian probability. See [Gagné et al. \(2014c\)](#) for more detail (their Section 5).

<sup>c</sup> Possible LCC contaminant.

NOTE—See Section 5 for more details.

## APPENDIX

### A. NEW OPTICAL AND NEAR-INFRARED SPECTRA

In this Section, new optical and near-infrared spectra described in Section 3 are displayed for reference (Figures A1, A2, A3, A4, and A5). The two new SpeX spectra (Section 3.3) are presented and discussed individually in Section 4.1.

### B. THE TOTAL MASS PROBABILITY DENSITY FUNCTION OF A BINARY SYSTEM

In this Appendix, the mathematical development leading to the total mass probability density function (PDF) of a system of two stars is carried out. In Section 6, a PDF  $\mathcal{P}(\ell)$  for the logarithm of the mass ( $\ell = \log_{10} m$ ) of each star in the sample is calculated. The determination of a systemic initial mass function (Section 8) thus requires that the PDF of the total mass of binary systems be calculated. Let the two stars have masses  $m_1$  and  $m_2$ , or  $\ell_1$  and  $\ell_2$  in logarithm space, and let  $m_t$  be the total mass of the system. It follows that:

$$\ell_t = \log_{10} m_t = \log_{10} (10^{\ell_1} + 10^{\ell_2}). \quad (\text{B1})$$

The problem is thus to determine  $\mathcal{P}_t(\ell_t)$  from  $\mathcal{P}_1(\ell_1)$  and  $\mathcal{P}_2(\ell_2)$ . To do this, the joint PDF  $\mathcal{P}_j(\ell_1, \ell_2)$  is introduced, and followed by a change of variable:

$$\mathcal{P}_j(\ell_1, \ell_2) = \mathcal{P}_1(\ell_1)\mathcal{P}_2(\ell_2), \quad (\text{B2})$$

$$\mathcal{P}'_j(\ell_1, \ell_t) d\ell_1 d\ell_t = \mathcal{P}_j(\ell_1, \ell_2) d\ell_1 d\ell_2. \quad (\text{B3})$$

It follows that :

$$\mathcal{P}'_j(\ell_1, \ell_t) = \mathcal{P}_j(\ell_1, \ell_2) |\mathbf{J}|, \quad (\text{B4})$$

where  $|\mathbf{J}|$  is the determinant of the Jacobian matrix of this transformation:

$$\mathbf{J} = \begin{bmatrix} \frac{\partial \ell_1}{\partial \ell_1} & \frac{\partial \ell_1}{\partial \ell_t} \\ \frac{\partial \ell_2}{\partial \ell_1} & \frac{\partial \ell_2}{\partial \ell_t} \end{bmatrix}. \quad (\text{B5})$$

It follows from Equation (B1) that:

$$|\mathbf{J}| = \frac{10^{\ell_t}}{10^{\ell_t} - 10^{\ell_1}} \quad (\text{B6})$$

The final PDF  $\mathcal{P}_t(\ell_t)$  can then be obtained by marginalizing  $\mathcal{P}'_j(\ell_1, \ell_t)$  over  $\ell_1$ , in the domain  $\ell_1 < \ell_t$  where the joint

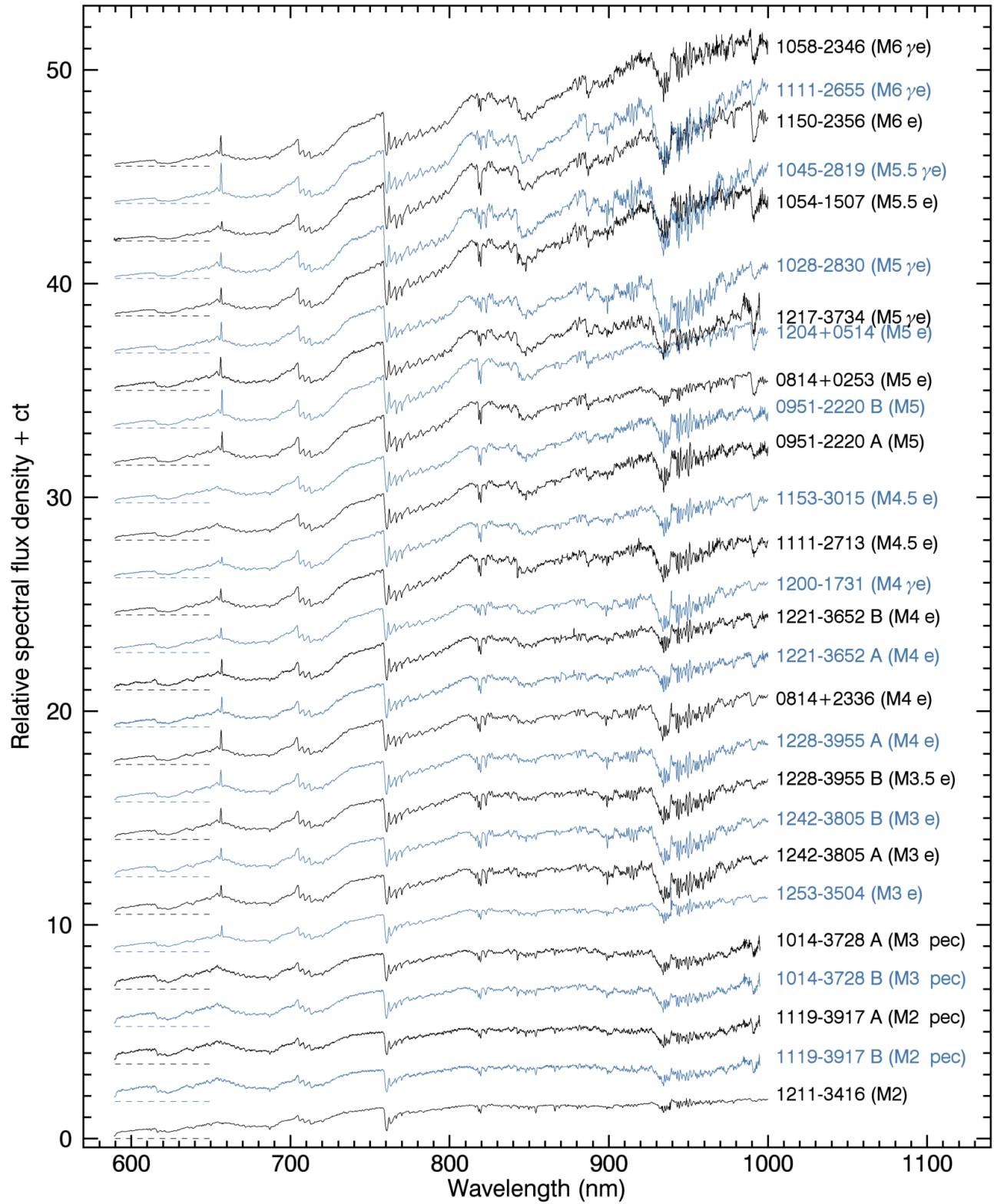


**Figure A1.** New GMOS spectra presented in this work. The individual zero flux levels are represented with horizontal dashed lines. See Section 3.2 for more details.

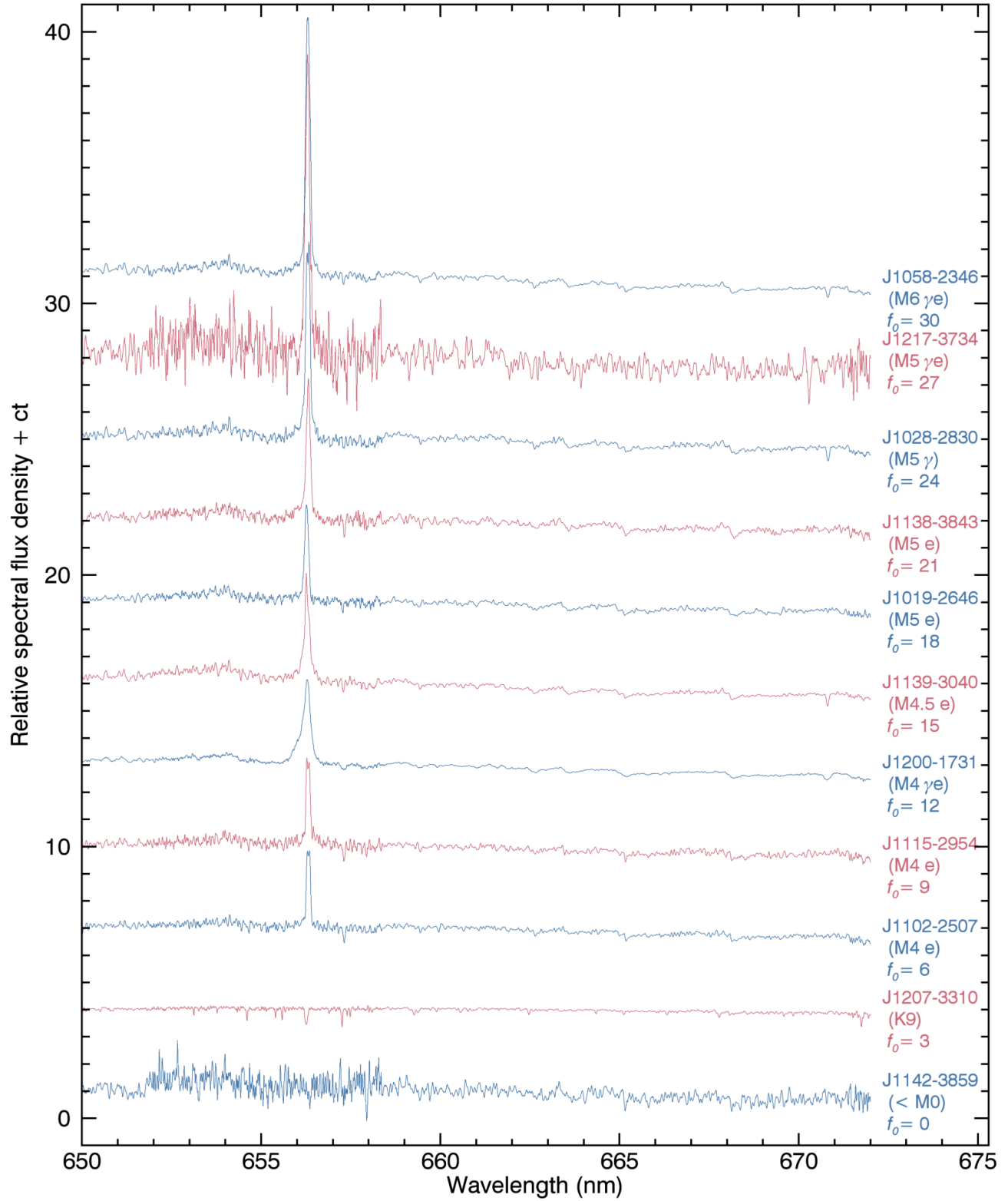


**Figure A2.** New ESPaDOnS spectra presented in this work. Zero levels in relative flux are indicated below object names and spectral types. See Section 3.5 for more details.

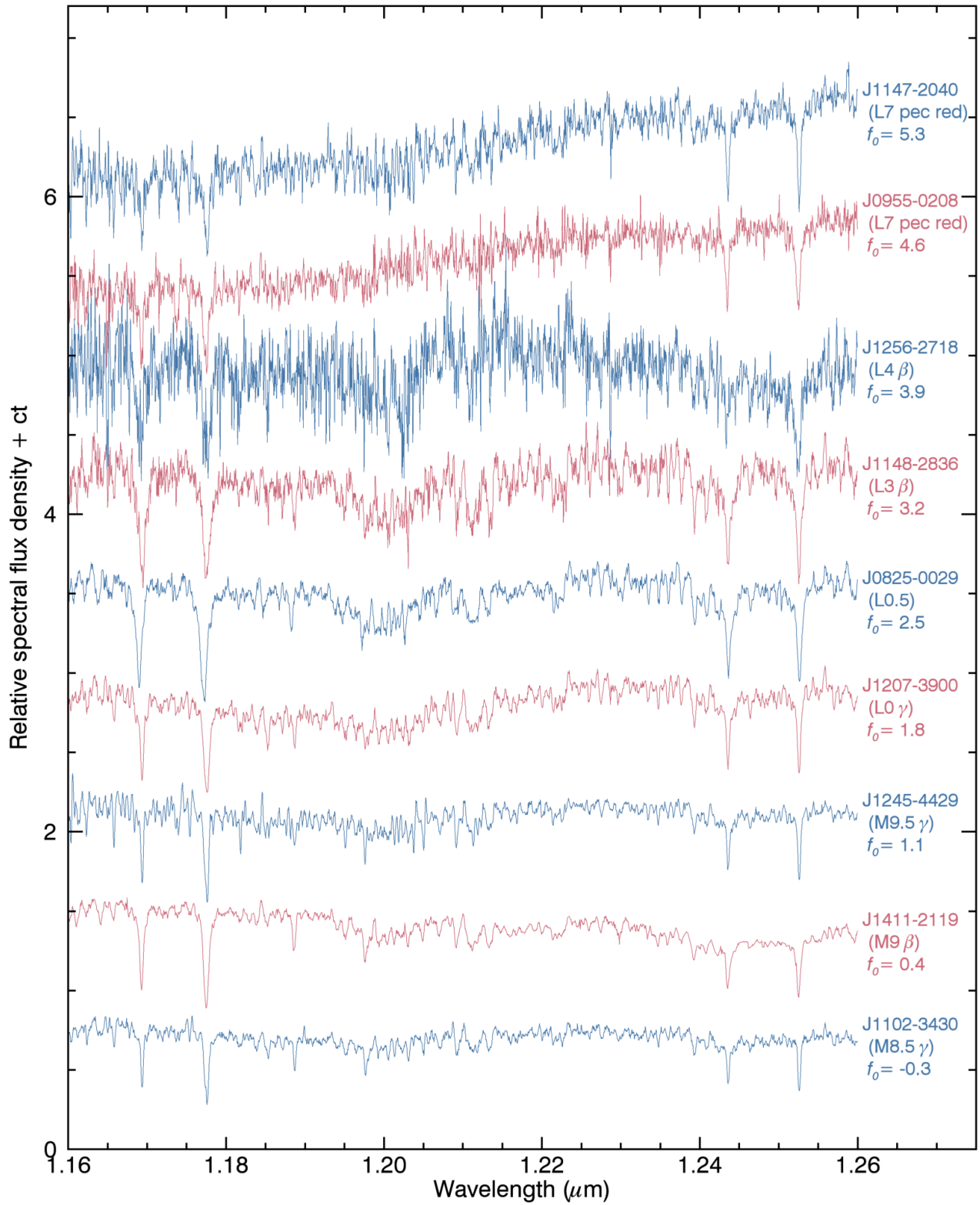


**Figure A3.** New  $J$ -band NIR spectra from FIRE obtained in echelle mode. Zero levels in relative flux are indicated below object names and spectral types. See Section 3.1 for more details.

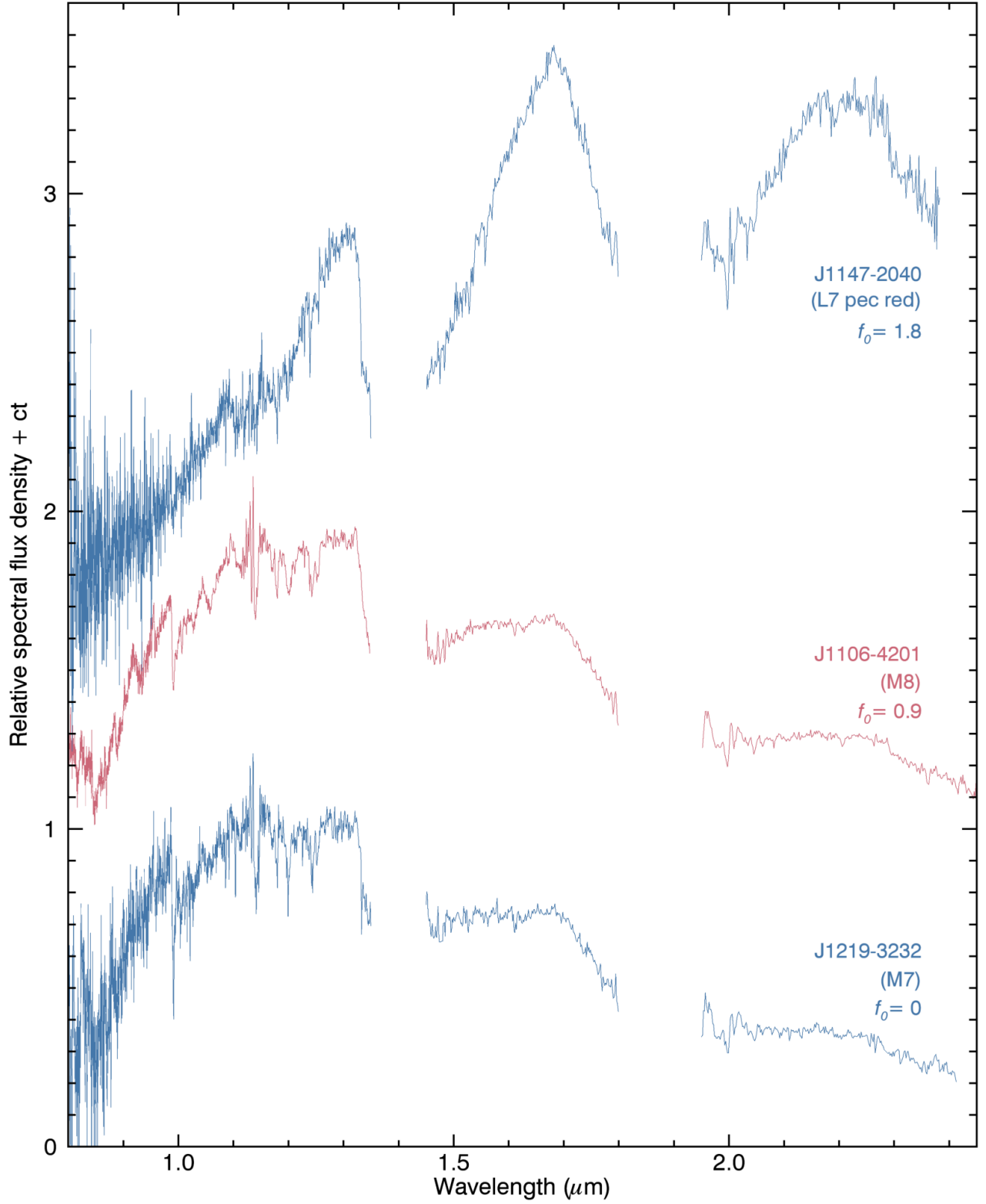


**Figure A4.** New NIR spectra from FIRE obtained in prism mode. Zero levels in relative flux are indicated below object names and spectral types. The slopes of all spectra were corrected using 2MASS photometry, as described in Section 4.1. 2MASS J12194846–3232059 and 2MASS J11063147–4201251 are normal low-mass stars with no signs of youth and were thus rejected as TWA candidates. 2MASS J11472421–2040204 (TWA 41) displays telltale signatures of youth such as a very red continuum and a triangular-shaped  $H$  band ( $\sim 1.5\text{--}1.8\ \mu\text{m}$ ). See Section 3.1 for more details.



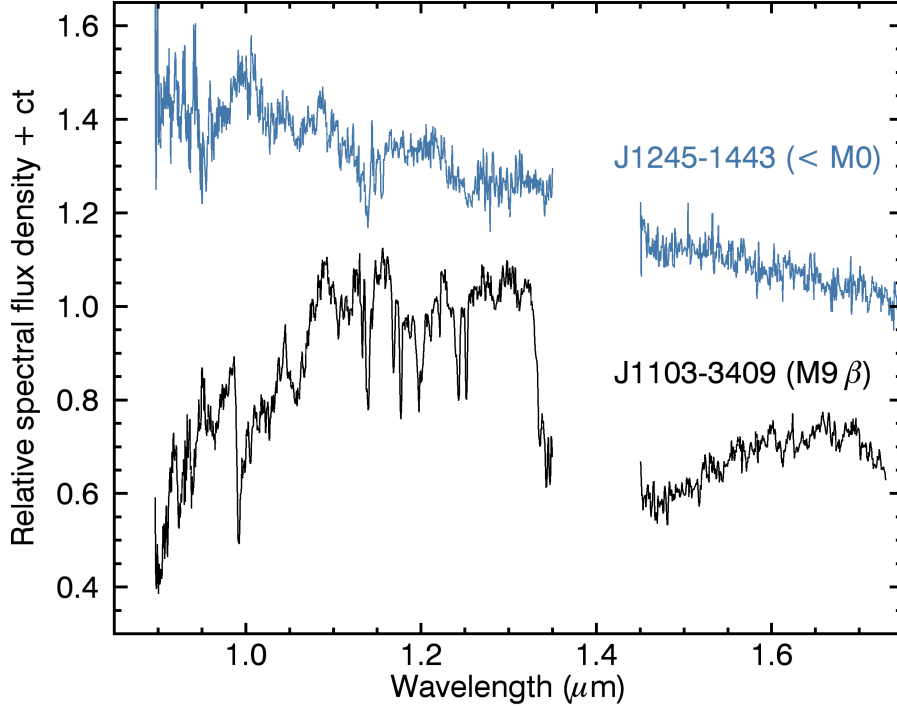


**Figure A5.** New Flamingos-2 spectra presented in this work. 2MASS J12451035–1443029 has a spectral type earlier than M0 and is likely a background contaminant, whereas 2MASS J11034950–3409445 is an M9  $\beta$  dwarf with tentative signs of a low surface gravity. The relative flux of 2MASS J11034950–3409445 was not offset, and that of 2MASS J12451035–1443029 was offset by 0.3. See Section 3.4 for more details.

PDF is defined:

$$\mathcal{P}_t(\ell_t) = \int_{-\infty}^{\ell_t} \mathcal{P}'_j(\ell_1, \ell_t) d\ell_1, \quad (\text{B7})$$

$$= \int_{-\infty}^{\ell_t} \mathcal{P}_j(\ell_1, \ell_2) |\mathbf{J}| d\ell_1, \quad (\text{B8})$$

$$= \int_{-\infty}^{\ell_t} \mathcal{P}_1(\ell_1) \mathcal{P}_2\left(\log_{10}(10^{\ell_t} - 10^{\ell_1})\right) \frac{10^{\ell_t}}{10^{\ell_t} - 10^{\ell_1}} d\ell_1. \quad (\text{B9})$$

This convolution-like integral representation of  $\mathcal{P}_t(\ell_t)$  is then solved numerically.

### C. REFERENCE PRIORS FOR THE MCMC FIT OF CUMULATIVE INITIAL MASS FUNCTIONS

The Markov Chain Monte Carlo (MCMC) fitting algorithm described in Section 8 requires the choice of a prior distribution on the parameters of the initial mass function (IMF) models to be fitted to the data. The numerical method described by Berger et al. (2009) was used to obtain non-informative priors, i.e., priors distributions that do not inject any information on the values of the IMF parameters that are not informed by the data.

In the case of a Salpeter IMF, this was done by defining a  $50 \times 50$  grid of parameters  $N = \phi_0 V_{\text{eff}}$  and  $\alpha$  defined in the ranges 10–100 and 0.3–4, respectively. For each values of  $N_i$  and  $\alpha_j$  on the grid, a random number of total TWA members  $N'_i$  was drawn from a Poisson distribution  $\mathcal{P}(x|N_i)$ . Each of these objects were attributed a mass following the IMF distribution described in Equation (1), with a parameter  $\alpha_j$ . The cumulative IMF was then constructed, and compared to the model with a Kolmogorov-Smirnov test. The likelihood probability density  $\mathcal{L}_{ij}(\mathcal{D}_{ij}|N_i, \alpha_i)$  was then calculated following Equation (18) at every point of the grid, where  $\mathcal{D}_{ij}$  is the simulated data.

Berger et al. (2009) define the value of the reference prior  $\pi_{ij}(\{\theta\})$  (where  $\{\theta\}$  is a set of parameters) as the mean value of  $\mathcal{L}_{ij}(\mathcal{D}_{ij}|\{\theta\})$  over a large number of trials. Obtaining a properly normalized prior distribution requires an additional step at each trial that was ignored in the present case; the resulting prior distribution is thus not normalized to unity, but this has no effect on the MCMC algorithm because it only relies on the relative value of the likelihood and prior at different steps in the parameter space. A total of 1000 trials were performed, and the resulting prior

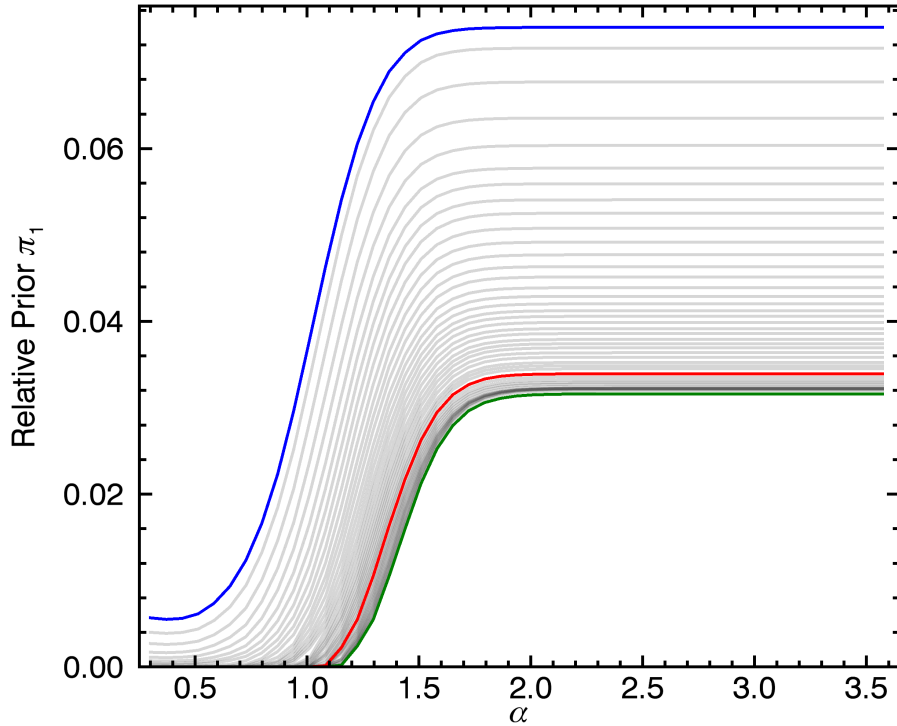


**Figure C6.** Reference priors in the Salpeter IMF case. The red curve corresponds to the case where  $N$  has been fixed to a typical value of 70, the blue and green curves correspond to minimal and maximal values of  $N$  respectively, and the grey curves to other values. All priors disfavour  $\alpha \lesssim 1.7$ , but become uniform above this value. Smaller numbers  $N$  of TWA members tend to be favoured.

array was smoothed in logarithmic space with a running box of  $6 \times 6$  elements. The resulting priors are displayed in Figure C6.

In the log-normal case, a similar calculation was performed on a  $50 \times 50 \times 50$  grid of parameters  $N = \phi_t V_{\text{eff}}$ ,  $\log_{10} m_c$  and  $\sigma$ , defined in the ranges 10–100,  $-2$ –0 dex (in  $\log_{10} M_{\odot}$ ) and 0.1–1.2 dex (in  $\log_{10} M_{\odot}$ ), respectively. Slices of the resulting reference prior cube are displayed in Figure C7.

## REFERENCES

- Abt, H. A., & Morrell, N. I. 1995, *Astrophysical Journal Supplement* v.99, 99, 135
- Aganze, C., Burgasser, A. J., Faherty, J. K., et al. 2016, *The Astronomical Journal*, 151, 46
- Allard, F., Homeier, D., & Freytag, B. 2012, *Philosophical Transactions of the Royal Society A: Mathematical*, 370, 2765
- Allers, K. N., Gallimore, J. F., Liu, M. C., & Dupuy, T. J. 2016, *The Astrophysical Journal*, 819, 133
- Allers, K. N., & Liu, M. C. 2013, *The Astrophysical Journal*, 772, 79
- Baraffe, I., Chabrier, G., Allard, F., & Hauschildt, P. H. 1998, *Astronomy & Astrophysics*, 337, 403
- Baraffe, I., Homeier, D., Allard, F., & Chabrier, G. 2015, *Astronomy & Astrophysics*, 577, A42
- Barrado Y Navascués, D. 2005, *II International GTC Workshop: Science with GTC 1st-light Instruments and the LMT* (Eds. A. M. Hidalgo-Gómez, 24, 217
- Barrado Y Navascués, D., Bouvier, J., Stauffer, J. R., Lodieu, N., & McCaughrean, M. J. 2002, *Astronomy & Astrophysics*, 395, 813
- Barrado y Navascués, D., & Martín, E. L. 2003, *The Astronomical Journal*, 126, 2997
- Basri, G. 1998, *Brown dwarfs and extrasolar planets*, 134, 394
- Bastian, N., Covey, K. R., & Meyer, M. R. 2010, *Annual Review of Astronomy & Astrophysics*, 48, 339
- Bell, C. P. M., Mamajek, E. E., & Naylor, T. 2015, *Monthly Notices of the Royal Astronomical Society*, 454, 593
- Berger, J. O., Bernardo, J. M., & Sun, D. 2009, *The Annals of Statistics*, doi:10.2307/30243652
- Bernardo, J. M. 1979, *Journal of the Royal Statistical Society Series B* ( . . .
- Bilir, S., Karataş, Y., Demircan, O., & Eker, Z. 2005, *Monthly Notices of the Royal Astronomical Society*, 357, 497
- Bochanski, J. J., Hawley, S. L., Covey, K. R., et al. 2010, *The Astronomical Journal*, 139, 2679
- Bochanski, J. J., Hawley, S. L., & West, A. A. 2011, *The Astronomical Journal*, 141, 98
- Bochanski, J. J., Hennawi, J. F., Simcoe, R. A., et al. 2009, *Publications of the Astronomical Society of the Pacific*, 121, 1409
- Boden, A. F., Sargent, A. I., Akeson, R. L., et al. 2005, *The Astrophysical Journal*, 635, 442
- Boller, T., Freyberg, M. J., Trümper, J., et al. 2016, *Astronomy & Astrophysics*, 588, A103
- Boucher, A., Lafrenière, D., Gagné, J., et al. 2016, arXiv.org, arXiv:1608.08259

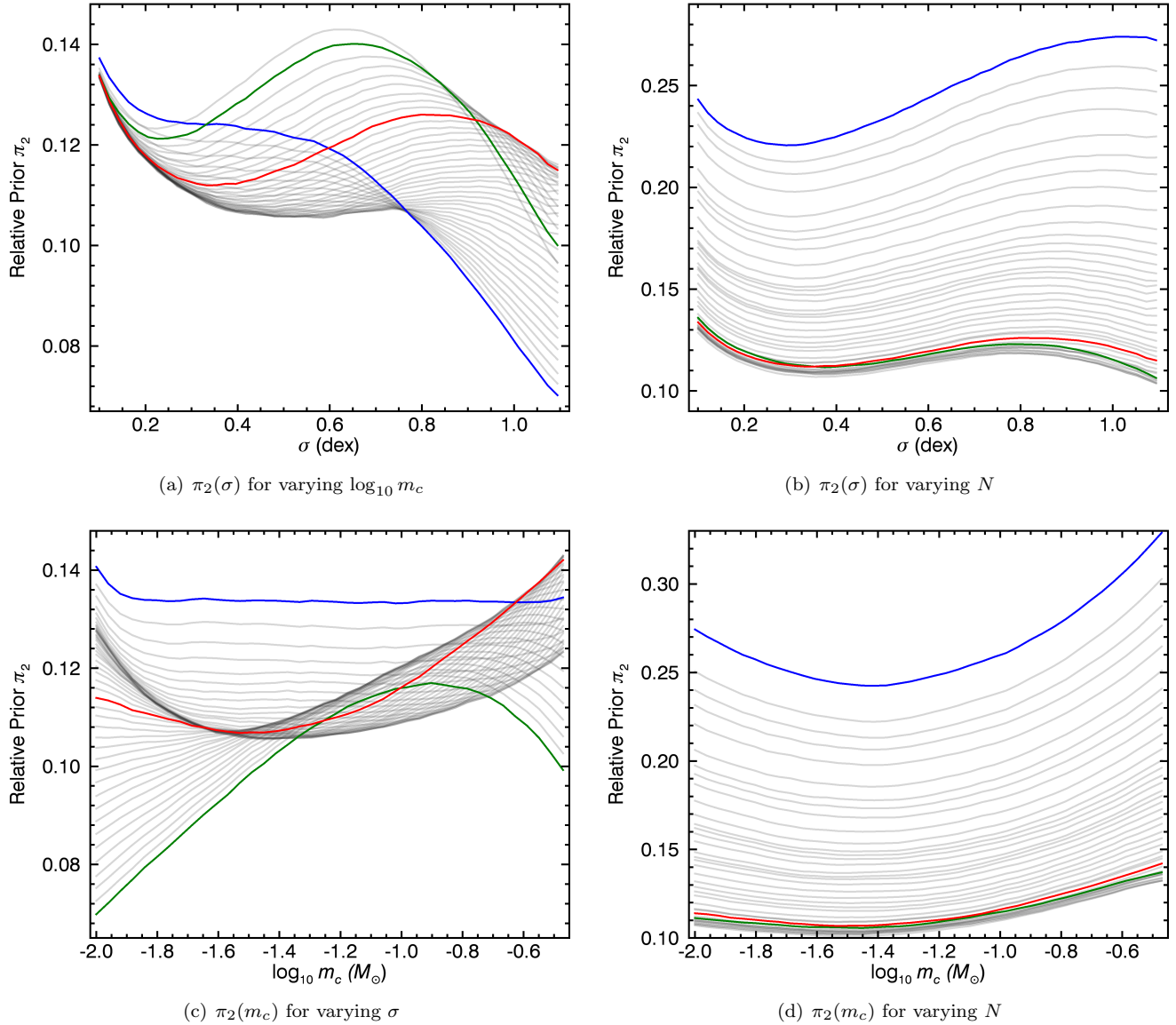


**Figure C7.** Reference priors in the log-normal IMF case. The red curves correspond to the cases where 2 out of 3 parameters have been fixed to typical values  $\{N, \log_{10} m_c, \sigma\} = \{70, 0.27, 0.75\}$ , the blue curves correspond to minimal parameter values, the green curves to maximal parameter values, and the grey curves to other values. Although the priors do not change in a drastic way, lower  $N$  tend to be favoured. The regions of  $\sigma$  that are favoured are dependent on the value of  $\log_{10} m_c$ ; small central masses favour high  $\sigma$  and vice-versa. Low values of  $\sigma$  result in a flat prior on the central mass.

- Burningham, B., Pinfield, D. J., Lucas, P. W., et al. 2010, *Monthly Notices of the Royal Astronomical Society*, 406, 1885
- Caballero, J. A. 2009, *COOL STARS*, 1094, 912
- Casagrande, L., Schönrich, R., Asplund, M., et al. 2011, *Astronomy & Astrophysics*, 530, A138
- Chabrier, G. 2003, *The Astrophysical Journal*, 586, L133
- . 2005, *The Initial Mass Function 50 years later*. Edited by E. Corbelli and F. Palte, 327, 41
- Chauvin, G., Lagrange, A.-M., Dumas, C., et al. 2004, *Astronomy & Astrophysics*, 425, L29
- Chiu, K., Fan, X., Leggett, S. K., et al. 2006, *The Astronomical Journal*, 131, 2722
- Choi, J., Dotter, A., Conroy, C., et al. 2016, *The Astrophysical Journal*, 823, 102
- Chubak, C., & Marcy, G. 2011, *American Astronomical Society*, 217, 434.12
- Comerón, F. 2011, *Astronomy & Astrophysics*, 531, A33
- Cruz, K. L., Kirkpatrick, J. D., & Burgasser, A. J. 2009, *The Astronomical Journal*, 137, 3345
- Cruz, K. L., Reid, I. N., Liebert, J., Kirkpatrick, J. D., & Lowrance, P. J. 2003, *The Astronomical Journal*, 126, 2421
- Cruz, K. L., Reid, I. N., Kirkpatrick, J. D., et al. 2007, *The Astronomical Journal*, 133, 439
- Cushing, M. C., Vacca, W. D., & Rayner, J. T. 2004, *The Publications of the Astronomical Society of the Pacific*, 116, 362
- Cushing, M. C., Kirkpatrick, J. D., Gelino, C. R., et al. 2011, *The Astrophysical Journal*, 743, 50
- David, T. J., & Hillenbrand, L. A. 2015, *The Astrophysical Journal*, 804, 146
- de Bruijne, J. H. J., & Eilers, A. C. 2012, *Astronomy & Astrophysics*, 546, A61
- de la Reza, R., Torres, C. A. O., Quast, G., Castilho, B. V., & Vieira, G. L. 1989, *Astrophysical Journal*, 343, L61
- de Wit, W. J., Bouvier, J., Palla, F., et al. 2006, *Astronomy & Astrophysics*, 448, 189
- de Zeeuw, P. T., Hoogerwerf, R., de Bruijne, J. H. J., Brown, A. G. A., & Blaauw, A. 1999, *The Astronomical Journal*, 117, 354
- Deacon, N. R., Schlieder, J. E., & Murphy, S. J. 2016, *Monthly Notices of the Royal Astronomical Society*, 457, 3191
- Delgado Mena, E., Bertrán de Lis, S., Adibekyan, V. Z., et al. 2015, *Astronomy & Astrophysics*, 576, A69
- Delorme, P., Delfosse, X., Albert, L., et al. 2008, *Astronomy & Astrophysics*, 482, 961
- Donaldson, J. K., Weinberger, A. J., Gagné, J., et al. 2016, *arXiv.org*, arXiv:1610.01667
- Donati, J. F., Catala, C., Landstreet, J. D., & Petit, P. 2006, *Solar Polarization* 4, 358, 362
- Donati, J. F., Semel, M., Carter, B. D., Rees, D. E., & Collier Cameron, A. 1997, *Monthly Notices of the Royal Astronomical Society*, 291, 658
- Ducourant, C., Teixeira, R., Galli, P. A. B., et al. 2014a, *Astronomy & Astrophysics*, 563, A121
- . 2014b, *Astronomy & Astrophysics*, 563, A121
- Egret, D., Didelon, P., McLean, B. J., Russell, J. L., & Turon, C. 1992, *Astronomy and Astrophysics (ISSN 0004-6361)*, 258, 217
- Eikenberry, S. S., Elston, R., Raines, S. N., et al. 2004, in *Ground-based Instrumentation for Astronomy*. Edited by Alan F. M. Moorwood and Iye Masanori. *Proceedings of the SPIE*, ed. A. F. M. Moorwood & M. Iye, University of Florida, USA (SPIE), 1196–1207
- Elliott, P., Bayo, A., Melo, C. H. F., et al. 2014, *Astronomy & Astrophysics*, 568, A26
- . 2016, *Astronomy & Astrophysics*, 590, A13
- ESA. 1997, *The Hipparcos and Tycho catalogues. Astrometric and photometric star catalogues derived from the ESA Hipparcos Space Astrometry Mission*, 1200
- Fabricius, C., Høg, E., Makarov, V. V., et al. 2002, *Astronomy & Astrophysics*, 384, 180
- Faherty, J. K., Alatalo, K., Anderson, L. D., et al. 2015, *arXiv.org*, arXiv:1505.01923
- Faherty, J. K., Riedel, A. R., Cruz, K. L., et al. 2016a, *The Astrophysical Journal Supplement Series*, 225, 10
- . 2016b, *arXiv.org*, arXiv:1605.07927
- Fernández, D., Figueras, F., & Torra, J. 2008, *Astronomy & Astrophysics*, 480, 735
- Filippazzo, J. C., Rice, E. L., Faherty, J., et al. 2015, *The Astrophysical Journal*, 810, 158
- Finch, C. T., Zacharias, N., & Henry, T. J. 2010, *The Astronomical Journal*, 140, 844
- Gagné, J., Burgasser, A. J., Faherty, J. K., et al. 2015a, *The Astrophysical Journal Letters*, 808, L20
- Gagné, J., Faherty, J. K., Cruz, K. L., et al. 2014a, *The Astrophysical Journal Letters*, 785, L14
- Gagné, J., Lafrenière, D., Doyon, R., et al. 2014b, *The Astrophysical Journal Letters*, 792, L17
- Gagné, J., Lafrenière, D., Doyon, R., Malo, L., & Artigau, É. 2014c, *The Astrophysical Journal*, 783, 121
- . 2015b, *The Astrophysical Journal*, 798, 73
- Gagné, J., Lambrides, E., Faherty, J. K., & Simcoe, R. 2015c, *Firehose v2.0*, Zenodo, Tech. rep., doi:10.5281/zenodo.18775
- Gagné, J., Faherty, J. K., Cruz, K. L., et al. 2015d, *The Astrophysical Journal Supplement Series*, 219, 33
- Gaia Collaboration. 2016, *arXiv.org*, 1609.04153v1
- Gaia Collaboration, Brown, A. G. A., Vallenari, A., et al. 2016, *arXiv.org*, arXiv:1609.04172
- Gizis, J. E. 2002, *The Astrophysical Journal*, 575, 484
- Gizis, J. E., Jao, W.-C., Subasavage, J. P., & Henry, T. J. 2007, *The Astrophysical Journal*, 669, L45
- Gizis, J. E., Reid, I. N., Knapp, G. R., et al. 2003, *The Astronomical Journal*, 125, 3302
- Gizis, J. E., Faherty, J. K., Liu, M. C., et al. 2012, *The Astronomical Journal*, 144, 94
- Głębocki, R., & Gnaniński, P. 2005, in *Proceedings of the 13th Cambridge Workshop on Cool Stars*, 571
- Gontcharov, G. A. 2006a, *Astronomy Letters*, 32, 759
- . 2006b, *Astronomical and Astrophysical Transactions*, 25, 145
- Gray, R. O., Corbally, C. J., Garrison, R. F., et al. 2006, *The Astronomical Journal*, 132, 161
- Gray, R. O., Corbally, C. J., Garrison, R. F., McFadden, M. T., & Robinson, P. E. 2003, *The Astronomical Journal*, 126, 2048
- Hartkopf, W. I., Mason, B. D., Finch, C. T., et al. 2013, *The Astronomical Journal*, 146, 76
- Henden, A. A., Templeton, M., Terrell, D., et al. 2016, *VizieR On-line Data Catalog*, 2336
- Holmberg, J., Nordström, B., & Andersen, J. 2007, *Astronomy & Astrophysics*, 475, 519
- Hoogerwerf, R. 2000, *Monthly Notices of the Royal Astronomical Society*, 313, 43
- Hook, I. M., Jørgensen, I., Allington-Smith, J. R., et al. 2004, *The Publications of the Astronomical Society of the Pacific*, 116, 425
- Houk, N. 1978, *Ann Arbor : Dept. of Astronomy*
- . 1982, *Michigan Catalogue of Two-dimensional Spectral Types for the HD stars. Volume 3. Declinations -40 to -26*.
- Isaacson, H., & Fischer, D. 2010, *The Astrophysical Journal*, 725, 875
- Ivezić, Z., Axelrod, T., Brandt, W. N., et al. 2008, *Serbian Astronomical Journal*, 176, 1
- Janson, M., Jayawardhana, R., Girard, J. H., et al. 2012a, *The Astrophysical Journal Letters*, 758, L2
- Janson, M., Hormuth, F., Bergfors, C., et al. 2012b, *The Astrophysical Journal*, 754, 44

- Jayawardhana, R., Coffey, J., Scholz, A., Brandeker, A., & van Kerkwijk, M. H. 2006, *The Astrophysical Journal*, 648, 1206
- Jaynes, E. T. 1968, . . . *Science and Cybernetics*
- Jeffreys, H. 1961, *Theory of Probability* (3rd ed.) Oxford University Press
- Jeffries, R. D. 2012, *Low-Mass Stars and the Transition Stars/Brown Dwarfs - EES2011*, 57, 45
- Jeffries, R. D., Naylor, T., Devey, C. R., & Totten, E. J. 2004, *Monthly Notices of the Royal Astronomical Society*, 351, 1401
- Jenkins, J. S., Murgas, F., Rojo, P., et al. 2011, *Astronomy & Astrophysics*, 531, A8
- Kastner, J. H., Zuckerman, B., & Bessell, M. 2008, *Astronomy & Astrophysics*, 491, 829
- Kastner, J. H., Zuckerman, B., Weintraub, D. A., & Forveille, T. 1997, *Science*, 277, 67
- Kellogg, K., Metchev, S., Gagné, J., & Faherty, J. 2016, *The Astrophysical Journal Letters*, 821, L15
- Kellogg, K., Metchev, S., Geißler, K., et al. 2015, *The Astronomical Journal*, 150, 182
- Kharchenko, N. V., Scholz, R. D., Piskunov, A. E., Röser, S., & Schilbach, E. 2007, *Astronomische Nachrichten*, 328, 889
- Kiraga, M. 2012, *Acta Astronomica*, 62, 67
- Kirkpatrick, D. J., Cutri, R. M., Skrutskie, M. F., et al. 2003, *VizieR On-line Data Catalog: II/246*. Originally published in: University of Massachusetts and Infrared Processing and Analysis Center, 2246, 0
- Kirkpatrick, J. D. 2005, *Annual Review of Astronomy & Astrophysics*, 43, 195
- Kirkpatrick, J. D., Barman, T. S., Burgasser, A. J., et al. 2006, *The Astrophysical Journal*, 639, 1120
- Kirkpatrick, J. D., Reid, I. N., Liebert, J., et al. 1999, *The Astrophysical Journal*, 519, 802
- Kirkpatrick, J. D., Cushing, M. C., Gelino, C. R., et al. 2011, *The Astrophysical Journal Supplement*, 197, 19
- Kirkpatrick, J. D., Gelino, C. R., Cushing, M. C., et al. 2012, *The Astrophysical Journal*, 753, 156
- Kirkpatrick, J. D., Schneider, A., Fajardo-Acosta, S., et al. 2014, *The Astrophysical Journal*, 783, 122
- Kolmogorov, A. N. 1933, *Sulla determinazione empirica di una legge di distribuzione*
- Konopacký, Q. M., Ghez, A. M., Duchêne, G., McCabe, C., & Macintosh, B. A. 2007, *The Astronomical Journal*, 133, 2008
- Kordopatis, G., Gilmore, G., Steinmetz, M., et al. 2013, *The Astronomical Journal*, 146, 134
- Kroupa, P. 2001, *Monthly Notices of the Royal Astronomical Society*, 322, 231
- Kroupa, P., Tout, C. A., & Gilmore, G. 1993, *Monthly Notices of the Royal Astronomical Society* (ISSN 0035-8711), 262, 545
- Kullback, S., & Leibler, R. A. 1951, *The annals of mathematical statistics*
- Lawson, W. A., & Crause, L. A. 2005, *Monthly Notices of the Royal Astronomical Society*, 357, 1399
- Leggett, S. K., Morley, C. V., Marley, M. S., & Saumon, D. 2015, *The Astrophysical Journal*, 799, 37
- Lindgren, L., Lammers, U., Bastian, U., et al. 2016, arXiv.org, arXiv:1609.04303
- Liu, M. C., Magnier, E. A., Deacon, N. R., et al. 2013, *The Astrophysical Journal Letters*, 777, L20
- Lodieu, N., Hambly, N. C., Jameson, R. F., et al. 2007, *Monthly Notices of the Royal Astronomical Society*, 374, 372
- Looper, D. L. 2011, *ProQuest Dissertations And Theses; Thesis (Ph.D.)—University of Hawai'i at Manoa*
- Looper, D. L., Bochanski, J. J., Burgasser, A. J., et al. 2010a, *The Astronomical Journal*, 140, 1486
- Looper, D. L., Burgasser, A. J., Kirkpatrick, J. D., & Swift, B. J. 2007, *The Astrophysical Journal*, 669, L97
- Looper, D. L., Mohanty, S., Bochanski, J. J., et al. 2010b, *The Astrophysical Journal*, 714, 45
- Lu, P. K. 1982, *Publications of the Astronomical Society of the Pacific*, 94, 304
- Luhman, K. L. 2007, *The Astrophysical Journal Supplement Series*, 173, 104
- . 2014, *The Astrophysical Journal Letters*, 786, L18
- Luhman, K. L., & Esplin, T. L. 2016, arXiv.org, arXiv:1605.06655
- Mace, G. N., Kirkpatrick, J. D., Cushing, M. C., et al. 2013, *The Astrophysical Journal Supplement*, 205, 6
- Makarov, V. V., & Fabricius, C. 2001, *Astronomy & Astrophysics*, 368, 866
- Malo, L., Artigau, É., Doyon, R., et al. 2014, *The Astrophysical Journal*, 788, 81
- Malo, L., Doyon, R., Lafrenière, D., et al. 2013, *The Astrophysical Journal*, 762, 88
- Mamajek, E. E. 2005, *The Astrophysical Journal*, 634, 1385
- Mamajek, E. E., & Bell, C. P. M. 2014, *Monthly Notices of the Royal Astronomical Society*, 445, 2169
- Mamajek, E. E., & Feigelson, E. D. 2001, *Young Stars Near Earth: Progress and Prospects*, 244, 104
- Mamajek, E. E., & Hillenbrand, L. A. 2008, *The Astrophysical Journal*, 687, 1264
- Mamajek, E. E., Meyer, M. R., & Liebert, J. 2002, *The Astronomical Journal*, 124, 1670
- Manara, C. F., Testi, L., Rigliaco, E., et al. 2013, *Astronomy & Astrophysics*, 551, A107
- Marocco, F., Day-Jones, A. C., Lucas, P. W., et al. 2014, *Monthly Notices of the Royal Astronomical Society*, 439, 372
- Marsakov, V. A., & Shevelev, Y. G. 1995, *Bulletin d'Information du Centre de Données Stellaires*, 47, 13
- Marsh, K. A., Plavchan, P., Kirkpatrick, J. D., et al. 2010, *The Astrophysical Journal*, 719, 550
- Martin, D. C., Fanson, J., Schiminovich, D., et al. 2005, *The Astrophysical Journal*, 619, L1
- McLean, I. S., McGovern, M. R., Burgasser, A. J., et al. 2003, *The Astrophysical Journal*, 596, 561
- Meshkat, T., Bonnefoy, M., Mamajek, E. E., et al. 2015, *Monthly Notices of the Royal Astronomical Society*, 453, 2378
- Messina, S., Desidera, S., Turatto, M., Lanzafame, A. C., & Guinan, E. F. 2010, *Astronomy & Astrophysics*, 520, A15
- Metchev, S. A., Kirkpatrick, J. D., Berriman, G. B., & Looper, D. 2008, *The Astrophysical Journal*, 676, 1281
- Miller, G. E., & Scalo, J. M. 1979, and J. M. Scalo. *Astrophysical Journal Supplement Series*, 41, 513
- Moffat, A. F. J. 1969, *Astronomy & Astrophysics*, 3, 455
- Mohanty, S., Jayawardhana, R., & Barrado y Navascués, D. 2003, *The Astrophysical Journal*, 593, L109
- Moraux, E., Bouvier, J., Stauffer, J. R., Barrado y Navascués, D., & Cuillandre, J. C. 2007, *Astronomy & Astrophysics*, 471, 499
- Moraux, E., Bouvier, J., Stauffer, J. R., & Cuillandre, J. C. 2003a, *Astronomy & Astrophysics*, 400, 891
- . 2003b, *Astronomy & Astrophysics*, 400, 891
- Murphy, S. J., Lawson, W. A., & Bento, J. 2015, *Monthly Notices of the Royal Astronomical Society*, 453, 2220
- Muzic, K., Scholz, A., Geers, V. C., & Jayawardhana, R. 2015, *The Astrophysical Journal*, 810, 159
- Nelder, J. A., & Mead, R. 1965, *The Computer Journal*, 7, 308
- Nordström, B., Mayor, M., Andersen, J., et al. 2004, *Astronomy & Astrophysics*, 418, 989
- Ochsenbein, F., Bauer, P., & Marcout, J. 2000, *Astronomy and Astrophysics Supplement*, 143, 23
- Oliveira, J. M., Jeffries, R. D., & van Loon, J. T. 2009, *Monthly Notices of the Royal Astronomical Society*, 392, 1034

- Pecaut, M. J., & Mamajek, E. E. 2013, *The Astrophysical Journal Supplement*, 208, 9
- . 2016, *Monthly Notices of the Royal Astronomical Society*, 461, 794
- Pecaut, M. J., Mamajek, E. E., & Bubar, E. J. 2012, *The Astrophysical Journal*, 746, 154
- Perryman, M. A. C., Lindegren, L., Kovalevsky, J., et al. 1997, *Astronomy and Astrophysics* 323, 323, L49
- Perryman, M. A. C., de Boer, K. S., Gilmore, G., et al. 2001, *Astronomy & Astrophysics*, 369, 339
- Pourbaix, D., Tokovinin, A. A., Batten, A. H., et al. 2004, *Astronomy & Astrophysics*, 424, 727
- Preibisch, T., & Mamajek, E. 2008, *Handbook of Star Forming Regions*, I, 235
- Qi, Z., Yu, Y., Bucciarelli, B., et al. 2015, *The Astronomical Journal*, 150, 137
- Rayner, J. T., Toomey, D. W., Onaka, P. M., et al. 2003, *The Publications of the Astronomical Society of the Pacific*, 115, 362
- Reid, I. N., Cruz, K. L., Kirkpatrick, J. D., et al. 2008, *The Astronomical Journal*, 136, 1290
- Reid, I. N., & Gizis, J. E. 1997, *Astronomical Journal* v.113, 113, 2246
- Reid, N. 2003, *Monthly Notice of the Royal Astronomical Society*, 342, 837
- Reid, N. I., Kirkpatrick, D. J., Gizis, J. E., et al. 2000, *AJ*, 119, 369
- Reipurth, B., & Mikkola, S. 2015, *The Astronomical Journal*, 149, 145
- Reyl , C., Delorme, P., Willott, C. J., et al. 2010, *Astronomy & Astrophysics*, 522, A112
- Riaz, B., Gizis, J. E., & Harvin, J. 2006, *The Astronomical Journal*, 132, 866
- Rice, E. L., Faherty, J. K., & Cruz, K. L. 2010, *The Astrophysical Journal Letters*, 715, L165
- Riedel, A. R. 2012, *ProQuest Dissertations And Theses; Thesis (Ph.D.)—Georgia State University*
- Riedel, A. R., Alam, M. K., Rice, E. L., Cruz, K. L., & Henry, T. J. 2016, *arXiv.org*, arXiv:1610.03867
- Riedel, A. R., Finch, C. T., Henry, T. J., et al. 2014, *The Astronomical Journal*, 147, 85
- Rizzuto, A. C., Ireland, M. J., & Robertson, J. G. 2011, *Monthly Notices of the Royal Astronomical Society*, 416, 3108
- Rodr guez, D. R., Bessell, M. S., Zuckerman, B., & Kastner, J. H. 2011, *The Astrophysical Journal*, 727, 62
- Roeser, S., Demleitner, M., & Schilbach, E. 2010, *AJ*, 139, 2440
- Rojas-Ayala, B., Covey, K. R., Muirhead, P. S., & Lloyd, J. P. 2012, *The Astrophysical Journal*, 748, 93
- Salpeter, E. E. 1955, *Astrophysical Journal*, 121, 161
- Schmidt, S. J., Hawley, S. L., West, A. A., et al. 2015, *The Astronomical Journal*, 149, 158
- Schneider, A., Melis, C., & Song, I. 2012a, *The Astrophysical Journal*, 754, 39
- Schneider, A., Song, I., Melis, C., Zuckerman, B., & Bessell, M. 2012b, *The Astrophysical Journal*, 757, 163
- Schneider, A. C., Windsor, J., Cushing, M. C., Kirkpatrick, J. D., & Wright, E. L. 2016a, *The Astrophysical Journal Letters*, 822, L1
- . 2016b, *arXiv.org*, 1603.07985v1
- Scholz, A., Jayawardhana, R., Muzic, K., et al. 2012, *The Astrophysical Journal*, 756, 24
- Scholz, R. D., McCaughrean, M. J., Zinnecker, H., & Lodieu, N. 2005, *Astronomy & Astrophysics*, 430, L49
- Schr der, K. P., & Pagel, B. E. J. 2003, *Monthly Notice of the Royal Astronomical Society*, 343, 1231
- Shannon, C. E., & Weaver, W. 1949, Urbana: University of Illinois Press
- Shkolnik, E. L., Anglada-Escud , G., Liu, M. C., et al. 2012, *The Astrophysical Journal*, 758, 56
- Shkolnik, E. L., Liu, M. C., Reid, I. N., Dupuy, T., & Weinberger, A. J. 2011, *The Astrophysical Journal*, 727, 6
- Siess, L., Dufour, E., & Forestini, M. 2000, *Astronomy & Astrophysics*, 358, 593
- Simcoe, R. A., Burgasser, A. J., Bernstein, R. A., et al. 2008, *Ground-based and Airborne Instrumentation for Astronomy II*. Edited by McLean, 7014, 70140U
- Simcoe, R. A., Burgasser, A. J., Schechter, P. L., et al. 2013, *Publications of the Astronomical Society of the Pacific*, 125, 270
- Skrutskie, M. F., Cutri, R. M., Stiening, R., et al. 2006, *The Astronomical Journal*, 131, 1163
- Smart, R. L., & Nicastr , L. 2013, *VizieR On-line Data Catalog*, 1324
- Song, I., Zuckerman, B., & Bessell, M. S. 2003, *The Astrophysical Journal*, 599, 342
- Soubiran, C., Jasniewicz, G., Chemin, L., et al. 2013, *Astronomy & Astrophysics*, 552, A64
- Stauffer, J. R., Schultz, G., & Kirkpatrick, J. D. 1998, *The Astrophysical Journal*, 499, L199
- Sterzik, M. F., Alcal , J. M., Covino, E., & Petr, M. G. 1999, *Astronomy & Astrophysics*, 346, L41
- Stock, J., & Wroblewski, H. 1972, *Astronomy & Astrophysics*, 18, 341
- Stoche, J. T., Morris, S. L., Gioia, I. M., et al. 1991, *Astrophysical Journal Supplement Series (ISSN 0067-0049)*, 76, 813
- Suchkov, A. A., Makarov, V. V., & Voges, W. 2003, *The Astrophysical Journal*, 595, 1206
- Sumi, T., Kamiya, K., Bennett, D. P., et al. 2011, *Nature*, 473, 349
- Tachihara, K., Neuh user, R., Frink, S., & Guenther, E. 2003, *Astronomische Nachrichten*, 324, 543
- Teixeira, R., Ducourant, C., Chauvin, G., et al. 2009, *Astronomy & Astrophysics*, 503, 281
- . 2008, *Astronomy & Astrophysics*, 489, 825
- ter Braak, C. J. F., & Vrugt, J. A. 2008, *Statistics and Computing*, 18, 435
- Tinney, C. G., Faherty, J. K., Kirkpatrick, J. D., et al. 2012, *The Astrophysical Journal*, 759, 60
- Tokovinin, A. A. 1999, *Astronomy Letters*, 25, 669
- Torres, C. A. O., Quast, G. R., da Silva, L., et al. 2006a, *Astronomy & Astrophysics*, 460, 695
- . 2006b, *Astronomy & Astrophysics*, 460, 695
- Torres, C. A. O., Quast, G. R., Melo, C. H. F., & Sterzik, M. F. 2008, *Handbook of Star Forming Regions*, I, 757
- Torres, G., Guenther, E. W., Marschall, L. A., et al. 2003, *The Astronomical Journal*, 125, 825
- Torres, R. M., Loinard, L., Mioduszewski, A. J., & Rodr guez, L. F. 2009, *The Astrophysical Journal*, 698, 242
- Turon, C., Cr z , M., Egret, D., et al. 1992, *Bulletin d'Information du Centre de Donnees Stellaires*, 41, 9
- Uppgren, A. R., Grossenbacher, R., Penhallow, W. S., MacConnell, D. J., & Frye, R. L. 1972, *Astronomical Journal*, 77, 486
- Vacca, W. D., Cushing, M. C., & Rayner, J. T. 2003, *The Publications of the Astronomical Society of the Pacific*, 115, 389
- van Leeuwen, F. 2007a, *Astronomy & Astrophysics*, 474, 653
- . 2007b, *Astronomy & Astrophysics*, 474, 653
- Webb, R. A., Zuckerman, B., Platais, I., et al. 1999, *The Astrophysical Journal*, 512, L63
- Weinberger, A. J., Anglada-Escud , G., & Boss, A. P. 2013, *The Astrophysical Journal*, 762, 118



- Weis, E. W. 1993, *Astronomical Journal* (ISSN 0004-6256), 105, 1962
- West, A. A., Bochanski, J. J., Hawley, S. L., et al. 2006, *The Astronomical Journal*, 132, 2507
- West, A. A., Hawley, S. L., Bochanski, J. J., et al. 2008, *The Astronomical Journal*, 135, 785
- Wright, E. L., Eisenhardt, P. R. M., Mainzer, A. K., et al. 2010, *The Astronomical Journal*, 140, 1868
- Wright, J. T. 2004, *The Astronomical Journal*, 128, 1273
- . 2005, *The Astronomical Journal*, 129, 1776
- Zacharias, N., Finch, C. T., Girard, T. M., et al. 2013, *The Astronomical Journal*, 145, 44
- Zuckerman, B., & Song, I. 2004, *Annual Review of Astronomy & Astrophysics*, 42, 685
- Zuckerman, B., Song, I., Bessell, M. S., & Webb, R. A. 2001a, *The Astrophysical Journal*, 562, L87
- Zuckerman, B., Webb, R. A., Schwartz, M., & Becklin, E. E. 2001b, *The Astrophysical Journal*, 549, L233